Faculty of Engineering Technology - Mechanical Engineering

Modelling study of the thermal management of a RSOC system

UNIVERSITY OF TWENTE.

Stan G. Wellen

Master Thesis
April 4, 2024

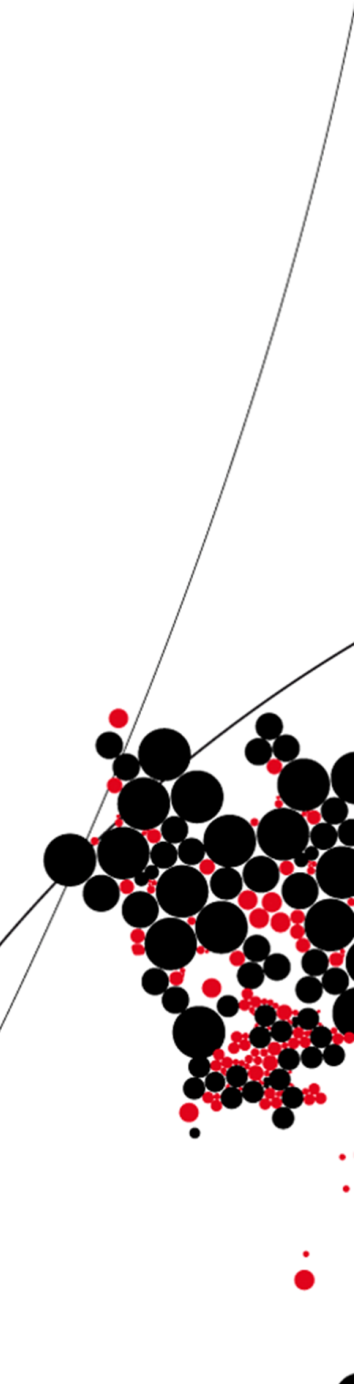

Supervisor(s)	Dr. S. Hajimolana
	Dr. A. Singh
Chair	Prof. dr. -ing. W. Rohlfs

Abstract

The source of energy in the grid is transitioning from fossil fuels towards renewable energy sources. With an increasing amount of electricity provided by offshore wind turbines, the source of the electricity becomes more intermittent. These variations within the source of electricity increase the challenge to match the supply and demand of electricity within the grid. To balance the supply and demand, electricity storage could be applied. To store electricity various solutions could be applied like batteries or by the electrochemical reaction of hydrogen. The electrolyser and fuel cell are the two components used to store and generate electricity by the conversion of hydrogen. One of the types of electrolyser and fuel cell is the solid oxide cell.

Reversible solid oxide cells (RSOC) are cells capable of both electrolysis and fuel cell operation. The RSOC is a promising solution for hydrogen storage due to its relatively high round-trip efficiency. Literature regarding the RSOC is still limited. Some models have been developed for the RSOC. However, models which include the balance-of-plant (BoP) required to operate the RSOC are not considered in the literature. The RSOC technology itself is still in the development stage and the development of variations in the BoP are limited. This study aims to develop and compare different concepts of the BoP to improve its performance and economic viability. For the comparison, a dynamic model for the BoP of the RSOC is developed.

For this purpose multiple variations of the BoP are described to be able to operate the RSOC. These include BoPs based on electric heaters and boiler. The use of heat recovery units to improve the performance of the system. The utilization of thermal energy storage (TES) and a heat pump to reduce the power consumption for evaporation. A concept based on the use of metal-hydride to store hydrogen and improve the thermal management. The dynamic model is developed to determine the performance of the different described BoPs. The performance of the different concepts is measured based on the efficiency and the levelized cost of electricity. It was found that the sole use of electric heaters results in a low overall efficiency. The use of metal hydrides to store hydrogen results in significantly higher costs. The differences in the levelized cost of the other concepts are small and dependent on the cost at which the components are obtained.

The developed model allows to determine the power consumption and required capacity of the different concepts. The model is used to compare different concepts of the BoP of the reversible solid oxide cell. However, for future elaboration of a single concept, a more detailed model should be used. For the comparison of the levelized cost of electricity (LCOE) further research and selection of components is required. Due to the range of the cost regarding components it could not be determined which is economically the best-suited solution.

Contents

1 Introduction

The increase of renewable energy sources like wind and solar requires challenges to be solved. The availability of renewable energy sources fluctuates throughout the year. Therefore balancing/storage of electricity is necessary to match supply and supply. One of these storage solutions is the conversion of electricity to hydrogen and vice versa by an electrochemical process. The reversible solid oxide cell (RSOC) system, operating in both high-temperature electrolysis and fuel cell mode, is a promising technology with low estimated cost of storage and potentially large storage capacity [1]. TNO has performed economic studies which identified the cost-of-storage to be 0.04 €/kWh, a round-trip efficiency of 50-55% and the potential of storage capabilities over 100 GWh for RSOC systems [1]. TNO is working on a model to integrate the RSOC into the electricity grid network. This requires a dynamic model which can be implemented in the existing electricity market model of TNO. The RSOC functions both as an electrolyser and fuel cell. Where in a solid oxide fuel cell an exothermic reaction takes place. While during electrolysis the efficiency of the process taking place could be improved if electricity is supplied as heat. This requires the balance-of-plant (BoP) to manage two scenarios for heat management. To optimise the response time and round-trip efficiency different variations of heat management within the BoP are investigated. Furthermore, a business case optimization should explore the components of the heat management of the balance-of-plant to investigate the viability of the different scenarios.

Research of TNO is focused on the design of the solid oxide cell to improve the durability and efficiency of the stack. However, the effects of the balance-of-plant on the round-trip efficiency are just as important. Prior to the investigation of a prototype of the balance-of-plant, it is desired to investigate the effects of different components and certain parameters. These are the temperature within the stack and the effects of pressure on the round-trip efficiency. The model is used to identify the round-trip efficiency and the size required for different components to determine the cost of the balance-of-plant.

The goal of this thesis is to select the optimal heat management scenario of the balance-of-plant of a reversible solid oxide cell. The research questions are defined as:

- What heat management scenario has the highest round-trip efficiency?
- Which concept has the lowest levelized cost of energy?
- How can the balance-of-plant be dynamically modelled, and integrated with an electricity market model?

To achieve the goals of this thesis and answer the research questions the thesis is divided into two objectives. The first is to investigate different concepts of the balance-of-plant. The second is to develop a dynamic model regarding the system.

The system includes the solid oxide cell and the other components of the balance-of-plant. The heat management scenarios assumes power generation by a wind park and the use of a base load demand from the grid. To select the optimal concept for the heat management, a business case analysis should be performed to include the economic aspects of the optimization of the balance-of-plant. To achieve the research objectives this thesis focuses on:

- Define the operating conditions of the stack.
- Develop multiple concepts for the design of the balance-of-plant with a focus on the thermal management of the balance-of-plant.
- Determine the expected response time for the different setups of the balance-of-plant
- The performance of the balance-of-plant in steady state and transient behaviour regarding required heat duty and efficiency.
- Develop a dynamic model of the stack and balance-of-plant
- Techno-economic analysis for the comparison of the concepts

This thesis focuses on the annual energy production and consumption, the efficiency and cost of the system. Therefore, different components of the balance-of-plant are assessed. These include the RSOC, heat exchangers and compressor. These components are necessary to achieve the operating conditions within the stack. A detailed description of each component is not part of the scope of this thesis. Therefore, the models and thesis do not include the components' detailed transient response and control. The design of the RSOC stack is considered out of the scope of this thesis. Except for general concepts which could alter the behaviour of the balance-of-plant, for example changing the method of cooling of the stack.

This thesis is structured as follows: Chapter 2 is a literature review. Chapter 3 discusses multiple concepts regarding the balance-of-plant. These concepts include electrical heaters, heat recovery, heat pumps and metal hydrides for hydrogen storage. Chapter 4 describes the models used for the electrochemical reaction and the balance-of-plant. The results of the models are presented in chapter 5 with a focus on the performance of the concepts. In chapter 6 the concepts are compared with a techno-economic analysis. In chapters 7 and 8 the conclusions and recommendations are formulated.

2 Literature review

The aim of this literature study focuses on the following questions: How do the SOFC and SOE work and how are these modelled, what are existing BoP designs for the SOFC and SOE, what are thermal management strategies for the SOE and SOFC?

2.1 Hydrogen conversion

The use of renewable energy sources results in the necessity to balance the varying supply and demand of electricity. To balance the supply and demand various storage solutions have been proposed. One is the conversion from electricity to chemical energy. Different types of fuel cell and electrolyzer designs exist and are described in the literature. These include the alkaline fuel cell (AFC), phosphoric acid fuel cell (PAFC), solid oxide fuel cell (SOFC), molten carbonate fuel cell (MCFC), proton exchange membrane fuel cell (PEMFC) and direct methanol fuel cell (DMFC). All these different fuel cells operate in a similar manner [2]. However, each type of cell has different advantages and disadvantages.

2.2 Solid oxide electrolysis and fuel cell

This section describes the use of solid oxide electrolyzer cells (SOEC) and SOFC. The SOEC is an electrochemical device which converts energy and H_2O into H_2. The SOFC operates in the opposite direction converting H_2 into power, heat and H_2O. Both solid oxide electrolysis (SOE) and the SOFC operate at high temperatures of 600 to 1000 °C. At these temperatures, the RSOC does not require a platinum catalyst [3], which results in lower cost. To become interesting for commercial use, SOC requires a low internal resistance and long durability. However, only a few reports on the durability are available in literature [4]. The operation of SOC is reversible, which allows it to both produce hydrogen and generate electricity within the same device.

The RSOC has received limited attention in its role of large-scale energy storage. Where most attention is given to the use of proton exchange membranes and alkaline cells [5]. In both of these cases relatively large over-potentials are required to achieve sufficiently high current densities [5]. SOFC has the potential to achieve an efficiency of 70-80% when using hydrocarbons as a fuel [6]. Hydrogen-based fuel cells operating at high temperatures, like the SOFC and MCFC could potentially achieve efficiencies up to 60 %. Compared to efficiencies of 40 to 50 % for low and medium temperature AFC and PEMFC fuel cells. Another advantage of the SOC is the ability to use the same cell for electrolysis and fuel cell operations. This allows for better system integration for thermal management which favours the efficiency of the SOC. Mottaghizadeh et al. [7] describe the possibility of a system integrating both SOE and SOFC modes in combination with thermal energy storage (TES), where heat is stored during SOFC mode and utilised during SOEC. The SOFC operation is an exothermic process where heat is generated within the stack. The heat could be used to supply heat during electrolysis if additional heat is required. The disadvantage of the SOC is the high operating temperature required to achieve the optimal

efficiency. This is due to the use of an oxide-ion conducting ceramic membrane which is in turn sensitive to mechanical failure. Mechanical failure is caused by the thermal stress due to variations in temperature within the RSOC. Other disadvantages of the SOC are the high cost and complexity of the SOC [8].

2.3 Modelling of SOC

The literature on the modelling of RSOC systems is limited and mostly focused on separate electrolysis and fuel cells. Several attempts at modelling the dynamic behaviour of RSOC systems can be found in the literature. Kazempoor and Braun present a 1D model for SOE based on hydrocarbons [9]. This paper focuses on the validation and steady-state results of their model regarding the electrolysis operation of a RSOC. This work is a continuation of a paper from the same authors [10] where the focus is on the validation of the fuel cell mode. To include both SOE and SOFC mode and the change of the current density Kazempoor and Braun [11] present a model which includes the entire range from SOE to SOFC. This paper presents the validation for the steady state of the voltage-current density relation over the entire range of a RSOC in steady-state .

Kazempoor and Braun developed a continuous model over the entire range of operation which simplifies the modelling. However, it is also possible to define an operator to model both modes separately. Papers regarding the change between the operational modes are limited. Jin and Xue [12] investigated the transient behaviour when switching between the electrolysis and fuel cell mode using a discrete operator. The authors developed a transient 2D isothermal model to investigate the switching between SOEC and SOFC and different compositions within the fuel channel. This model was only used for comparison with steady-state results.
System level evaluations require reduced order models with less complexity. These models should be detailed enough to accurately represent the electrochemical reaction and the flow and pressure characteristic [10]. Motylinski et al. [13] developed a 0D model of a reversible solid oxide cell, which is used for system-level modelling. To model the dynamic response of the balance-of-plant Mottaghizadeh et al. used an area-specific resistance (ASR) based on experimental results [7]. The ASR could be used to describe the polarization losses within the SOFC.
The models regarding the dynamic behaviour of the RSOC at the system level are limited and are used for small periods of time. Furthermore, the literature considering the dynamic response is focused on the RSOC cell itself with limited focus on the full BoP [13]. Additionally, the focus is on the transition between electrolysis to fuel cell operation and in the opposite direction [12, 13].

2.4 Balance-of-plant of the RSOC

The described balance-of-plant found in the literature focuses on different applications for the SOC such as the SOFC, SOEC and RSOC. Although SOFC and SOEC are the same electrochemical cell the opposite direction of the process results in different strategies for the management of

the process. These different processes require different setups for the balance-of-plant. Therefore all three applications of the RSOC are reviewed. Literature about the SOFC is the most prevalent due to the use of fuel cells in combination with natural gas as a replacement for conventional power generation.

2.4.1 Reversible solid oxide cell

The number of papers describing the BoP of a RSOC is limited. Therefore models for SOE and SOFC are taken into account in this review. Several attempts can be found in the literature on how to increase the efficiency of the system or to store heat and hydrogen. The dynamic model presented by Motylinski et al. [13] utilized a BoP to satisfy heat demand and thermal management of the stack. [7] et al. modelled both SOE and SOFC using a reversible solid oxide cell. The designed BoP includes heat storage to increase the performance of the BoP. However, the RSOC research is based on methane and carbon dioxide in contrast to hydrogen. Therefore further research is required on whether or not the proposed BoP is suited for a process utilizing hydrogen as the main component. Giap et al. [14] described a BoP using a different storage method of hydrogen. Giap et al. make use of the metal hydride MgH_2 for hydrogen storage in contrast to most papers. These use the combination of a compressor and pressure vessels to store hydrogen [7, 13, 15]. Metal hydrides absorb hydrogen and de-absorb hydrogen if below or above a certain temperature. The use of metal hydrides is advantageous due to the high storage density and the removal of the required high compression ratio for hydrogen storage [14].

2.4.2 Solid oxide fuel cell

SOFC systems have been extensively investigated for their high efficiency and low environmental impact. SOFC can use different types of fuel such as natural gas or pure hydrogen. In literature, different systems such as the BoP for SOFC are described [16, 17]. The use of SOFC and the corresponding balance-of-plant are therefore more often described as RSOC systems.
The solid oxide fuel cell is not the only device mode to convert hydrogen to power. The proton-exchange membrane fuel cell is developed for transportation. PEMFC and AFC operate at lower temperatures and are more commonly investigated in steady-state and varying load conditions [18].

2.4.3 Solid oxide electrolysis

The described solid oxide electrolyzers could be split into two variants. The first is based on electrolysis which uses only water as fuel and converts the water to hydrogen. Papers which propose an electrolysis system based on H_2O are Alzahrani and Dincer [15], Mansilla et al. [19] and Peter et al.[20]. The second variant is based on the co-electrolysis of CO_2 and H_2O resulting in a syn-gas/methane. Systems for the co-electrolysis of CO_2 and H_2O are proposed by Ali et al. [21] and Gotz et al. [22].

Alzahrani and Dincer [15] describe the BoP of a SOE system. However, this paper does not include the models for components besides the solid oxide cell. The results are validated and

show steady-state results relating to the current density and pressure. The BoP described is similar to the BoP used for reversible operation by Motylinski et al. [13]. However, Alzahrani and Dincer focus on the effects of pressure during SOE mode. Therefore only the mechanical components such as the compressor and pump are included in the model. It was found that the storage as compressed hydrogen might reduce the overall efficiency of the BoP, including the RSOC, with 6% [15].

2.5 Durability and degradation

Research shows that the change in temperatures results in a different RSOC resistance over time. The change in the temperature causes thermal stress. The thermal stresses within each cell cause delamination between the different layers within the cell. The thermal stresses are partly caused by the difference in thermal expansion coefficients of the materials used within the RSOC [23]. The change in the cell resistance is investigated by Bujalski et al. where due to the repeated temperature changes of the cell, small changes in cell resistance are observed over time. Hereby a rate of change of the temperature of 2 °C/min is used [24]. For the design of the RSOC thermal management is required to manage the temperatures and keep the temperature within operational range. This is due to the thermal expansion coefficients change for different temperatures [25]. The rate of temperature change is related to the increase or decrease of the current within the cell. The current density could theoretically be increased rapidly. Xie et al. put a SOC under a step change of the cell voltage and found that the current density changed rapidly from 1.5 A/cm2 to 3.8 A/cm2 [26]. This paper does not investigate the degradation of the cell due to temperature variations.
The response time of the RSOC stack depends on the ramp rate of the current density within each cell. The change of temperature ($\frac{dT}{dt}$) is related to the ($\frac{dA}{dt}$), where a lower ramp rate for the current density results in smaller changes in temperature per minute [13]. The literature describes the effects of large temperature differences of the RSOC [23]. The effect of thermal cycling reduces the cell potential over a period of time as ASR increases during the number of cycles [23]. Reducing the change of the current density results in a lower temperature gradient over time [13].

2.6 Thermal management of RSOC

Cooling of the fuel cell is required to manage the temperature distribution in the cell. The most common method of temperature management in the SOFC is the use of increased airflow through the cell. This is relative to the stoichiometrically required airflow. The availability of literature about the other methods of cooling for the SOFC is limited. However, the air required for the thermal management of the SOFC results in high parasitic electricity consumption. Due to the low heat capacity of air, the required flow of air is large to limit the temperature rise of the cell. Research has been summarized and could be categorized into three different types: Passive cooling, liquid cooling and phase change materials [27, 28].

2.6.1 Passive cooling

Passive cooling can reduce the temperature gradient in the cell. For PEMFC multiple passive cooling techniques are described by Zhang [29]. Heat can be removed more easily from the edges of the cell and does not require any circulation of coolant. The principle of passive cooling is based on the conduction of heat from the central region of the cell to the edge of the stack. Since solid oxide cells operate at a high-temperature, heat losses to radiation are inevitable. However, the effects of the ambient temperature are minor on the cell's performance. However, heat losses due to radiation are minimal in a full stack of cells [30].

2.6.2 Liquid cooling

An external cooling solution may be favourable due to the reduction of the air required. The BoP parasitic energy consumption is related to the increased airflow through the system during SOFC. A possibility to cool fuel cells is the use of coolant liquids. The use of heat pipes for the thermal management of SOE and SOFC is described by Dillig and Karl [31]. Their numerical model showed that heat pipes can reduce the thermal temperature variation within the stack. The use of heat pipes was experimentally validated. This shows that the use of heat pipes reduces the temperature gradient [32, 33]. Furthermore, heat pipes can reduce the parasitic electricity consumption of the RSOC and use the heat of secondary processes [34].

2.6.3 Phase change materials

The use of heat pipes or other liquid cooling requires the temperature of the coolant to increase the removal of the heat. Promsen et al. [35] propose cooling using phase-change material (PCM). The use of saturated water can significantly reduce parasitic power consumption. Saturated water-cooled SOFC is not commonly used. However, cooling with saturated water can drastically reduce temperature variations in the stack; 295K to 62K at 3500 A/m^2 for tubular SOFC and 186K to 26K at 9000 A/m^2 for planar SOFC [35]. Water cooling is a promising solution to limit the temperature differences within the RSOC. However, there are challenges in applying this and might lead to increased sizes, complexity and higher cost.

The cooling of the fuel cell stack by air is the most prevalent method of cooling the cell. The use of secondary channels, heat pipes or phase change materials within the stack significantly increases the complexity of the stack. However, the cost of the BoP components can be reduced using dedicated cooling due to the reduction in parasitic power consumption.

2.7 Heat management

Due to overpotential in the stack the SOC can operate in both endothermic as well as exothermic modes [7]. The reaction taking place for SOFC is exothermic and requires cooling to remain within the operational conditions of the fuel cell.

2.7.1 Heat recovery

The air and fuel gasses leave the SOEC and SOFC at high temperatures. The heat within the gasses could be used to pre-heat the incoming air and fuel streams through the use of heat recovery units [15]. Heat recovery units have been used to heat the air and fuel entering the RSOC in different studies [7, 13].

2.7.2 Heat storage

Due to the reversible operations of the RSOC, the exothermic SOFC and endothermic/thermoneutral SOE, heat storage is investigated. The energy supplied by wind turbines varies throughout the year. Because heat is required for the production of hydrogen, it is necessary to store thermal energy for a long time. Different thermal energy storage methods have different properties and thus advantages and disadvantages.

TES System	**Efficiency (%)**	**Storage Period**	**Cost (€/kWh)**
Sensible	50-90	days/months	0.1 -10
Latent	75–90	hours/months	10–50
Chemical	75–100	hours/days	8–100

Table 1: Parameters thermal energy storage [36]

Novo et al. [37] states that seasonal heat storage can be provided by underground thermal energy storage, by phase change materials or by chemical reactions.
A second criterion used for thermal energy storage (TES) is the response time of the storage medium. The response time is the speed at which energy is released or absorbed. This varies from a few seconds to minutes, depending on the medium [38].

TES System	**Response time**	**Source**
Sensible	2.5 [min]	[39, 40]
PCM	5 - 20 [min]	[41]
Thermochemical	10 -30 [min]	[42]

Table 2: TES response time

Sensible heat storage is generally the cheapest form of thermal energy storage. In addition, the response time of 2.5 min to tens of minutes is faster compared to latent heat storage and thermochemical storage. However, the disadvantage of sensible heat storage is the low energy storage density. Phase change materials and thermochemical storage have the advantages of high storage density, long duration of storage and low losses of heat [43]. However, the low thermal conductivity of PCM results in an increase in the response time. Since the heat transfer is limited by thermal conductivity, this slows down the process of releasing and storing energy [44].

3 Proposed concepts

This chapter discusses the different scenarios developed for the balance-of-plant (BoP). The concepts are required to achieve three operating conditions. Firstly the concepts have to increase the temperature of the fuel and air flows to the operating temperature of the RSOC. In addition, the temperature within the RSOC must be regulated. Finally, the hydrogen must also be prepared for storage at a pressure of 350 bar. The goal is to design different concepts of the heat management of an entire RSOC facility. The heat and flow management within the balance-of-plant is necessary to ensure the operation conditions within the RSOC in both SOFC and SOEC modes. For the thermal management within the stack, different techniques are used which allow a variety of thermal management scenarios. The different concepts are based on literature and components that are identified to consume a large amount of electricity.

The concepts are assumed to be stand-alone systems connected to the grid and wind park. Therefore no external heat sources are available. The power supplied and generated by the RSOC is treated separately from the other components of the BoP as shown in figure 1.

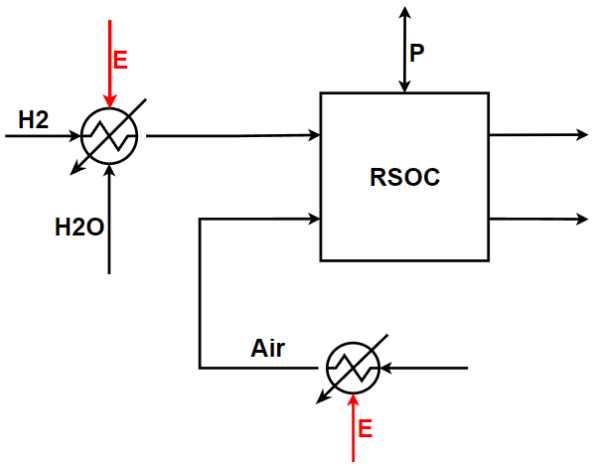

Figure 1: To meet the requirements to operate the RSOC the fuel (H_2 and H_2O) and air are pre-heated. The energy required to operate the RSOC stack is determined by the difference between demand and supply from the grid and windpark (P). Power required to operate the BoP, excluding the RSOC stack, is supplied by the grid(E).

To investigate different solutions to improve thermal management and round-trip efficiency five concepts are developed. The concepts are developed for a specific set of requirements and fixed parameters. Pre-defined parameters include the composition and minimum and maximum temperature of the stack. The temperature of the RSOC is set to be between 700 and 750 °C. Where the temperature of 700 °C is the operating temperature of the SOEC and the maximum temperature is 750 °C during SOFC operational mode. The inlet composition for the evaluation and

modelling is pre-defined and set by TNO [1]:

$$x_{\text{SOFC,in}} = \begin{cases} x_{H_2} = 0.95 \\ x_{H_2O} = 0.05 \end{cases}$$

For electrolysis, the inlet composition changes to increase the fraction of steam within the cell.

$$x_{\text{SOEC,in}} = \begin{cases} x_{H_2O} = 0.9 \\ x_{H_2} = 0.1 \end{cases}$$

The conversion between hydrogen and steam is constant for both SOFC and SOFC. The conversion rate is set at a fuel utilization of U_f = 0.8. The pressure for each of the concepts is set at atmospheric pressure. An increased pressure positively affects the Nernst-potential and polarization curve for fuel cells [45]. Mottaghizadeh investigated both the effects of pressure on the fuel cell efficiency and the efficiency of the BoP. Where a higher operating pressure resulted in an increased efficiency of the fuel cell [7]. Increased pressure can increase the cell efficiency with 5-7% compared to atmospheric pressure [46]. However, the efficiency of the complete BoP is found to be reduced. The reduction in the efficiency is attributed to the increased energy consumption required to compress the air within the system [7]. The influence of these parameters on the fuel cell's performance is elaborated in appendix A.

An overview of the concepts is given below. A more detailed description can be found in this chapter. The goal of these concepts is to identify possible improvements in the balance-of-plant.

- Concept 1: The simplest form of a system for a RSOC to be able to satisfy the requirements concerning temperature and pressure. All heat is supplied by electric heaters or boiler.
- Concept 2: This is a variant which is more efficient due to the heat recovery taking place of the outgoing streams of fuel and air.
- Concept 3: A more efficient SOC for power generation by including a thermal energy storage solution, and a heat pump for steam generation as a replacement for the boiler.
- Concept 4: This is an iteration of concept 2, the attempt is to integrate high-temperature heat storage as a replacement for electric boilers and heaters.
- Concept 5: This concept incorporates metal hydrides as hydrogen storage. The chemical reaction of metal hydrides is exothermic when the hydride matrix absorbs H_2. Metal hydrides can replace the high-pressure vessel and reduce the external energy required for evaporation.

3.1 Concept 1: Electric heaters

The first concept is the most basic concept to achieve the inlet requirements for the RSOC. Furthermore, the concept is used to investigate the energy consumption of different components of

the BoP. The concept for the BoP aims to provide air and hydrogen at pre-set temperatures. Air is extracted from the environment since if the air if the air is in a closed-loop cycle the air could be depleted from or enriched with oxygen. Where the depleted air will not be able to satisfy the stochiometric requirements of the reaction.

To be able to process the required air and fuel concept 1 consists of electric heaters. Water, blue in figure 2, is supplied from the environment to provide sufficient steam for the process. The water is pre-heated to the evaporation temperature by an electric heater. Where the evaporation of water takes place in the electric boiler. Similarly, the air is fed into the system from the environment and pre-heated to 700 °C. The air is presented as the green line in figure 3. The purple line represents the mixture of hydrogen and water. The mixture is super-heated to 700°C by the heater. After the reaction in the RSOC the hydrogen and water are separated. Before separation, the water vapour is condensed which allows the water to be removed from the system. The hydrogen is subsequently compressed to 350 bar. The goal is to investigate the efficiency of a RSOC without any heat recovery and to determine the components required to run the RSOC. The BoP is shown in figure 2.

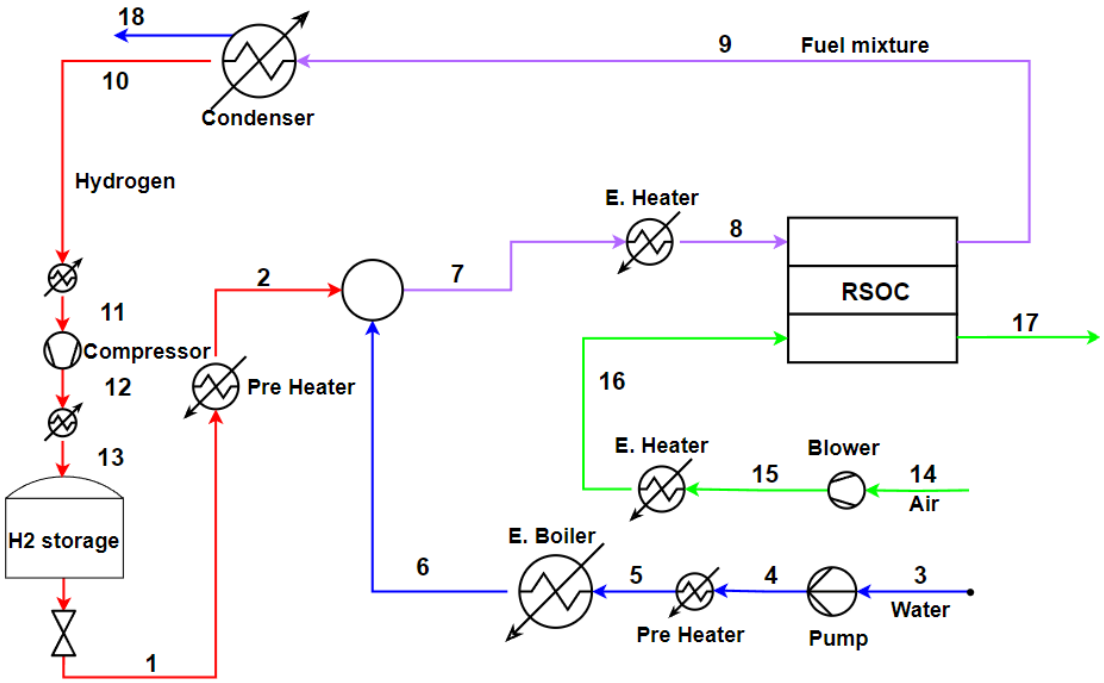

Figure 2: Schematic overview of concept 1, heat is provided for both flows by means of electric heaters and boiler. Red represents the flow of H_2, blue represents the flow of H_2O, purple represents the mixture (H_2 and H_2O) and green represents the flow of air. The corresponding molar-flow rates and temperature is presented in table 11 in appendix B.1 for each part of the BoP.

The system is based on the operation of a solid oxide cell connected to a grid. The flow diagram is presented in figure 2 and the corresponding temperatures are shown in table 11. To achieve the operating conditions water is heated from ambient temperature to the evaporation

temperature of 100 °C and subsequently evaporated to generate steam. The hydrogen, stored at a pressure of 350 bar, is extracted from the storage vessel. Subsequently, the hydrogen is expanded to the operating pressure of the system and heated to the required temperature. The expanded hydrogen and produced steam are mixed. The mixture of hydrogen and steam is then superheated to a temperature of 700 °C with the use of electrical heaters. Depending on the operational mode the RSOC consumes hydrogen or steam. Similarly to the fuel side of the BoP air is fed from the environment into the system at ambient temperatures and is subsequently heated. The amount of air required is determined by two criteria. Firstly, during electrolysis, the molar flow of air is used to prevent the oxygen content from exceeding 23.5% of the air. Secondly, during SOFC operational mode the air is used to manage the heat within the stack and to satisfy the stoichiometric requirement of the reaction. The airflow is used to manage the temperate increase of the stack so it does not exceed a temperature of 750 °C. During electrolysis, the stack operates at an endothermic voltage. Where the heat supplied is equal to the evaporation of water. This means that the temperature inside the fuel channel will remain constant. The amount of air required is therefore determined by the maximum oxygen content of the air. The air is subsequently released into the environment. The fuel mixture is fed into a condenser. The steam is condensed which is required to separate the two components. The condensed water is extracted from the system. The hydrogen is cooled to 25 °C before entering the compressor where the pressure is increased to 350 bar for storage. It is evident that using electric heaters and boilers results in parasitic electricity losses. The use of steam instead of liquid water reduces the required electricity input within the stack itself per mole of hydrogen produced. However, if the steam is generated by an electric boiler the efficiency of the total concept does not improve. The large energy consumption for the heaters and boilers could be reduced by the use of the heat available at the outlet of the stack.

3.2 Concept 2: Heat recovery units

For concept 1 it is expected that a large part of auxiliary energy use is consumed by the electric heaters for heating air and fuel to operating temperatures. Commonly used for SOFC are systems with integrated heat recovery to re-utilise the heat in the exhaust flow of the RSOC. Heat recovery is assumed to be vital for the efficiency of the system due to the high flow rate for both the fuel and air channels. Heat exchangers could provide the heat required for the incoming flow and can increase the overall efficiency of the BoP. In SOFC the outlet temperature is expected to be 50 °C higher relative to the inlet temperature of the flows. The heat recovery units are required to have at least a minimal temperature difference between the two flows. For SOFC it is assumed the heat recovery can provide all heat required for heating the inlet streams to operational temperatures. During SOE additional heat is expected to be required to reach the operating temperature. The additional heat is provided by electrical heaters. The schematic overview of the concepts including heat recovery is shown in figure 3, and the corresponding temperature and compositions are shown in table 12.

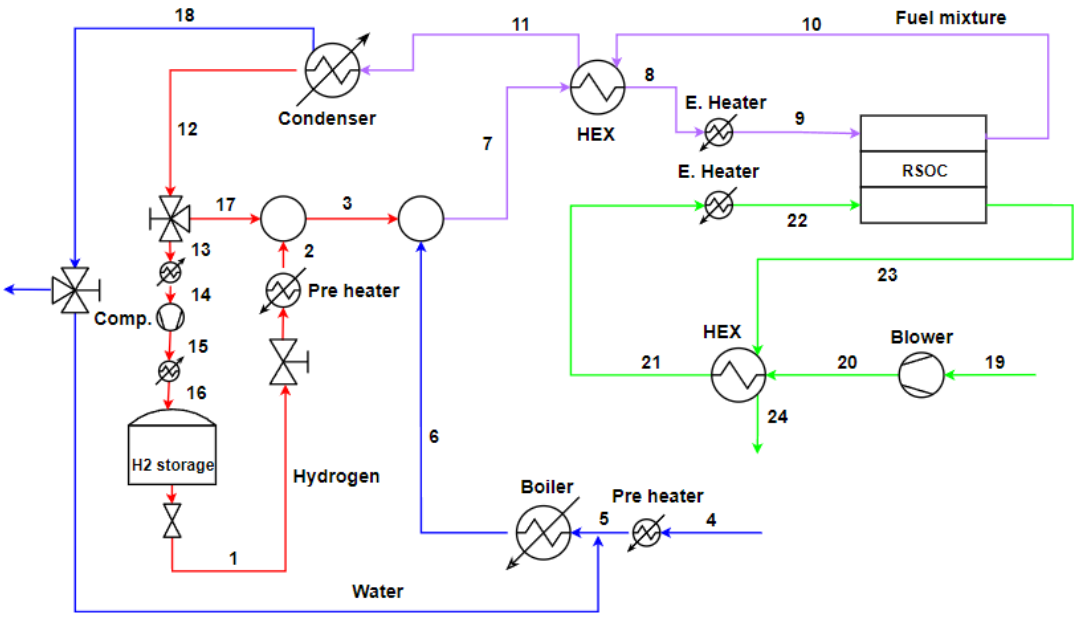

Figure 3: Schematic overview of concept 2, the heat is provided with the combination of electric heaters and heat recovery units. Water is evaporated with an electric boiler. Red represents the flow of H_2, blue represents the flow of H_2O, purple represents the mixture (H_2 and H_2O) and green represents the flow of air. The corresponding molar-flow rates and temperature is presented in table 12 in appendix B.1 for each part of the BoP.

Selecting a type of heat exchanger is important for the performance of the heat recovery unit. The two main types of heat exchangers are parallel-flow and counter-flow heat exchanger setups. The parallel-flow heat exchanger has the advantage of the possibility of a high heat flux [47]. Whereas counter-flow heat exchangers have the potential for higher heat recovery. This is advantageous as the outlet temperatures of the incoming streams require less additional heat to reach the operational temperature. In case the heat is provided with electric heaters the round-trip efficiency of the system drops.

3.3 Concept 3: Heat pump and heat storage

With heat recovery, the heat required for heating the air and fuel streams could be reduced. However, to reduce the power required by the RSOC water could be supplied as steam to the RSOC. In previous concepts, an electric boiler converts one unit of electricity into approximately one unit of heat. However, this does not reduce the power consumption of the BoP. However, both in SOEC and SOFC modes heat is released by the condensation of steam before separation of H_2 and H_2O. Where during SOFC steam is generated within the SOFC. For SOE not all steam generated in the boiler is used due to a fuel utilization of 80%. The temperature at which the heat is released is insufficient to be reused for the evaporation process. However, the released heat during condensation could function as a heat source for a steam-generating heat pump.

The heat released by condensation during SOFC is sufficient to serve as a heat reservoir for a heat pump. The heat recovery during electrolysis could provide approximately 15 to 20% of the heat required for evaporation. The heat released by the condensation during SOFC is larger than required for the evaporation of water. Thus further improvements regarding the efficiency could be made by implementing thermal heat storage (TES). So the surplus of heat could be stored and used during electrolysis where insufficient heat is available within the BoP.

The overview of the system is shown in figure 4. The heat is extracted from the mixture during the condensation of the steam. During SOFC mode the heat available is sufficient to provide the heat required by the heat-pump to evaporate water. The surplus of heat is stored in the TES. The low-temperature storage stores the heat at temperatures below 100 °C. If required during electrolysis the TES functions as the heat reservoir for the heat-pump.

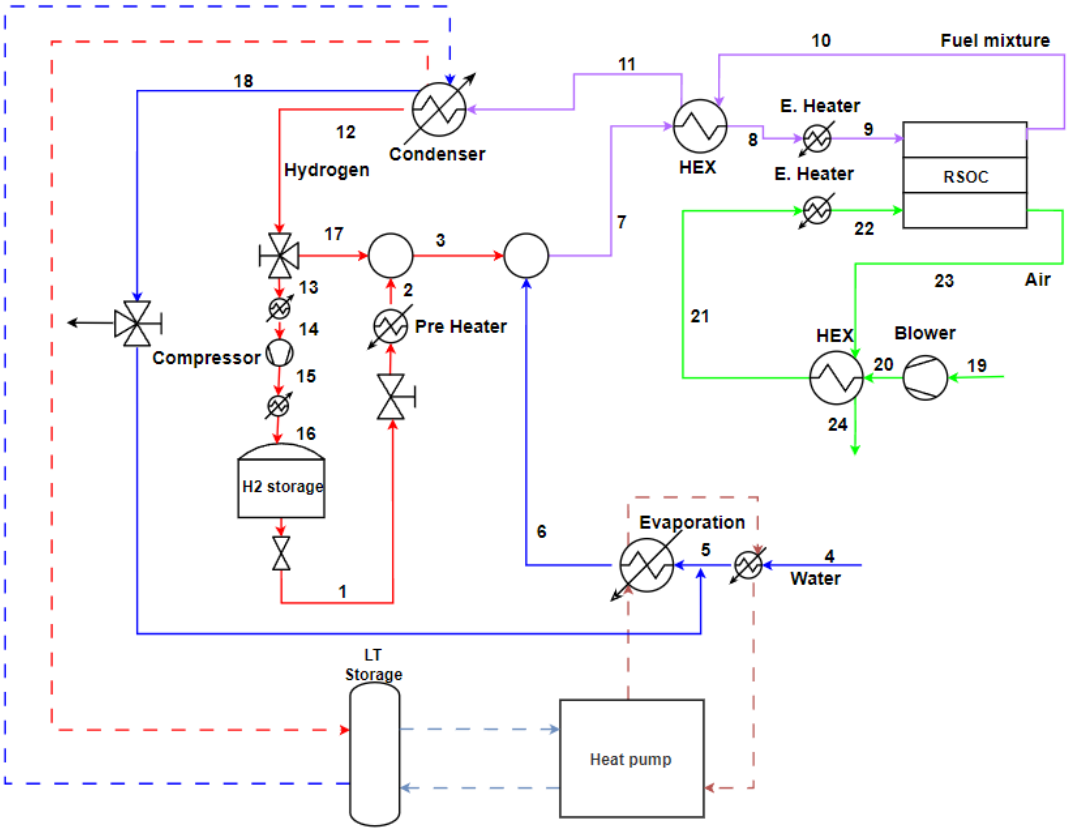

Figure 4: Schematic overview of concept 3, the heat is provided with the combination of electric heaters and heat recovery units. Water is evaporated with a heat pump. Excess heat is stored to be used during electrolysis. Red represents the flow of H_2, blue represents the flow of H_2O, purple represents the mixture (H_2 and H_2O) and the green represents the flow of air. The corresponding molar-flow rates and temperature is presented in table 13 in appendix B.1 for each part of the BoP.

The use of an electrically driven heat pump could increase the performance of the system. Very high-temperature heat pumps (VHTHP) release heat at temperatures above 100 °C and can op-

erate with ambient temperature heat sources [48]. With the utilization factor U_f= 0.8 during both SOFC and SOE heat is removed within the condenser which provides a high-temperature heat source. Heat pumps can operate more efficiently if the temperate difference between evaporation and condensation is small. The efficiency or coefficient of performance (COP) is used to investigate the performance of the heat pump. The COP is calculated by the heat output and the input.

$$COP_{\text{heating}} = \frac{\dot{Q}_{\text{H}}}{\dot{Q}_{\text{H}} - \dot{Q}_{\text{C}}} \tag{1}$$

Where $\dot{Q}_{\text{H}}$ - $\dot{Q}_{\text{C}}$ is equal to the additional power input. The maximum theoretical performance of a heat pump is calculated by the Carnot Efficiency.

$$COP_{\text{heating}} = \frac{T_{\text{H}}}{T_{\text{H}} - T_{\text{C}}} \tag{2}$$

A COP of 6.1 has been achieved using water as a refrigerant with an evaporation temperature of 85 °C and condensation temperature of 117 °C [49]. Tveit et al. [50] presents a series of heat pumps generating steam at 10 bar and a temperature of 184 °C with a source of 80-90 °C.
Equation (2) shows that the temperature of the heat source is an important factor for the performance of the heat pump. With the heat extracted from the condensation of steam. Therefore a small temperature difference between the flow of condensing steam and the cooling fluid is desired. The condensation is theoretically possible at a small temperature difference. The use of a logarithmic mean temperature difference (LMTD) of 9.5 °C is used for condenser for a power plant [51]. The temperature of the lower reservoir heat pump is desired to be as high as possible. However, the temperature of the lower reservoir is bound to at least two heat exchanges, $T_{con} > T_{cool} > T_{storage} > T_C$, where the storage might be used as the low-temperature reservoir A more detailed description of the chosen type of heat pump and the order of the heat pump and cooling is presented in appendix B.2.

The thermal energy storage can be implemented to store the excessive heat of condensation not directly used by the heat pump. Two forms of TES are considered, sensible heat and latent heat storage. Sensible heat storage can be a cost-effective method of storing heat. The drawbacks of sensible heat are the energy density and thermal stability during discharging [43]. Water is a solution for storing energy at the required range of temperature, especially for temperatures below 100 °C [52]. The use of sensible heat storage gives additional design freedom since the temperature of storage is variable. Another possibility is the use of latent heat storage. It is advantageous that these materials have a higher energy density [52]. The major drawback of latent heat storage is the low thermal conductivity of the phase change materials used, which influences the response time of the TES. However, the charge and discharging can be improved by the use of heat transfer enhancing methods [53]. The response time of heat-pumps is in general much quicker than the response time of the heat storage [54]. However, MacArthur [55] reports a time response of 5 minutes until the heat flux of the TES reaches a steady-state.

3.4 Concept 4: Integrated cooling and heat storage

In this section, the fourth concept is described. The generated heat within the stack during SOFC is partly lost due to temperature differences required within the heat recovery units. The combination of a large airflow and these temperature differences result in high losses of heat. Furthermore, this loss of energy could potentially be utilized for pre-heating of the air and fuel flows during electrolysis. To transfer the heat over time heat storage should be implemented. The stored heat could then be used during electrolysis where additional heat is expected to be required.

Besides the use of TES, it is investigated whether the amount of air used for cooling can be reduced during SOFC mode. The large airflow for cooling affects the required size of the heat exchangers as the air must be heated to the operating range of the RSOC. By using different cooling techniques, it is possible to extract high-temperature heat from the RSOC and reduce the size of the heat exchangers. The cooling techniques are shown in section 2.6. Since air is not used as the main component of the cooling the airflow could be reduced to the stoichiometrically required flow rate of air. For air, the size of heat recovery units could thus be reduced. The expected size of the heat exchanger is approximately four times smaller, based on the largest air flows identified, as shown in table 14. For this purpose heat pipes will be used in this concept. Which could be used as a closed environment for cooling. Therefore the coolant does not have to be cooled to ambient temperatures for each cycle. Secondly, more of the heat recovered during SOFC mode could be stored and utilized during SOE mode. This setup with a separate flow for cooling allows for more high-quality heat to be stored.

The recovered heat is subdivided into two different thermal energy storages. Firstly, the heat stored for heating the fuel and air flows should be above 700°C. Which is shown in figure 5a as the A section of the HT storage. It is expected that heat recovered during SOFC exceeds the additional heat required during SOE. Therefore, TES can be used to replace the electrical heaters. The second part of the TES is the heat stored for the evaporation of water. The heat provided during SOFC mode is sufficient for the evaporation. However, during electrolysis additional heat is required. The heat stored for the evaporation of water should be stored between 100 and 700°C. The TES is denoted as section B of the heat storage in figure 5a. With a heat transfer fluid (HTF) used within the heat pipes operating at 700 - 750°C all heat generated by the SOFC could be stored. The setup for this concept is shown in figures 5a and 5b for SOE and SOFC respectively.

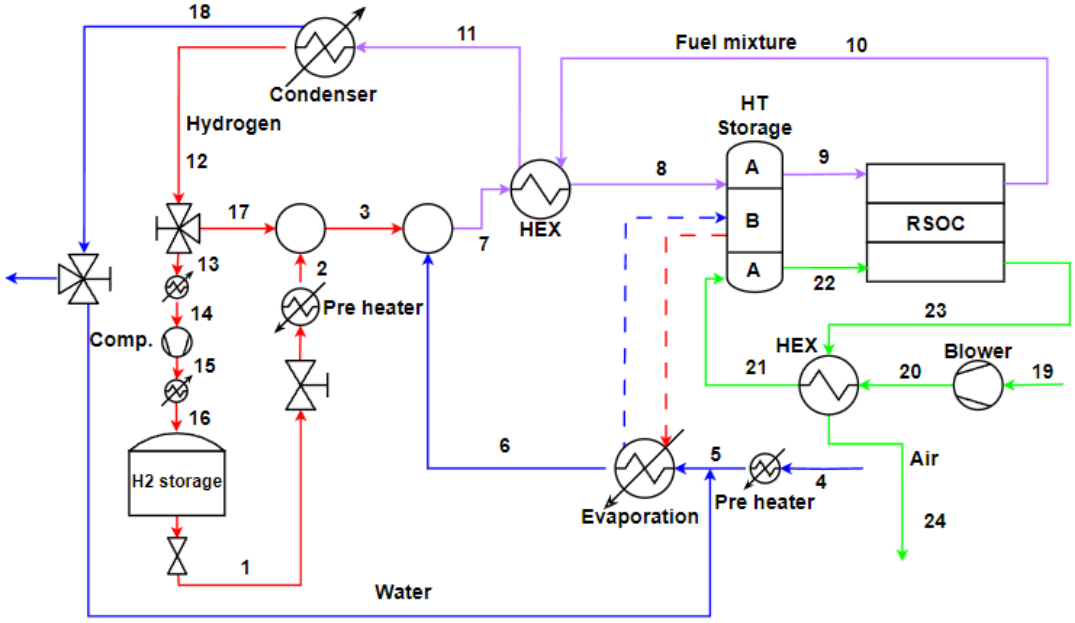

(a) Concept 4 in SOEC mode, the heat is provided with the combination of electric heaters and heat recovery units. Water is evaporated with a heat exchanger. Heat is provided during electrolysis from the heat storage.

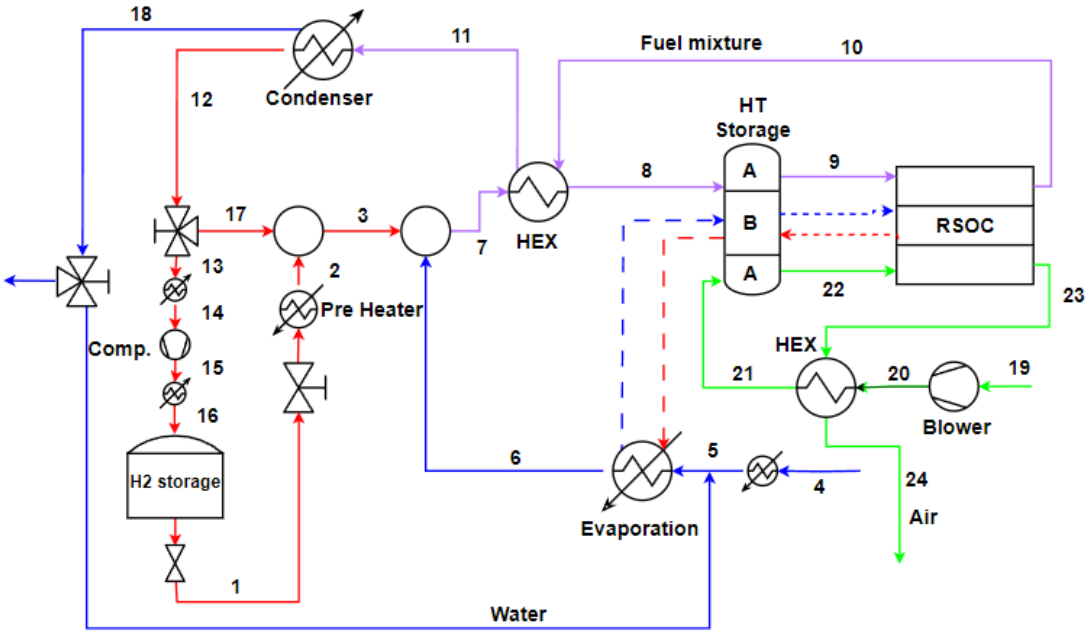

(b) Concept 4 in SOFC mode, the heat is provided with the combination of electric heaters and heat recovery units. During SOFC mode the heat-storage is charged.

Figure 5: Schematic overview of concept 4, Red represents the flow of H_2, blue represents the flow of H_2O, purple represents the mixture (H_2 and H_2O) and green represents the flow of air. The corresponding molar-flow rates and temperature is presented in table 14 in appendix B.1 for each part of the BoP.

The temperatures for the steady state in both electrolysis and fuel cell mode are listed in table 14, appendix B.1. The use of heat storage to replace electrical heaters for heating the air and fuel flows to 700 °C is required to satisfy $T_H > T_{HTF} > T_{st} > T_C$. Where T_H is the temperature of the stack which has a maximum of 750 °C. Where T_{HTF} is the heat transfer fluid, the cooling of the stack can only be done up to the temperature of the HTF. The small temperature difference between the inlet temperature and the stack temperature requires a TES with small temperature fluctuations. Therefore, the use of the latent heat of phase change materials is investigated [56]. The PCM investigated are required to have a change in their phase between 700 - 750 °C.

Table 3: PCM material 700 - 750 °C [56]

Material	Melting Temperature (°C)	Δh (J/g)
LiF–30MgF2	728	520
NaF–23CaF2–12MgF2	743	568
LiF–33MgF2	746	947
LiF–13KF–13MgF2	749	860

The second heat storage is used for the heat required for evaporation. The TES used for evaporation is expected to be larger compared to the TES used for heating the air/fuel stream. However, the temperature difference between the SOFC and the evaporation temperature allows for a variety of heat storage techniques. Including sensible heat storage where it is possible to leverage the large temperature difference between the SOFC and evaporation temperatures.

3.5 Concept 5: Metal hydride storage of hydrogen

In this section, the fifth concept is described. This concept investigates the possibility of storing the excess heat generated during SOFC mode using thermochemical reactions to store and release heat. For low-temperature thermal energy storage, two forms of thermochemical reactions are considered. These are salt hydrates which react with H_2O and metal hydrides which react with H_2. This could potentially remove the requirement for the condenser and separator. Metal hydrides are applicable to store hydrogen since the metal hydrides react with hydrogen. Therefore, the use of salt hydrates and metal hydrides is investigated for possible improvements concerning evaporation and storage. The reaction of the salt hydrates and metal hydrides is in general described as:

$$A(s) + B(g) \longleftrightarrow AB(s) + \Delta E \tag{3}$$

Salt hydrates

Salt hydrates react with H_2O and are a possibility to store and release heat.

$$SrBr_2 + H_2O = SrBr_2H_2O + 72\,kJmol^{-1} \tag{4}$$

The use of salt hydrates does not have an advantage over the use of condensation and evaporation based on an integrated TES solution. It can be expected that salt hydrates release energy during fuel cell operation and require energy for dissociation during electrolysis. However, the heat required to release the H_2O is supplied during SOE and that reduces the effect of the thermochemical heat storage capacity of the salt hydrate.

Metal hydride

Metal hydrides are considered for the storage of hydrogen, primarily for mobility applications due to their high energy storage densities. However, the use of metal hydrides could result in a significant improvement of the balance-of-plant [14]. Metal hydride storage has a specific advantage over compressed hydrogen storage. Since the reaction is exothermic for the absorption of hydrogen which results in a release of heat during electrolysis. Therefore, metal hydrides could store the hydrogen and provide heat for the generation of steam. During SOFC mode the metal hydride operates in an endothermic process. Where the process within the SOFC is exothermic. The heat released within the SOFC could be used for the release of the hydrogen from the metal hydride storage. For this concept, MgH_2 is used due to the relatively low cost [14]. The reaction of magnesium and hydrogen is described by [57]:

$$Mg + H_2 \rightarrow MgH_2 + 75\,kJmol^{-1} \tag{5}$$

MgH_2 is a very active material which self-ignites when exposed to air and does react with water if it comes in contact [58]. Additional disadvantages are the slow kinetics and high energy requirement for discharge [59]. The advantages of magnesium hydrides are low cost and good reversibility. Besides the release of heat during electrolysis metal hydrides based on MgH_2 could provide hydrogen storage by the chemical reaction. Which allows the storage of hydrogen at lower pressures. In contrast to previous concepts where hydrogen is stored at a pressure of 350 bar. This allows for a reduction of the consumed power required for the compression of hydrogen. To be able to maximize the efficiency the metal hydride must satisfy:

$$R_{\mathrm{H_2}} \Delta E \leq \dot{Q}_{\mathrm{SOFC}} \tag{6}$$

If equation (6) is satisfied, the release of hydrogen does not require additional energy. Depending on the thermal management of the RSOC the available heat might not be sufficient. For low current densities, the losses within the SOFC are low. Which results in less heat to be generated by the SOFC.

During electrolysis heat is released during the process of charging the hydrogen storage. This could be used for the evaporation of water to increase the efficiency of the system. Assuming $R_{H_2} = R_{H_2O}$ the following expression has to be satisfied:

$$\Delta E \geq h_{\mathrm{fg}} * R_{\mathrm{H_2O}} \tag{7}$$

ΔE is the heat release of reaction and h_{fg} is the latent heat of water at atmospheric pressure. Since the MgH_2 reacts with water, the exhaust gasses are to be condensed and separated before entering the storage. The flow of water is heated in a separate system to prevent the water from coming in contact with the metal hydride. The heat transferred between RSOC and metal hydride is represented with the dotted line in figure 6b.

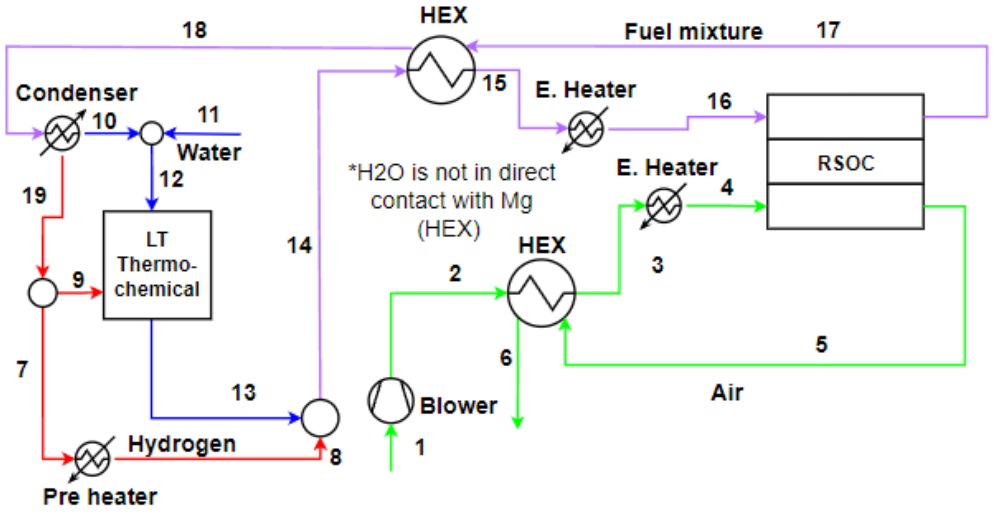

(a) Concept 5 in SOEC mode, metal hydrides react with hydrogen in an exothermic reaction. The heat generated is sufficient for the evaporation of water.

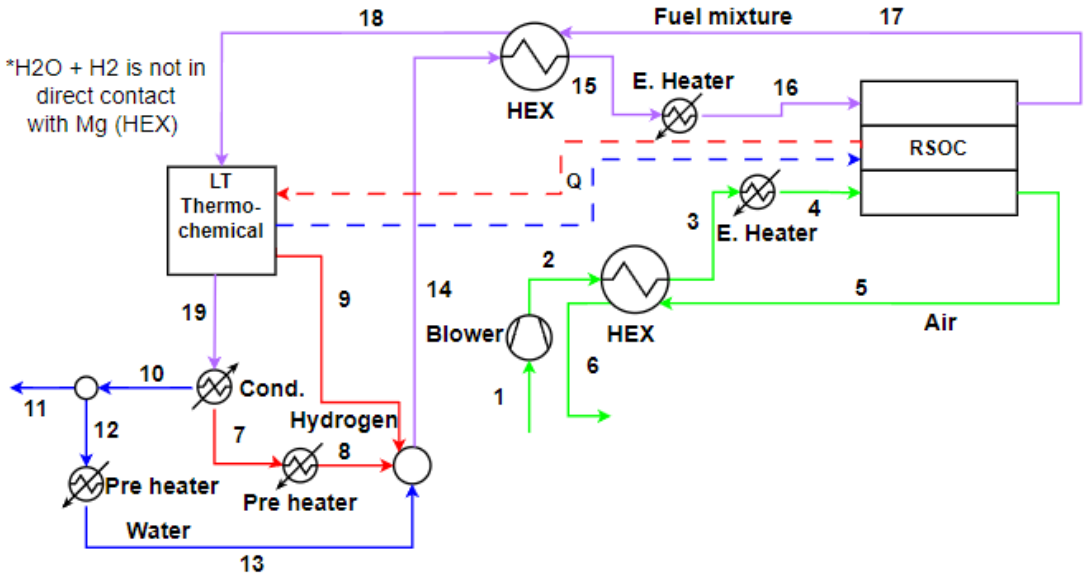

(b) Concept 5 in SOFC mode, during SOFC heat is required to dislocate the hydrogen from the metal hydride storage. The heat is supplied by the exothermic reaction of the SOFC.

Figure 6: Schematic overview of concept 5, Red represents the flow of H_2, blue represents the flow of H_2O, purple represents the mixture (H_2 and H_2O) and green represents the flow of air. The corresponding molar-flow rates and temperature is presented in table 15 in appendix B.1 for each part of the BoP.

3.6 Comparison of concepts

The five concepts have different approaches to the thermal management of the balance-of-plant. The concepts of the BoP have been investigated in steady-state and dynamic behaviour, of which the results are presented in chapter 5. Furthermore, the economic viability is investigated in the techno-economic analysis which is presented in chapter 6. Each of the concepts has advantages and disadvantages, which are presented below.

1. The electricity consumption of concept 1 is expected to be substantial due to the use of the electric heater to heat the air and fuel flow.

2. Concept 2 is expected to be an improvement compared to concept 1. The use of heat recovery units reduces the electricity consumption of the electrical heaters. The concept is slightly more complex as it increases the number of components. The combined size of the electric heaters and heat recovery units is expected to be approximately equal to the size of the electric heaters in concept 1.

3. Compared to concept 2, the third concept has the advantage of increased efficiency due to the reduction of external energy required for the evaporation of water. The concept is functioning similarly to concept 2. Disadvantages are the increasing complexity of the system and higher initial costs due to additional components required.

4. A RSOC which uses heat pipes for cooling removes the need for cooling with the airflow. This reduces the size of the heat recovery units to correlate to the stoichiometrically required flow for the electrolysis process. The separate cooling allows for heat to be stored at higher quality. In previous concepts, the quality of the heat is degraded by the heat recovery units. The expected disadvantage of this concept is the high cost of the adjusted RSOC stack, which is not quantified in the literature.

5. Metal hydrides are a promising technique for hydrogen storage. This allows the removal of the compressor and the electric boiler. However, the cost of metal hydride is substantially higher compared to the pressurized storage of hydrogen.

With these five concepts, the impact of different solutions to improve the efficiency of the RSOC balance-of-plant can be investigated. The dynamic model is described in section chapter4.

Based on the finding of the steady-state analysis it is decided to not dynamically model concept 1. Because it is judged to be inefficient compared to the other concepts. The required electricity input for the electric heaters exceeds SOFC electricity output. The electricity generated by the SOFC is thus all consumed by the BoP, see 5.1. The fifth concept is found to be an efficient solution as will be shown in section 5.1. However, the cost of metal hydride is high compared to pressurized hydrogen storage. The hydrogen storage is connected to a wind farm. The size of the storage is determined by seasonal fluctuations in energy production. The combination

of the large size of the storage and the high cost of metal hydrides make concept 5 economically unfeasible. Therefore concept 5 is not dynamically modelled. The comparison between the storage techniques can be found in the techno-economic analysis presented in chapter 6.2. The dynamic model used for concepts 2 to 4 is presented in 4. The results of the different concepts are presented in section 5.2.

4 Modelling RSOC and BoP

This chapter describes the model used for the RSOC and the auxiliary components of the balance-of-plant. These include pumps, blowers, compressors, heat exchangers, condensers and the evaporator. The dynamic model is used to find the overall efficiency of the proposed concepts. Another aim of the model is to determine the allowable response time for the components, based on the ability to cope with fluctuations in the load. Furthermore, the dynamic model is used to determine the size of the heat storage and the capacity of the different components. The basis of the different concepts is similar. Therefore, the second concept is used as a basis for the dynamic model. For example concept 4, the components are similar except for the heat storage. Concept 3 requires an additional model for the heat pump. This chapter will start with a description of the assumptions made to model the stack and other components in the BoP. Furthermore, the assumptions regarding the inputs of the system are described, see figure 7.

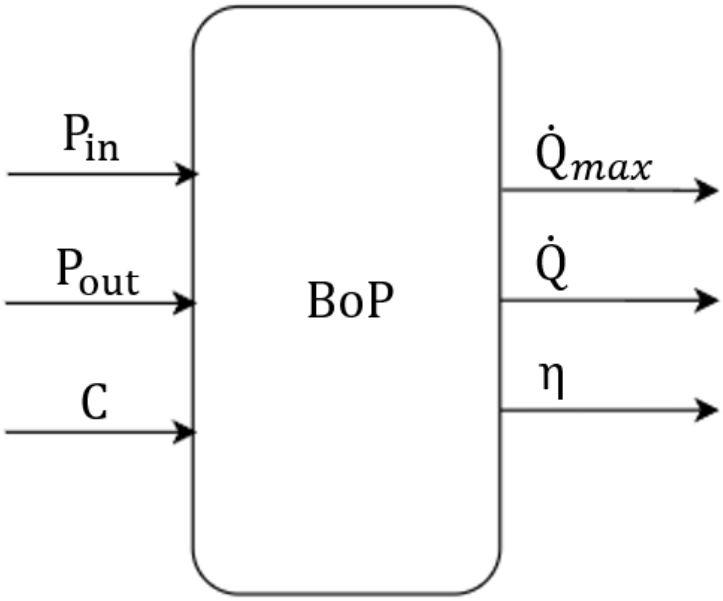

Figure 7: The inputs of the model and respective output. P_{in} and P_{out} are the supplied electricity from the wind and the load demand of the grid, C are parameters such as ambient temperature and composition of the streams. Outputs are the different energy consumption of components ($\dot{Q}$), the maximum energy consumption of each component ($\dot{Q}_{max}$) and the efficiency of the system (η).

4.1 Model assumptions

The following assumption has been made for modelling the RSOC stack and the BOP.

1. The stack is represented as one single cell. The stack's performance can be characterized by a single cell [60]. Udagawa et al. state that [61] a common method used to represent large SOC stacks is to use a small cell with proper boundary conditions. It is assumed the

modelled cell is at the centre of a large stack, so there are no effects of the surrounding [7, 61].

2. Due to computational time, a 0D model of the stack is used. The stack is modelled as a lumped model for the stack, which shows to be accurate [62]. Resulting in constant conditions over the stack. However, since temperature and flow rates are of interest, the air and fuel channels are modelled as 1D-model. Where it is assumed that air and fuel outlet temperatures are equal [7].

3. Duration of charge is assumed to be equal to discharging [7]. The kinetics of the thermal chemical process is faster than the temperature change of the stack [13].

4. The stack is perfectly insulated, so the losses to the surroundings due to convection and radiation are disregarded [30]. The pressure drop within the stack is assumed to be 0.05 kPa [63].

5. Temperature of air and fuel does not exceed the temperature of the stack $T_{air} \leq T_{stack}$.

6. The cooling of the stack is based on Newton's Law of cooling [13], the thermal control strategy regarding the removal from the stack is done by fuel and the airflow. The outlet gasses for both SOE and SOFC consist of hydrogen gas and steam. The air is the main contributor to the cooling of the stack. For thermal management, the flow of air is adjusted based on the stack operational temperature and the heat flux from the stack to the fluids.

7. Inside the solid oxide cell it is assumed that the gas in both the air and fuel side of the cell are of sufficiently high temperatures and low pressure. So that the behaviour of the gas can be assumed to be described by the ideal gas law.

8. Heat exchangers are assumed to be perfectly insulated, and the pressure drop is assumed to be zero. The heat exchangers are modelled as a zero-capacity model. The pressure drop in the heat exchanger is neglected.

9. The mechanical components and electric heaters are assumed to be faster than the stack and are therefore modelled as quasi-steady state components.

4.1.1 Model inputs

The dynamic model is required to be compatible with data regarding the power generation of wind turbines and the demand of a grid. The demand of the grid is assumed to be a constant load. Therefore the model's input is based on data from the power production of the wind park at IJmuiden provided by TNO.

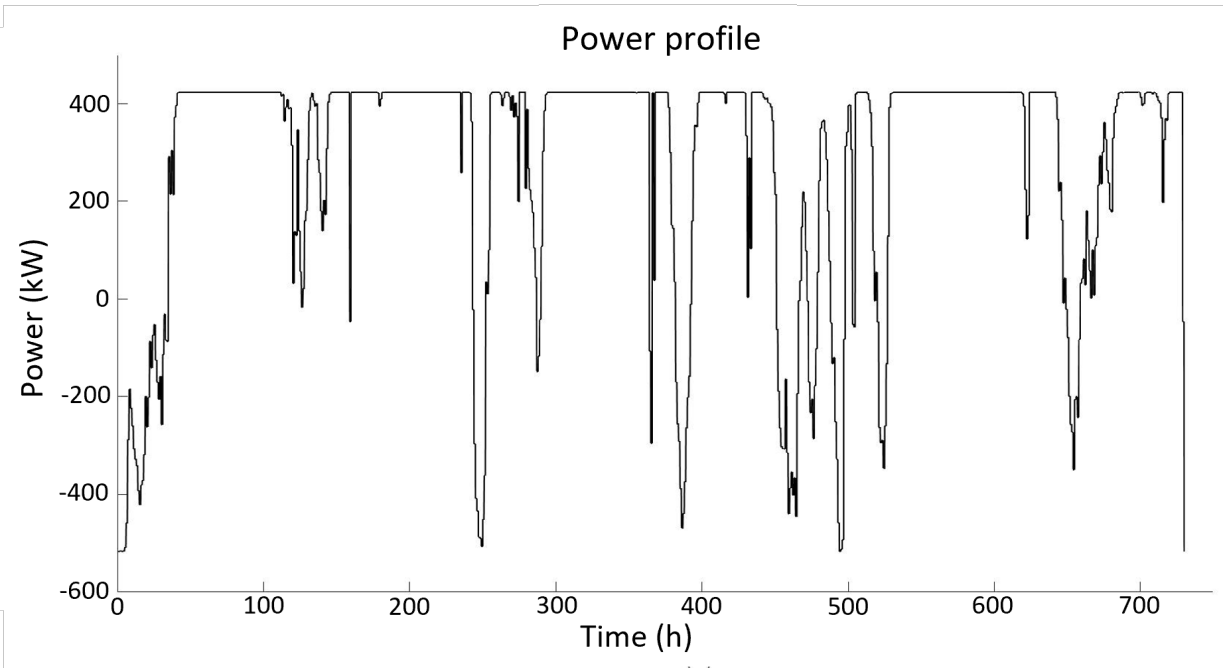

Figure 8: The required supply and demand of the RSOC based on the power production of the wind park and a base load, January 2008.

The model uses the wind park's power provided to the grid and a base load for power consumption. The power provided by the RSOC is calculated as follows:

$$P = P_{\text{wp}} - P_{\text{bl}} \tag{8}$$

P= Power of the RSOC, P_{wp} = power provided by the wind park and P_{bl} = Power consumed by the grid. The input data from the wind park is measurements over one-hour intervals. Resulting in power distribution for January 2008 as shown in figure 8.

4.1.2 Dynamic response time

This section discusses the response time of the different components. The limitation given to the current density change reduces the system's ability to cope with the variations in the supply and demand of electricity.

The goal of the RSOC is to operate at maximum efficiency. It is assumed that information like weather prediction and historical data on the demand of the grid are not available. This requires a quick response time for all components within the BoP. It is assumed the response time of the balance-of-plant should be faster than the RSOC stack. The response time is determined by the ramp rate of the current within the stack. Motylinski et al. report an increase/decrease rate of 5 A min^{-1} [13] as a maximum ramp rate for a 100x100 mm cell. Commonly used for SOFC and SOE, like the boiler, compressor and heat recovery units are found to have a response faster than the stack itself or are limited to start-up and shutdown of the components. However, the

start-up and shutdown of the system are assumed not to be prevalent within the scope/goal of the model. The heat recovery units remain at similar operating temperatures for SOE and SOFC. Furthermore, the response times of the mechanical components like the blower and compressor are assumed to be faster than the stack.

Concepts 3 till 5 propose a system which uses nonstandard components for both SOE and SOFC namely: A heat pump, heat storage and metal hydrides. The three groups of heat storage are sensible, latent and thermochemical heat storage. Sensible heat storage has the fastest response time. The response of the latent heat storage depends on the thermal conductivity [64].

TES System	Response time	Source
Sensible	2.5 [min]	[39, 40]
PCM	5 - 20 [min]	[41]
Thermochemical	10 - 30 [min]	[42]

Table 4: Response time TES

The metal hydride is assumed to be equal to the response time of thermochemical heat storage. The range of the response time of metal hydrides is rather large, shown in table 5. Where most of the are approximately papers report response times of 10 - 30 min for magnesium-based hydride [59].

TES System	Response time	Source
Heat pump	15 [min]	[55]
Metal hydride	0.45 - 1440 [min]	[59]

Table 5: Response time for replacement of electric boiler.

Electric boilers have sufficiently fast ramp-up speeds [65]. Therefore it is assumed electric boilers can cope with changes in the demand of the RSOC. Similarly, heat pumps are found to have fast response time [66]. However, these numbers do not include the time for the subsequent evaporation of water [55]. The components could potentially slow down the response of the system. However, it cannot be concluded that either the methods for evaporation or the thermal energy storage are increasing the response time. Therefore, the electric boilers and heat pump are modelled as quasi-steady state.

4.2 Electrochemical model

The model used to describe the processes within the cell is described as a 0D model. Firstly, the electrochemical model of the stack is modelled as a 0D model. Secondly, the heat and mass transfer within the stack and channels is modelled. The RSOC stack is developed as a black box model to determine the output in terms of temperature, flow rates and power. The electrochem-

ical model relates the cell voltage and the current density.
The modelling convention regarding the current is that the current is positive during SOFC and negative in SOEC mode. Furthermore, the voltage applied during electrolysis is equal to the thermoneutral voltage. The thermoneutral voltage is the voltage at which the temperature does not change.

4.2.1 Nernst equation

The open circuit voltage (OCV) is the voltage when no external load is applied. To determine the OCV, the Gibbs potential and Nernst potential are used. The Nernst potential is used to calculate the reversible voltage. The Nernst equation is used to calculate the cell potential for non-standard cell conditions. The standard cell potential is based on the Gibbs free energy.

$$H_2O \rightarrow H_2 + \frac{1}{2}O_2 \tag{9}$$

And for the SOFC operation:

$$H_2 + \frac{1}{2}O_2 \rightarrow H_2O \tag{10}$$

The thermodynamics of the cell can be described with equation (11). This shows that according to Gibbs's free energy equation, the temperature affects the required energy to be supplied as electricity.

$$\Delta H = \Delta G + T\Delta S \tag{11}$$

Where ΔH is the enthalpy of the formation of water, ΔG is Gibb's free energy, T is the temperature, and ΔS is the entropy difference. The entropy calculation is described in appendix C.1. The reaction enthalpy can be determined using Kirchhoff's Law for the enthalpy:

$$\Delta H_{\mathrm{f}}(T) = \Delta H^0(298K) + \int_{298\ \mathrm{K}}^{T} \Delta c_{\mathrm{p}} dT \tag{12}$$

At 25°C the ΔH is 285 kJ/mol for liquid water and 241 kJ/mol for steam. For the reaction during SOE the thermoneutral voltage is used. The thermal neutral voltage is based on the enthalpy of formation. The thermoneutral voltage can be determined using the reaction enthalpy:

$$U_{\mathrm{th}} = \frac{\Delta H}{2F} \tag{13}$$

The Gibbs potential is the open circuit voltage under standard conditions.

$$E_0 = \frac{\Delta G}{2F} \tag{14}$$

The OCV is calculated using the Nernst equation which accounts for the composition of the flow and pressure. [9–11].

$$E_{\mathrm{Nernst}} = E_0 + \frac{RT}{2F} ln\left(\frac{x_{\mathrm{H_2}}\sqrt{x_{\mathrm{O_2}}}}{x_{\mathrm{H_2O}}}\right) + \frac{RT}{2F} ln\left(\frac{P_{\mathrm{A}}}{P_{\mathrm{amb}}}\right) \tag{15}$$

4.2.2 Area specific resistance

The voltage of the cell is higher than the Nernst potential during electrolysis and lower during fuel cell mode due to the ohmic, activation and concentration over-potentials.

$$E_{\text{cell}} = E_{\text{Nernst}} - \eta_{\text{ohm}} - \eta_{\text{act}} - \eta_{\text{conc}} \tag{16}$$

Where η_{ohm} is the ohmic over-potential, η_{act} is the activation over-potential and η_{conc} the concentration over-potential [10]. The U-j curve for the electrolysis and fuel cell is for simplicity approximated as a straight line. Modelling of the U-j curve using a simplified model substantially reduces the computational time and can thus give more versatility to the model. The used area-specific resistance (ASR) is assumed to be constant for SOE, SOFC and temperature for the model.

$$ASR = r_{\text{ohm}} + r_{\text{act}} + r_{\text{conc}} \tag{17}$$

The area-specific resistance includes the ohmic, activation and concentration overpotentials. The ASR could be determined by experimental results. The Nernst potential and ASR show the relation between the current and voltage of a cell.

$$E_{\text{cell}} = E_{\text{Nernst}} - (ASR)i \tag{18}$$

Where i is the current density, ASR is the area-specific resistance. Figure 9 shows the U-j curve with an ASR of 0.3 Ω/cm^2, with composition as shown in equation (33) for SOE and for the SOFC composition as shown in equation (32).

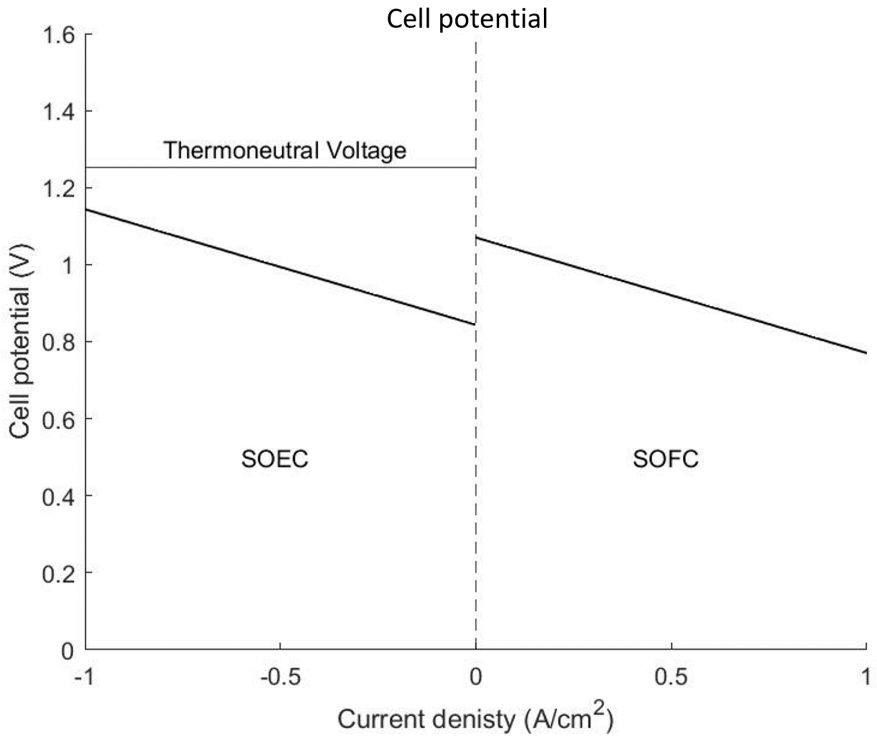

Figure 9: Cell potentials

4.2.3 Hydrogen to Power

The integration of the model with an external power source requires the model to convert power input and outputs to current and voltage. Therefore the relationship between power and hydrogen consumption/production is determined. The reaction rate of the production and consumption of hydrogen is dependent on the current. The relation between current and hydrogen production and consumption is described by Faraday's Law of electrolysis [67].

$$R_{\mathrm{H_2}} = \frac{I}{nF} \tag{19}$$

Where n is the number of electrons transferred in the reaction (for water electrolysis n = 2), I is the current, F is Faraday's constant and $R_{\mathrm{H_2}}$ is the rate of reaction. The relation between the current density and voltage is determined in equation (18).
The relation between the power and hydrogen consumption and production is derived from the relation between the power which is a function of voltage and current.

$$P = IV \tag{20}$$

Dividing both sides of equation (20) with the area of the cell results in a relation between the power density and current density.

$$p = iV \tag{21}$$

Where p is the power density, i the current density and V is the voltage. Substituting the calculation to determine the cell potential, equation (18), in equation (21) the relation becomes:

$$p = i(E_{\mathrm{Nernst}} - (ASR)i) \tag{22}$$

Where p = P/Area ($\mathrm{W/cm^2}$) and i = I/Area ($\mathrm{A/cm^2}$). Note for SOE the voltage is determined by the thermoneutral voltage.

$$E_{\mathrm{cell}} = \frac{\Delta H_{(g)}}{2F} \tag{23}$$

Substituting equations (24) and (23) describe the power consumption during electrolysis.

$$p = iE_{\mathrm{cell}} \tag{24}$$

4.2.4 Molar balance

The molar balance is used to compute the composition of the air and fuel in the channels of the RSOC. The molar balance is used to compute the exhaust composition of the air and fuel. The ratio of the reaction between the components is defined as:

$$R_{\mathrm{H_2}} = -R_{\mathrm{H_2O}} = 2R_{\mathrm{O_2}} \tag{25}$$

Where the rate of conversion of R_{H_2} is calculated as shown in equation (19). The rate of production and consumption of H_2 is dependent on the current as described by Faraday's Law of electrolysis, shown in equation (19). The molar balance for the fuel channel is defined as:

$$\frac{dn_{\text{fuel}}}{dt} = \dot{n}_{\text{fuel,out}} - \dot{n}_{\text{fuel,in}} \tag{26}$$

The total molar flow consists of the molar flow of H_2 and the molar flow of H_2O. Where $\dot{n}$ is the molar flow entering and leaving. The n_{fuel} represents the number of moles within the fuel channel of the RSOC.

$$\dot{n}_{\text{fuel}} = \dot{n}_{H_2} + \dot{n}_{H_2O} \tag{27}$$

Where $\dot{n}_{H_2}$ and $\dot{n}_{H_2O}$ are flow of the number of moles of H_2 and H_2O respectively. The outlet stream $\dot{n}_{\text{fuel,out}}$ is determined based on equations (19), (34), (35) and (36). The number of moles of H_2 and H_2O are determined using the rate of production of hydrogen R_{H_2} and the relation between the reaction rates R_{H_2} and R_{H_2O} shown equation (25). The change of the hydrogen within the fuel channel is determined by the conservation of mass.

$$\frac{d(x_{H_2} n_{\text{fuel}})}{dt} = \dot{n}_{\text{fuel,in}} x_{H_2,\text{in}} - \dot{n}_{\text{fuel,out}} x_{H_2,\text{in}} - R_{H_2} \tag{28}$$

Similarly the conservation of steam within the fuel channel.

$$\frac{d(x_{H_2O} n_{\text{fuel}})}{dt} = \dot{n}_{\text{fuel,in}} x_{H_2O,\text{in}} - \dot{n}_{\text{fuel,out}} x_{H_2O,\text{in}} - R_{H_2O} \tag{29}$$

The molar balance for the air side is defined as:

$$\frac{dn_{\text{air}}}{dt} = \dot{n}_{\text{air,in}} - \dot{n}_{\text{air,out}} - R_{O_2} \tag{30}$$

The restrictions regarding the oxygen content in the SOC and BoP requires management of the air flow. The oxygen content within the air channel is determined as:

$$\frac{d(x_{O_2} n_{\text{air}})}{dt} = \dot{n}_{\text{air,in}} x_{O_2,\text{in}} - \dot{n}_{\text{air,out}} x_{O_2,\text{in}} - R_{O_2} \tag{31}$$

It is assumed the fraction of the oxygen content increases by electrolysis linearly over the length of the channel. For the model the two situations for fuel composition are regarded. Firstly. a fuel composition for operations during SOFC mode and secondly during SOE mode. The composition used during fuel cell mode is:

$$x_{\text{SOFC,in}} = \begin{cases} x_{H_2} = 0.95 \\ x_{H_2O} = 0.05 \end{cases} \tag{32}$$

During SOE, the inlet composition changes to increase the fraction of steam within the cell.

$$x_{\text{SOE,in}} = \begin{cases} x_{\text{H}_2\text{O}} = 0.9 \\ x_{\text{H}_2} = 0.1 \end{cases} \tag{33}$$

When the RSOC converts hydrogen and oxygen into water and electricity or in the reverse direction, the composition changes. However, the cell is assumed not to be able to convert all steam or hydrogen. Therefore the utilization factor is used to determine the total flow of fuel for each of the modes.

$$U_{\text{f}} = \frac{R_i}{\dot{n}_i} \tag{34}$$

For this project, the fuel utilization factor is assumed to be constant. The utilization factor (U_f) is set as, U_f = 0.8.

$$SOFC: \qquad x_{\text{H}_2,\text{out}} = 1 - x_{\text{H}_2} U_{\text{f}} - x_{\text{H}_2\text{O}} \tag{35}$$

$$SOE: \qquad x_{\text{H}_2\text{O},\text{out}} = 1 - x_{\text{H}_2\text{O}} U_{\text{f}} - x_{H_2} \tag{36}$$

The inlet molar fractions of hydrogen and steam and a utilization factor of 0.8 results in a composition at the outlet of the SOFC as:

$$x_{\text{SOFC,out}} = \begin{cases} x_{\text{H}_2} = 0.19 \\ x_{\text{H}_2\text{O}} = 0.81 \end{cases} \tag{37}$$

For SOE, the composition after the SOC changed to:

$$x_{\text{SOE,out}} = \begin{cases} x_{\text{H}_2\text{O}} = 0.18 \\ x_{\text{H}_2} = 0.82 \end{cases} \tag{38}$$

4.2.5 Energy balance

The energy balance is used to determine the effect of heat generation and heat consumption. Since the model should obey the law of energy conservation, the temperatures of the exhaust gasses can be determined.

$$dH = dU + VdP + PdV \tag{39}$$

The energy balance over the fuel channel is:

$$\frac{d(n_{\text{fuel}} h_{\text{fuel}})}{dt} = \dot{n}_{\text{fuel}} h_{\text{fuel,in}} - \dot{n}_{\text{fuel}} h_{\text{fuel,out}} + \Delta\dot{Q}_{\text{PEN,fuel}} + \Delta\dot{Q}_{\text{int,fuel}} \tag{40}$$

Where $\Delta Q_{\text{PEN,fuel}}$ and $\Delta Q_{\text{int,fuel}}$ are the heat fluxes from the positive-electrolyte-negative (PEN) and interconnect to the fuel channel. Similarly the energy balance of the air channel:

$$\frac{d(n_{\text{air}} h_{\text{air}})}{dt} = \dot{n}_{\text{air}} h_{\text{air}} - \dot{n}_{\text{air}} h_{\text{air}} + \Delta\dot{Q}_{\text{PEN,air}} + \Delta\dot{Q}_{\text{int,air}} \tag{41}$$

The heat transfer from and to the air channel from the PEN structure is defined $\Delta Q_{PEN,air}$. $\Delta Q_{int,air}$ is the heat-flux between the air channel and the interconnect. The temperature change of the PEN is described by the conservation of energy:

$$\dot{n}c_p\frac{dT}{dt} = \Delta H_f R_{H_2} - V_{cell}i - \dot{Q}_{PEN,fuel} - \dot{Q}_{PEN,air} \tag{42}$$

The energy conservation for the interconnect is defined as:

$$\dot{n}c_p\frac{dT}{dt} = \dot{Q}_{int,fuel} + \dot{Q}_{int,air} \tag{43}$$

For the model, the following assumptions regarding the temperature distribution and heat fluxes are made. Within the cell the temperature of the PEN structure and interconnect are assumed to be equal. Therefore, the heat exchange between the interconnect and PEN structure through radiation could be disregarded [30]. The energy balance within the air channel follows from:

$$\dot{n}c_p\frac{\partial T}{\partial t} = \Delta\dot{Q} - \dot{n}c_p\frac{\partial T}{\partial\frac{x}{L}} + R_{O_2}h_{O_2} \tag{44}$$

Similar to the air channel the temperature of the fuel side can be determined. With the assumption $\dot{n}_{fuel,in} = \dot{n}_{fuel,out}$ the energy balance can be written as:

$$\dot{n}c_p\frac{\partial T}{\partial t} = \Delta\dot{Q} - \dot{n}\frac{\partial h}{\partial\frac{x}{L}} \tag{45}$$

Where h is the energy contained within the fuel.

4.2.6 Thermal management of RSOC

The thermal management used for SOE and SOFC is different. The thermal management of the stack during electrolysis is determined by the thermoneutral voltage. The thermoneutral voltage results in a constant temperature within the fuel channel. For modelling isothermal conditions within the PEN and interconnect are assumed [12]. Furthermore, the temperature within the PEN and interconnect is assumed to be equal.

$$T_{PEN}(x,t) = T_{int}(x,t) \tag{46}$$

It is further assumed that there are no heat losses to the environment [68]. Therefore all heat generated and required by the electrochemical reaction is supplied and removed through fuel and air flows. The rate of cooling is assumed to be determined by Newton's Law of cooling [13]. Furthermore, the outlet temperature of the fuel channel is equal to the outlet temperature of the air channel [7, 13, 19]. The model is designed in a way that it calculates the amount of air required to extract the heat released by the PEN during SOFC. And secondly, takes into account the management of the airflow to control the oxygen content. The two possible scenarios SOFC and SOE require different management strategies for the flow and heat. Both SOE and SOFC

have to satisfy two requirements. Firstly, the temperature of the stack should be between 700 - 750 °C. Secondly, the oxygen content within the air channel should not exceed 23.5%.

The heat generated from within the PEN is calculated as:

$$\Delta\dot{Q}_{\text{gen}} = \left(\frac{\Delta H_{(\text{l})}}{2F} - E_{\text{cell}}\right) i \tag{47}$$

Where i is positive during SOFC and negative for SOE. A voltage larger than $\frac{\Delta H_{\text{g}}}{2F}$ during electrolysis results in an exothermic reaction. If the voltage is smaller than $\frac{\Delta H_{\text{g}}}{2F}$ then the SOE process is endothermic.

Fuel cell

The heat released during the fuel cell is partly consumed by the change in composition over the fuel channel. However, the heat generated within the stack is calculated with the enthalpy of the formation of water. However, due to the high temperature, it is assumed to be in the form of steam at the outlet for both SOE and SOFC. The required energy to satisfy the water as steam is:

$$\dot{Q}_{\text{fuel}} = \dot{n}_{\text{fuel}} \left[h_{\text{H}_2} \frac{\partial x_{\text{H}_2}}{\partial\left(\frac{x}{L}\right)} + h_{\text{H}_2\text{O}} \frac{\partial x_{\text{H}_2\text{O}}}{\partial\left(\frac{x}{L}\right)} \right] \tag{48}$$

The remainder of the heat, which corresponds to the Δ $\text{H}_{(\text{g})}$ is distributed over the two channels where it satisfies $\text{T}_{\text{fuel,in}} = \text{T}_{\text{fuel,out}}$.

$$\Delta\dot{Q} = hA(T_{\text{h}} - T_{\text{c}}) \tag{49}$$

Where hA is assumed to be constant. The heat removed by air is determined as:

$$\Delta\dot{Q}_{\text{air}} = \Delta\dot{Q} - \Delta\dot{Q}_{\text{fuel}} \tag{50}$$

The energy balance over the air channel is described as:

$$\dot{n}c_{\text{p}}(T)\frac{\partial T}{\partial t} = \dot{n}_{\text{air}}c_{\text{p}}(T)\frac{\partial T}{\partial\left(\frac{x}{L}\right)} - R_{\text{O}_2}h_{\text{O}_2}(T) - \Delta\dot{Q}_{\text{air}} \tag{51}$$

Similarly the energy balance of the fuel channel:

$$\begin{aligned} \dot{n}c_{\text{p}}\frac{\partial T}{\partial t} &= \dot{n}_{\text{fuel}}c_{\text{p}}(T_{\text{in}} - T_{\text{out}}) + \Delta\dot{Q}_{\text{fuel}} \\ c_{\text{p}} &= x_{\text{H}_2}c_{\text{p,H}_2}(T) + x_{\text{H}_2\text{O}}c_{\text{p,H}_2\text{O}}(T) \end{aligned} \tag{52}$$

The molar flow through the fuel channel is determined by the electrochemical reaction. The molar flow through the air channel is determined according to the boundary conditions regarding the maximum temperature increase of the cell. This is given as $\text{T}_{\text{out}} = \text{T}_{\text{in}} + 50$ °C or equal to the

cell temperature $T_{out} = T_{stack}$. For the electrolysis process, the requirement for the enrichment of the air is taken into account.

The air is used to control the temperature within the stack. The molar flow required of the air is determined as:

$$\Delta\dot{Q}_{air} = \dot{n}_{air} c_p(T) \frac{\partial T}{\partial(\frac{x}{L})} - R_{O_2} h_{O_2}(T) + n c_p(T) \frac{\partial T}{\partial t} \tag{53}$$

The molar flow follows from:

$$\dot{n}_{air} = \frac{\Delta\dot{Q}_{air} + R_{O_2} c_{p,O_2}(T) T_{out} - n c_p(T) \frac{\partial T}{\partial t}}{c_p(T) \frac{\partial T}{\partial(\frac{x}{L})}} \tag{54}$$

Electrolysis
The second condition states that the airflow has to satisfy the maximum oxygen enrichment of $x_{O_2} = 0.235$ at the outlet. This condition is found to be critical for SOE due to the thermoneutral voltage applied.

$$\frac{\dot{n}_{O_2}}{\dot{n}_{air}} = \frac{\dot{n}_{air} x_{O_2} - R_{O_2}}{\dot{n}_{air} - R_{O_2}} \tag{55}$$

The value at the outlet of the RSOC is defined as $x_{O_2,out} = 0.235$.

$$\dot{n}_{air} = \frac{x_{O_2,out} R_{O_2} - R_{O_2}}{x_{O_2,out} - x_{O_2}} \tag{56}$$

Furthermore, the thermoneutral conditions have to be satisfied. Since enthalpy of formation is ΔH_l. This is the energy required for one mole of water to be split into oxygen and hydrogen. Since the thermoneutral voltage for the cell is related to the ΔH_g, additional heat is to be supplied. The additional energy is supplied by the latent heat of steam which is released during the reaction. With the assumptions of a constant temperature for the fuel side of the cell, the required heat to sustain the constant temperature is shown in equation (48).

4.3 Model balance-of-plant

This section describes the models used for components besides the electrochemical model of the RSOC.

4.3.1 Heat exchanger

This section describes the models used for the heat exchangers in heat recovery units. For the transient behaviour of the heat exchanger, the heat exchange to or from a fluid is described by the energy conservation laws [69]. The equations (57), (58) and (59) are used to define the final equations used in the model.

The change of energy over time in the wall:

$$MC\frac{\partial T_{\mathrm{w}}}{\partial \tau} - (hA)_{\mathrm{h}}\left(T_{\mathrm{h}} - T_{\mathrm{w}}\right) + (hA)_{\mathrm{c}}\left(T_{\mathrm{w}} - T_{\mathrm{c}}\right) = 0 \tag{57}$$

The heat exchange and corresponding change of a medium can be described as follows:

$$C_{\mathrm{c}}\frac{\partial T_{\mathrm{c}}}{\partial \tau} - (hA)_{\mathrm{c}}\left(T_{\mathrm{w}} - T_{\mathrm{c}}\right) + (\dot{n}cL)_{\mathrm{c}}\frac{\partial T_{\mathrm{c}}}{\partial x} = 0 \tag{58}$$

And the hot stream:

$$C_{\mathrm{h}}\frac{\partial T_{\mathrm{h}}}{\partial \tau} + (hA)_{\mathrm{h}}\left(T_{\mathrm{h}} - T_{\mathrm{w}}\right) + (\dot{n}cL)_{\mathrm{h}}\frac{\partial T_{\mathrm{h}}}{\partial x} = 0 \tag{59}$$

With the assumption of a zero capacity model for the heat exchangers equation (57) can be written as equation (61). Since then an infinitely small amount of heat could change the temperature, the transient behaviour of equation (57) becomes:

$$MC\frac{\partial T_{\mathrm{w}}}{\partial \tau} = 0 \tag{60}$$

The change in temperature within the wall does not affect the heat transfer between the two fluids.

$$(hA)_{\mathrm{h}}\left(T_{\mathrm{h}} - T_{\mathrm{w}}\right) = (hA)_{\mathrm{c}}\left(T_{\mathrm{w}} - T_{\mathrm{c}}\right) = \dot{Q}_{\mathrm{transfer}} \tag{61}$$

And similarly, for equations (58) and (59).

$$C_{\mathrm{c}}\frac{\partial T_{\mathrm{c}}}{\partial \tau} = C_{\mathrm{h}}\frac{\partial T_{\mathrm{h}}}{\partial \tau} \tag{62}$$

Therefore equation (59) can be substituted in equation (58) and can be written as (63).

$$\dot{n}_{\mathrm{c}}c_{p_c}\frac{\partial T_{\mathrm{c}}}{\partial\left(\frac{x}{L}\right)} = \dot{n}_{\mathrm{H}}c_{p_H}\frac{\partial T_{\mathrm{H}}}{\partial\left(\frac{x}{L}\right)} \tag{63}$$

The dynamic model for the cold size, note C_c is assumed to be infinitely small:

$$C_c\frac{dT}{dt} = (hA)_{\mathrm{h}}(T_{\mathrm{w}} - T_{\mathrm{c}}) - \dot{n}c_{\mathrm{p,c}}\frac{dT}{\left(\frac{x}{L}\right)} \tag{64}$$

Similarly, the C_{h} and C_{w} are assumed to be infinitely small.

$$\left(C_{\mathrm{h}} + C_{\mathrm{w}}\right)\frac{dT}{dt} = \dot{n}c_{\mathrm{p,h}}\frac{dT}{\left(\frac{x}{L}\right)} - (hA)_{\mathrm{h}}(T_{\mathrm{h}} - T_{\mathrm{w}}) \tag{65}$$

External heating

The heat provided is constrained by the temperature difference between the two streams within the heat exchanger. The heat that is still needed to reach the desired inlet temperature of the RSOC is to be provided by an additional heat source. For example an electric heater or heat

storage.

$$\dot{Q}_{\text{ext}} = \dot{n} c_{\text{p,c}} (T_{\text{opr}} - T_{\text{hex,out}}) \tag{66}$$

4.3.2 Steam generation

The heat duty for the production of steam is split into two parts. Firstly the sensible heat is required to preheat the water to a saturated liquid and secondly, the evaporator converts saturated liquid into saturated vapour.

Pre-heating of water

The pre-heating of water consists of two parts. The re-circulation of water vapour in the exhaust gas of the RSOC and additional water added to the system.

$$\dot{n}_{\text{RSOC,in}} = \begin{cases} \dot{n}_{RSOC} \;\; if \;\; \dot{n} > \dot{n}_{\text{RSOC}} \\ \dot{n} \;\; if \;\; \dot{n} < \dot{n}_{\text{RSOC}} \end{cases} \tag{67}$$

Electrolysis requires additional water to be inserted into the system since the system outlet streams consist mostly of hydrogen gas.

$$\dot{n}_{\text{ext}} = \begin{cases} \dot{n} - \dot{n}_{\text{RSOC}} \;\; if \;\; \dot{n} > \dot{n}_{\text{RSOC}} \\ 0 \;\; if \;\; \dot{n} < \dot{n}_{\text{RSOC}} \end{cases} \tag{68}$$

In the case of a surplus of water, during SOFC, the redundant water is extracted from the system and fed into the surroundings, resulting in thermal heat loss. The combined molar flow of water fed into the system is described as follows:

$$\dot{n}_{\text{in}} = \dot{n}_{\text{RSOC}} + \dot{n}_{\text{ext}} \tag{69}$$

Prior to condensing, the exhaust gas does contains a fraction of the heat not recovered by the heat recovery units. The remaining heat could potentially be utilized for the pre-heating of hydrogen and water. The sensible heat could be used to increase the temperature of water up to the saturation temperature of water. In the case $\mathrm{Q}_{sen} > \mathrm{Q}_{H_2O}$ the remaining heat is used to (partially) pre-heat the hydrogen stream as well. The additional heat required to pre-heat the stream is calculated as:

$$\dot{Q}_{\text{req}} = M_{\text{c}} c_{\text{p,c}} \frac{dT}{dt} + \dot{n}_{\text{c}} c_{\text{p,c}} \frac{\partial T}{\partial(\frac{x}{L})} \tag{70}$$

The available heat is defined as:

$$\dot{Q}_{\text{av}} = M_{\text{h}} c_{\text{p,h}} \frac{dT}{dt} + \dot{n}_{\text{h}} c_{\text{p,h}} \frac{\partial T}{\partial(\frac{x}{L})} \tag{71}$$

The heat is transferred between the outlet flow of the RSOC and the pre-heaters of water.

$$\dot{Q}_{\text{HEX}} = \begin{cases} \dot{Q}_{\text{av}} \;\; if \;\; \dot{Q}_{\text{req}} > \dot{Q}_{\text{av}} \\ \dot{Q}_{\text{req}} \;\; if \;\; \dot{Q}_{\text{req}} < \dot{Q}_{\text{av}} \end{cases} \tag{72}$$

The heat required if not sufficient heat is available, the heat is provided externally.

$$\dot{Q}_{\text{ext}} = \begin{cases} \dot{Q}_{\text{req}} - \dot{Q}_{\text{av}} \;\; if \;\; \dot{Q}_{\text{req}} > \dot{Q}_{\text{av}} \\ 0 \;\; if \;\; \dot{Q}_{\text{req}} < \dot{Q}_{\text{av}} \end{cases} \tag{73}$$

$$\dot{Q}_{\text{PH}} = \dot{Q}_{\text{HEX}} + \dot{Q}_{\text{ext}} \tag{74}$$

Steam generator

Steam is required to be condensed prior to the separation of H_2 and H_2O. Therefore no possibility to reduce the energy consumption by re-circulating the steam into the system. The energy balance over the evaporator, with the assumption of a perfect insulated system:

$$V\frac{\partial(\rho H)}{\partial t} = \dot{n}_{\text{in}} h_{\text{l}} - \dot{n}_{\text{out}} h_{\text{g}} - \dot{Q} \tag{75}$$

The assumption of zero capacity results in the following:

$$\dot{Q}_{\text{SG}} = (h_{\text{g}} - h_{\text{f}})\dot{n} \tag{76}$$

The additional energy required for the production of steam is calculated as:

$$\dot{Q} = \dot{Q}_{\text{PH}} + \dot{Q}_{\text{SG}} \tag{77}$$

4.3.3 Pre-heating and storage and H_2

To maximize the efficiency, hydrogen and water are recirculated to satisfy the demand of the SOE/SOFC. Hydrogen is recirculated during both SOFC and SOE. During SOE, the hydrogen produced is sufficient for the hydrogen needed in the cell. The composition of the flow of the components leaving the cell is calculated. The hydrogen and water fractions within the exhaust stream for electrolysis are described as follows:

$$\begin{aligned} \dot{n}_{\text{H}_2,\text{RSOC}} &= \dot{n}_{\text{H}_2\text{O}} U_{\text{f}} + \dot{n}_{\text{H}_2} \\ \dot{n}_{\text{H}_2O,\text{RSOC}} &= \dot{n}_{\text{H}_2\text{O}}(1 - U_{\text{f}}) \end{aligned} \tag{78}$$

Similar to the fuel cell, the composition of the exhaust gas is described as follows:

$$\begin{aligned} \dot{n}_{\text{H}_2\text{O},\text{RSOC}} &= \dot{n}_{\text{H}_2} U_{\text{f}} + \dot{n}_{\text{H}_2\text{O}} \\ \dot{n}_{\text{H}_2,\text{RSOC}} &= \dot{n}_{\text{H}_2}(1 - U_{\text{f}}) \end{aligned} \tag{79}$$

Molar balance hydrogen

For electrolysis, the hydrogen used to satisfy composition requirements is extracted from the exhaust stream of fuel, as shown in figure 10

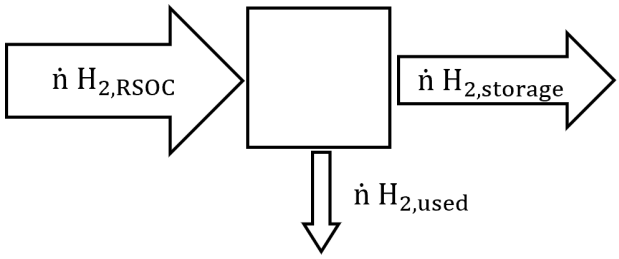

Figure 10: Hydrogen distribution between use and storage during SOE.

Hydrogen consumption during SOFC is high. However, not all hydrogen is consumed. The remaining hydrogen in the exhaust gas is separated from the water vapour after condensation. All hydrogen within the exhaust gas is added to the hydrogen extracted from the storage vessel. This hydrogen stream is mixed with the incoming steam, as shown in figure 11.

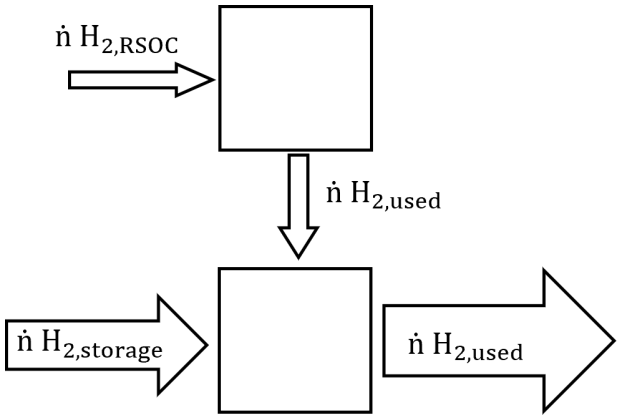

Figure 11: Hydrogen management to be used during SOFC.

The molar-flow rate recirculated within the system is determined as:

$$\dot{n}_{\text{RSOC,in}} = \begin{cases} \dot{n}_{\text{RSOC}} \ \ if \ \ \dot{n} > \dot{n}_{\text{RSOC}} \\ \dot{n} \ \ if \ \ \dot{n} < \dot{n}_{\text{RSOC}} \end{cases}$$

The additional flow of hydrogen is required to be pre-heated the hydrogen extracted from the storage is defined as:

$$\dot{n}_{\text{st}} = \begin{cases} \dot{n} - \dot{n}_{\text{RSOC}} \ \ if \ \ \dot{n} > \dot{n}_{\text{RSOC}} \\ 0 \ \ if \ \ \dot{n} < \dot{n}_{\text{RSOC}} \end{cases}$$

The total amount of hydrogen used is determined as:

$$\dot{n} = \dot{n}_{\text{RSOC,in}} + \dot{n}_{\text{st}} \tag{80}$$

In the case of SOE, the hydrogen available in the outlet stream is larger than required $\dot{n}_{RSOC} > \dot{n}_{RSOC,in}$. The excess hydrogen is extracted from the system and stored.

Energy balance

The heat required for the pre-heating of the hydrogen is defined as:

$$\dot{n}_{\mathrm{RSOC,in}} c_{\mathrm{p}} \Delta T_{\mathrm{RSOC}} + \dot{n}_{\mathrm{st}} c_{\mathrm{p}} \Delta T_{\mathrm{st}} = \dot{Q}_{\mathrm{PH}} \tag{81}$$

$\dot{n}_{\mathrm{RSOC}}$ is the molar-flow from exhaust flow, $\Delta \mathrm{T_{RSOC}}$ = $\mathrm{T_{sat}}$ - $\mathrm{T_{con}}$, $\dot{n}_{\mathrm{in}}$ is the additional molar-flow required, $\Delta \mathrm{T_{st}}$= $\mathrm{T_{sat}}$ - $\mathrm{T_{st}}$. The system operates at increased temperatures relative to the surroundings. Therefore the temperature of the fuel and air streams is elevated to 700 °C.

H_2 storage

The hydrogen is assumed to be stored at 25 °C and a pressure of 350 bar. The temperature of the hydrogen is cooled before entering the compressor to 25 °C which decreases the required power consumption. The compression results in a pressure and temperature increase. After the compression of the hydrogen, the temperature is again reduced to 25 °C. The compression and subsequent temperature increase are described in section 4.3.5. The heat extracted during the cooling of the hydrogen is described as:

$$\dot{Q} = \dot{n}_{\mathrm{H_2}} c_{\mathrm{p}} \Delta T \tag{82}$$

4.3.4 Condenser

Condensation of water is a critical step and is required to separate the hydrogen gas from the water vapour. Before the separation of hydrogen and water, the water vapour is condensed.

$$V \frac{\partial(\rho H)}{\partial t} = \dot{n}_{\mathrm{in}} h_{\mathrm{g}} - \dot{n}_{\mathrm{out}} h_{\mathrm{l}} - \dot{Q} \tag{83}$$

The heat extracted from the stream is:

$$\dot{Q}_{\mathrm{con}} = \dot{n}_{\mathrm{fuel}} \left((h_{\mathrm{g}} - h_{\mathrm{f}}) x_{\mathrm{H_2O}} + c_{\mathrm{p,fuel}} \Delta T \right) \tag{84}$$

Where $c_{\mathrm{p,fuel}} = c_{\mathrm{p}_{\mathrm{H_2O}}} x_{\mathrm{H_2O}} + c_{\mathrm{p}_{\mathrm{H_2}}} x_{\mathrm{H_2}}$. Before condensation of the water vapour the sensible heat, not extracted from the stream during the heat recovery, is used to preheat the water and hydrogen streams. The available sensible heat is described as:

$$\dot{Q}_{\mathrm{sen}} = M c_{\mathrm{p}} \frac{\partial T}{\partial t} + \dot{n} c_{\mathrm{p}} \frac{\partial T}{\partial \frac{x}{L}} \tag{85}$$

The sensible heat available as shown in equation (85), is utilized to (partially) pre-heat the inlet water and hydrogen gas to the saturation temperature of the water.

$$\dot{Q}_{\text{sen,con}} = \begin{cases} \dot{Q}_{\text{sen}} - (\dot{Q}_{H_2} + \dot{Q}_{H_2O}) \;\; if \;\; \dot{Q}_{\text{sen}} > (\dot{Q}_{H_2} + \dot{Q}_{H_2O}) \\ 0 \;\; if \;\; \dot{Q}_{\text{sen}} < (\dot{Q}_{H_2} + \dot{Q}_{H_2O}) \end{cases}$$

The required heat removed from the outlet flow, necessary to fully condensate the water vapour, is thus defined as:

$$\dot{Q}_{\text{con}} = \dot{n} x_{H_2O} (h_{\text{g}} - h_{\text{f}}) + \dot{Q}_{\text{sen,con}} \tag{86}$$

The change in the cooling liquid can be described as:

$$\dot{n}(h_{\text{out}} - h_{\text{in}}) = \dot{Q}_{\text{con}} \tag{87}$$

4.3.5 Compressor & blower

A substantial part of the electric power is consumed by the BoP components. Motylinski et al. found that 19-36 % of the electricity requirements of the BoP can be attributed to mechanical components of the BoP [13]. The blower and compressor are modelled using the same expression. The compressor is used to pressurize the hydrogen. It is assumed that the mechanical components of the balance-of-plant can be modelled as steady-state due to their fast response time [13, 70]. The power consumption due to polytropic compression is:

$$W = \left(\frac{m}{m-1}\right) z_1 \frac{R T_{\text{in}}}{M} \left[\left(\frac{P_{\text{out}}}{P_{\text{in}}} \right)^{\frac{m-1}{m}} - 1 \right] \tag{88}$$

The corresponding pressure increases due to polytropic compression and can be determined with equation (89).

$$T_{\text{out}} = T - \text{in} \left(\frac{P_{\text{out}}}{P_{\text{in}}} \right)^{\frac{m-1}{m}} \tag{89}$$

It is assumed that T_{in} and $\frac{P_{\text{out}}}{P_{\text{in}}}$ remain constant. Compression results in a temperature increase, which does not have to be supplied by a heat exchanger. The efficiencies are shown in table 19. With the storage pressure of 350 bar, the temperature increase can be calculated. To reduce the temperature increase and improve the efficiency multiple stages are used. The use of the serial setup allows for the inter-cooling of the compressor, which reduces the power consumption of the compressor. For modelling purposes, a five-stage compressor is selected. A more detailed explanation of the selection of the number of stages is presented in appendix C.2.

4.4 Evaluation of the model

The presented model is evaluated to determine whether it is compatible with the energy conservation law. Therefore the model is applied to a steady-state scenario with an output of 10 kW from the SOFC. The majority of the energy supplied is supplied as electricity during electrolysis. For the fuel mixture, the composition at the inlet and outlet is taken into account to evaluate the

energy conservation. Since the change in composition is significant. For airflow, the energy contained at the inlet and outlet of the cycle is not taken into account. A slight deviation is observed for SOE to hydrogen. This is caused by a difference between the heat used for evaporation and the difference between LHV and HHV of hydrogen.

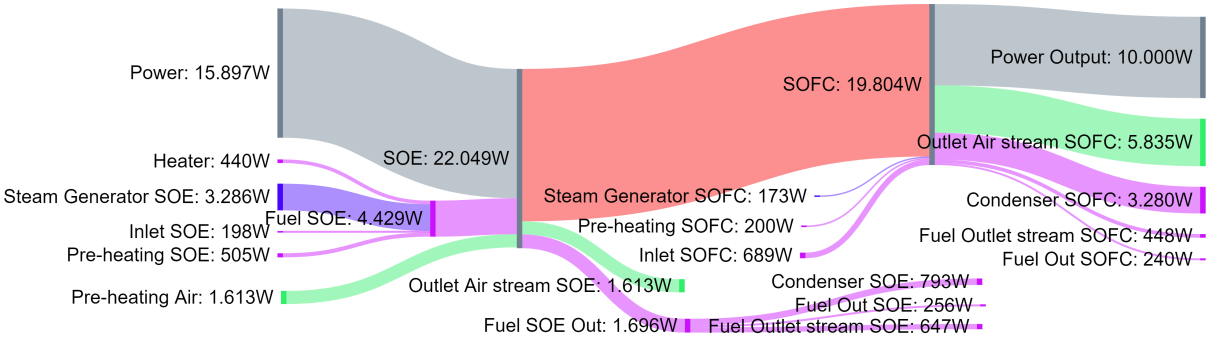

Figure 12: The Inputs and outputs of the balance-of-plant for a 10 kW output in SOFC mode.

To evaluate the model used for the electrochemical reaction the resulting round-trip efficiency is compared to previous studies. The round-trip efficiency found for the RSOC is higher in comparison to previous modelling studies. The difference in performance is caused by a different resistance within the cell. Mottaghizaed et al. use a higher value of the area-specific resistance. As a result, the round-trip efficiency of the RSOC reaction is lower [7].

5 Results

This chapter describes the results of the round-trip efficiency of the different concepts. First, the steady state efficiency is determined including the use of TES. Secondly, the results of the dynamic model are presented. Which includes the consequences of the selected control strategy and discusses a method to improve the performance of the BoP. Furthermore, the effects of the response time and size of the TES are discussed.

The results presented were described in chapter 3. These concepts are:

- Concept 1: Electric heater
- Concept 2: Heat recovery units
- Concept 3: Heat pump with TES
- Concept 4: TES with integrated cooling in RSOC
- Concept 5: Metal hydride hydrogen storage

5.1 Steady state

This section discusses the steady-state results of the five concepts presented in 3. The steady-state calculations are made to give an initial estimation of the performance of the BoP. The results are based on calculations for a constant power output which are obtained with different current densities. The amount of hydrogen converted is related to the applied current. Where the amount of moles of hydrogen converted increases for an increasing current.

Since operating voltage is dependent on the current density, as shown in chapter 4.2, the increase of the current reduces the performance of the cell. Therefore effect of the operating voltage on the round-trip efficiency of the cell is investigated. The results are shown in 13. It is shown that round-trip efficiency is reduced for a decrease in the voltage during SOFC. The decreasing operating voltage corresponds with an increase in the current density. Therefore during SOFC, to obtain a constant power output a decrease in the voltage results in an increase in the current density and thus a higher hydrogen consumption.

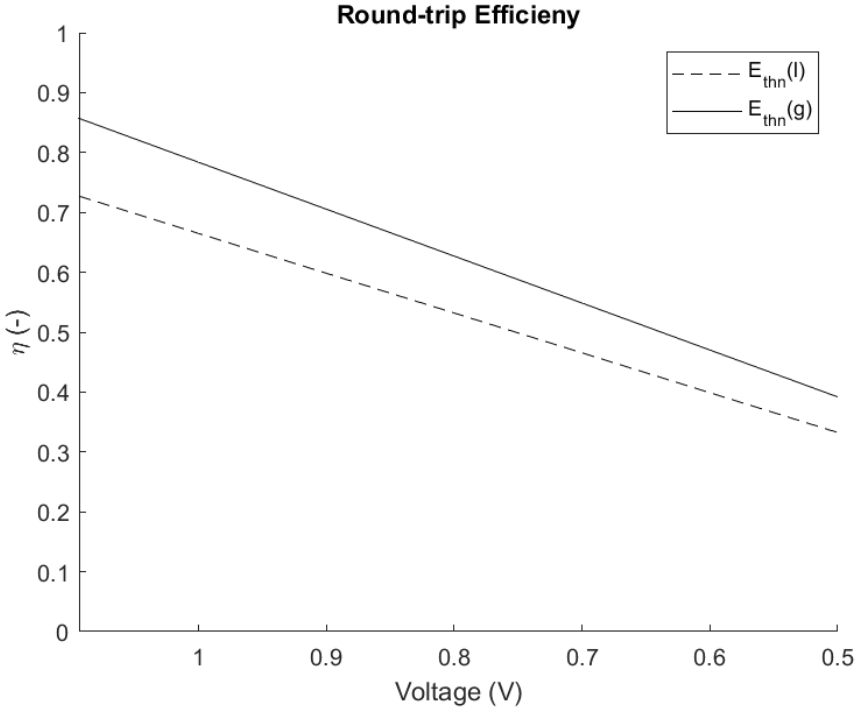

Figure 13: Relation between the voltage in SOFC mode and corresponding maximum electric round-trip efficiency. The operating voltage is dependent on the current density.

The round-trip efficiency of the different concepts is investigated, the results are shown in figure 14. The assumption is that for concepts 3 and 4 the size and state of charge of the TES are sufficiently large to obtain the maximum efficiency. The efficiency of the steady state calculation based on input and output is defined as:

$$\eta = \frac{P_{\text{out}}}{P_{\text{in}}} = \frac{P_{\text{SOFC,out}}}{P_{\text{SOE,in}} + P_{\text{SOFC,in}}} \tag{90}$$

Since the required output of the SOFC is constant for the concepts the efficiency differs due to different power consumption of the components within the BoP. The decrease in the efficiency over the current density is caused by the lower performance of the RSOC.

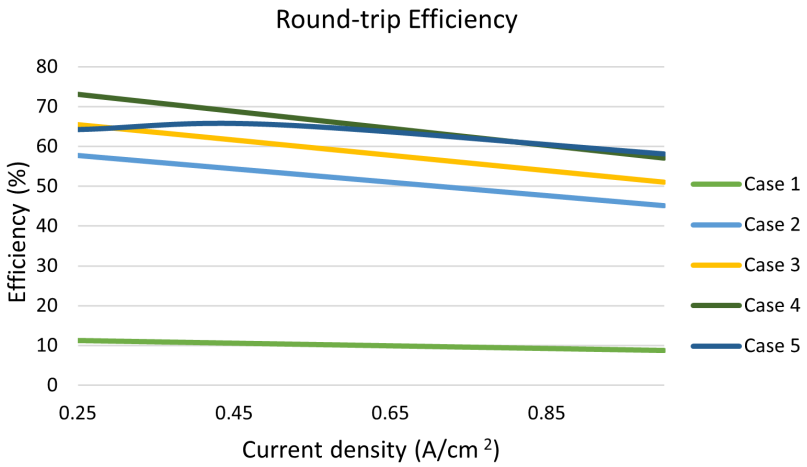

Figure 14: Relation between current density and round-trip efficiency for steady-state calculation.

The hydrogen required to generate a constant amount of electricity increases for higher current densities during SOFC. Since higher current densities during SOFC mode result in larger losses, see section 4.2. This reduction in the efficiency for increasing current densities is caused by the lower performance of the cell in SOFC mode. The differences between the different concepts are caused by the BoP, the performance of the BoP differs mainly during electrolysis. Except for concept 1 where the BoP consumes more electricity during the SOFC mode. The power consumption of the BoP at different current densities is shown in appendix D. During SOFC, concepts 4 and 5 are found to have the least parasitic losses. Since both are assumed to provide sufficient heat from the RSOC additional electricity for evaporation is not required. In figure 14 it is shown that the efficiency of concept 5 does not reduce at low current densities (0.25 to 0.5 A/cm^2) in contrast to the other concepts. For the release of hydrogen from the metal hydride storage during SOFC mode heat is required. The heat generated increases for higher current densities since this increases the losses within the electrochemical process. At low current densities, the hydrogen is converted more efficiently to electricity, as is shown in figure 13. At higher current densities the less efficient conversion to electricity causes more heat to be generated.

Since the aim of the RSOC is to produce additional electricity during times when demand from the grid exceeds supply from the wind turbines. The performance of the BoP during SOFC mode is separately investigated. It is found that concept 1 does consume significantly more external energy compared to the other concepts. Therefore, concept 1 is disregarded due to the low overall efficiency and high external energy consumption during SOFC mode.

The breakdown of the external energy input during SOE is shown in figure 15. Where the power consumption by the RSOC is constant for the different concepts. Concepts 3 and 4 are assumed to be operating with TES which could provide all heat required. Concept 5 does not require additional heat for the heating of air and fuel due to the chemical storage with metal hydride.

Furthermore, it is assumed that metal hydride storage operates at atmospheric pressure which results in the omission of the compressor.

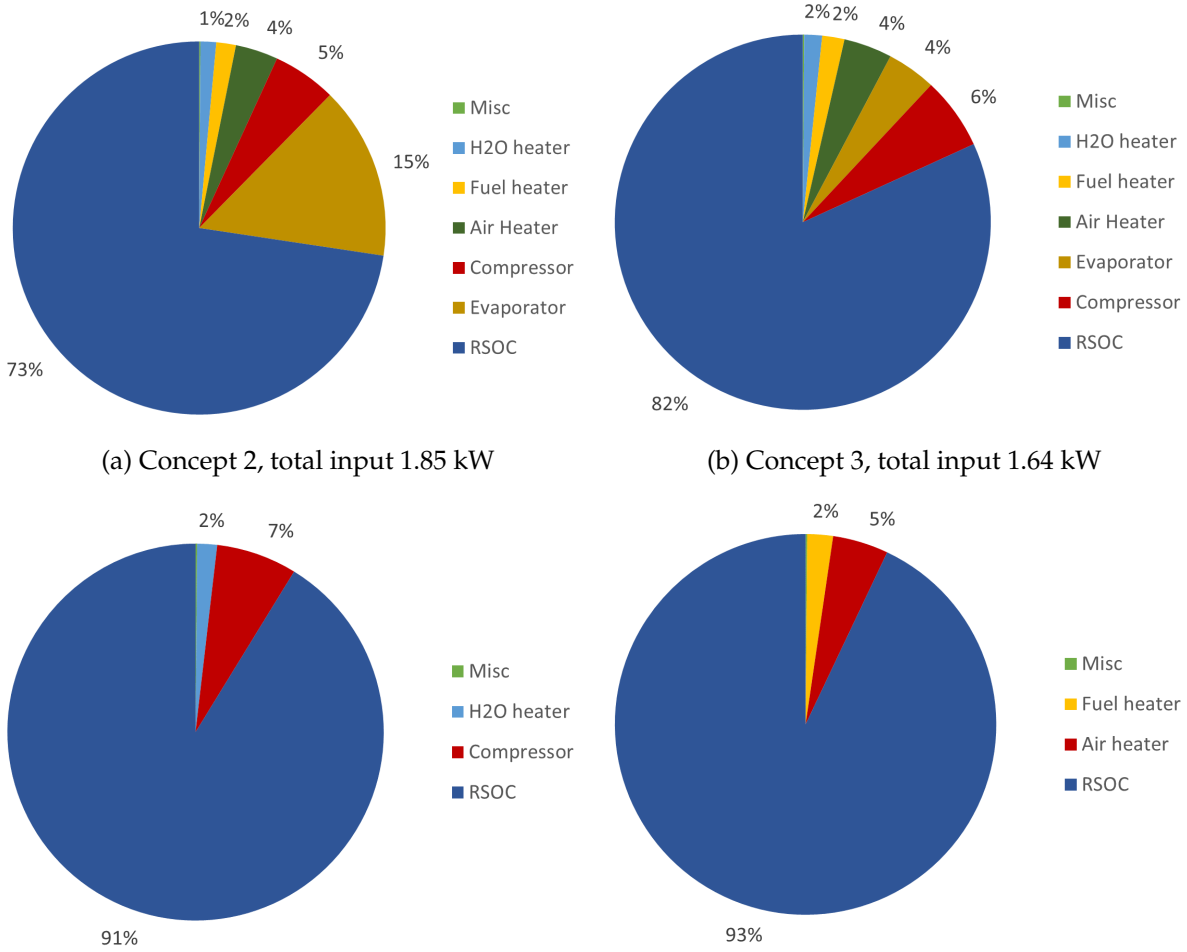

(a) Concept 2, total input 1.85 kW

(b) Concept 3, total input 1.64 kW

(c) Concept 4, total input 1.47 kW

(d) Concept 5, total input 1.44 kW

Figure 15: The breakdown of SOE the external energy input for concepts 2 to 5, for 0.5 A/cm^2.

5.2 Dynamic model

Previous results were based on steady-state calculation. For the dynamic models, multiple variations are investigated. This includes the temperature management strategy within the stack and the effects of the changing rate of the current density.

5.2.1 Thermal management strategy of the RSOC

The initial thermal management strategy of the stack was based on Newton's law of cooling. Where the airflow is adjusted to remove the exact amount of heat released by the stack. However, it is observed that the variations in the outlet temperature result in a reduction in the performance of the heat recovery unit. Therefore the impact of a different thermal management strategy is investigated. This strategy includes a constant temperature at SOFC independent of the current and a constant temperature during SOE.

The reduction in round-trip efficiency is caused by the lower outlet temperature of the RSOC compared to the initial design temperature of 750 °C. Resulting in higher demand for electric heaters for pre-heating air and fuel. The design temperature is not obtained due to the chosen thermal management strategy and assumption of Newton's law of cooling. The temperature of the stack varies for different power densities, which occur due to varying loads. An example is shown with the temperature profile shown in figure 16a which corresponds to the power generation and cooling shown in figure 16b.

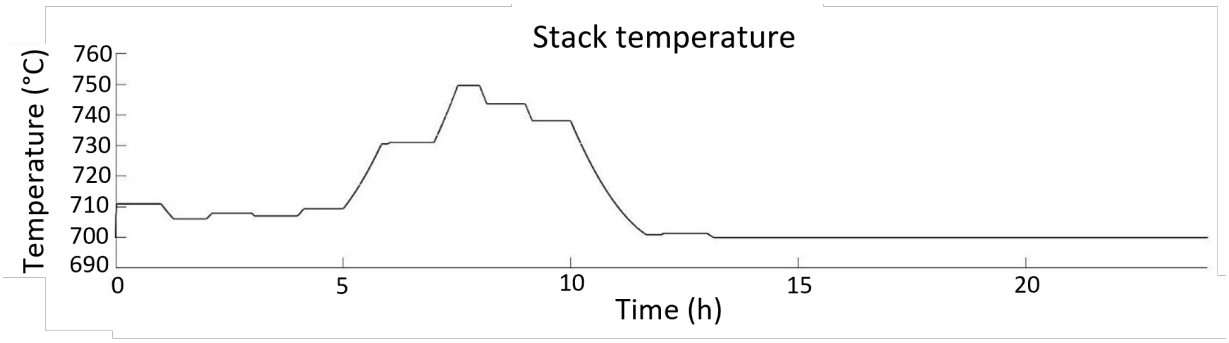

(a) Stack temperature

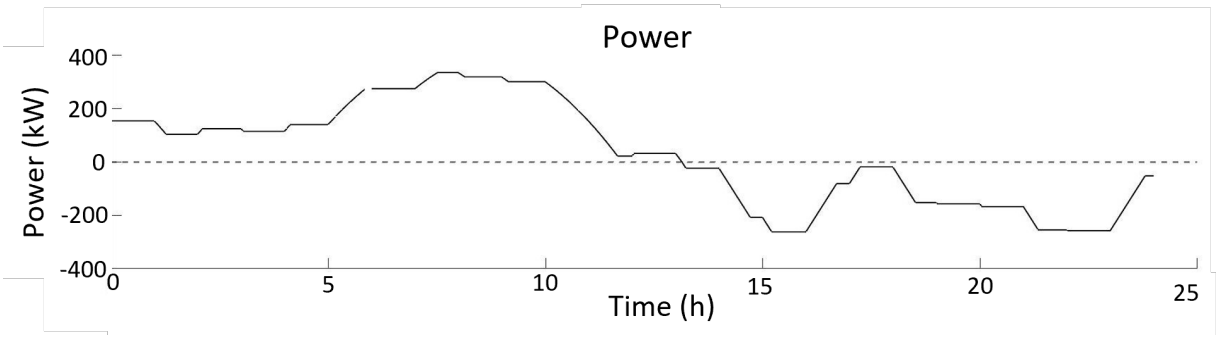

(b) Power generation and consumption

Figure 16: Example of stack temperature and Power, June 30^{th} 2008.

The temperature is correlated to the power within the stack. Figure 16b shows SOFC mode for the first half of the day. It shows that the temperature of the stack is increasing for higher power outputs. During SOFC operations the temperature of the stack is managed by the varying in the airflow. Where the outlet temperature of the air can not exceed the temperature of the stack. The assumption to relate the temperature of the stack to the power generated in the stack is found to cause an increase in energy consumption within the BoP. For small differences in temperature between the air at the inlet and the stack the airflow is required to be large. Since for small temperature differences the potential energy increase per mole is small. Which increases the required airflow. Furthermore, the temperature of the hot airflow in the heat recovery unit is not sufficiently high. Which requires the electric heaters to supply additional heat for the in going airflow. In the initial design, the use of the electrical heaters was only expected during

SOE mode. The electricity consumption of electric heaters during SOFC is the largest parasitic consumer of electricity in the BoP, see figure 18. The parasitic electricity consumption by the electric heaters should be kept to a minimum to increase the performance of the system.
Figures 17 and 18 show an example of high parasitic losses due to BoP electricity consumption from the air heaters. The net power generation, in SOFC mode, between 0 and 5 hours is relatively small see figure 18 for example. However the consumption of electricity by the air heater is high, see figure 17. Between hours 5 to 10, the generated electricity by the SOFC is high. The high power output increases the temperature of the outlet gasses, see figure 16. This results in more efficient heat recovery which can be seen as the electricity consumption is reduced, shown in figure 18.

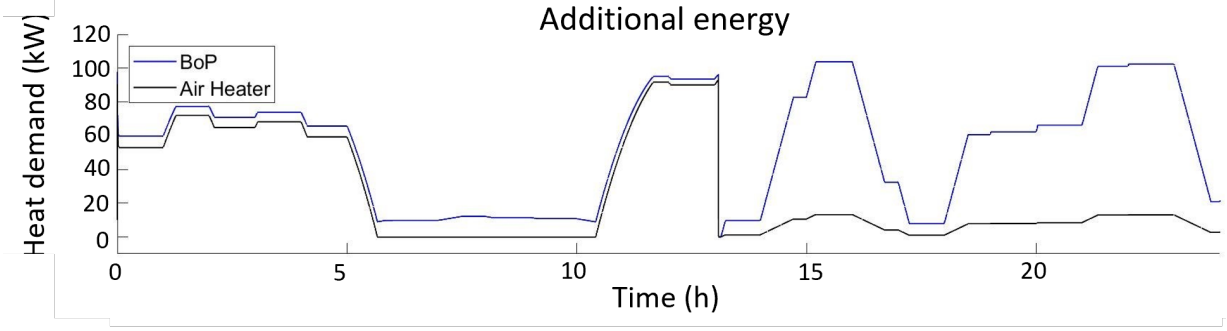

Figure 17: Balance-of-plant & Air electric heater energy consumption June 30^{th}.

The balance-of-plant power consumption due to the high energy consumption by the heaters could exceed the power produced by the RSOC, as shown in figure 18.

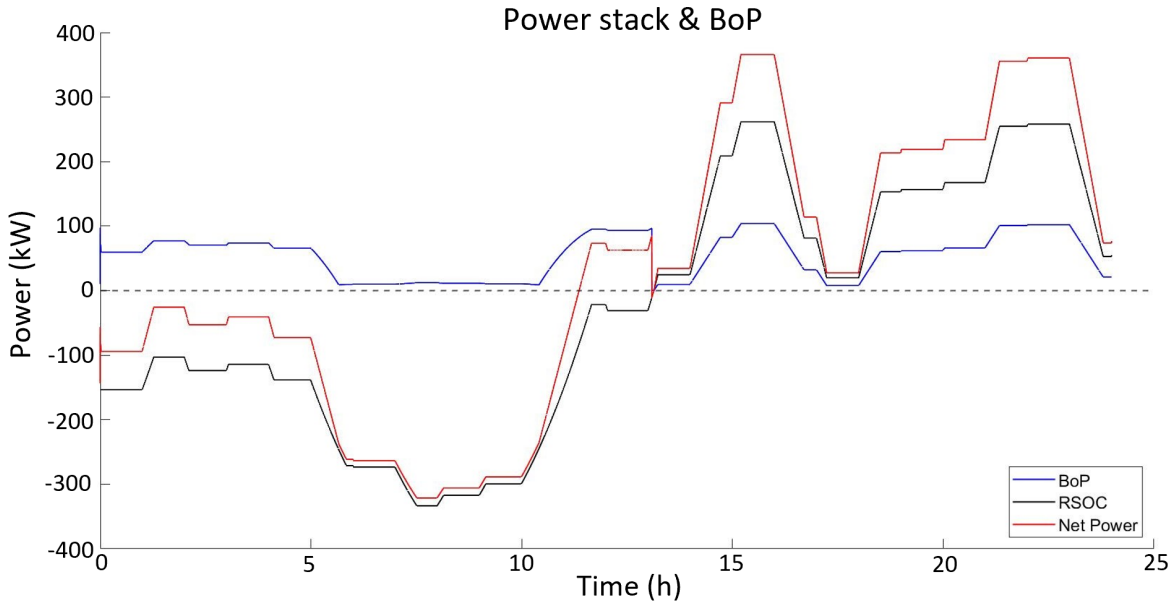

Figure 18: Balance-of-plant & air electric heater energy consumption June 30^{th}. Negative power represents power generation and positive the consumption of electricity by the BoP or RSOC.

To reduce power consumption a different thermal management is applied. This thermal man-

agement is not based on maximizing the cooling of the stack. However, this thermal management strategy is based on a constant temperature of the stack for each mode. The stack temperature is independent of the current density/power density by reducing the airflow rate, which alters the cooling of the stack.

$$T_{\text{RSOC}} = \begin{cases} 700°C \ \ if \ \ i < 0 \\ 750°C \ \ if \ \ i > 0 \end{cases} \tag{91}$$

The temperature of the stack remains constant after the required temperature is achieved. The resulting power consumption of the balance-of-plant is subsequently reduced, due to the reduced airflow required for cooling and the increased temperature of the hot stream of the heat recovery unit. The effect of the BoP on the power consumption and generation of the system is shown in figure 19. The resulting power consumption of electrical heaters only increases for larger temperature differences during electrolysis.

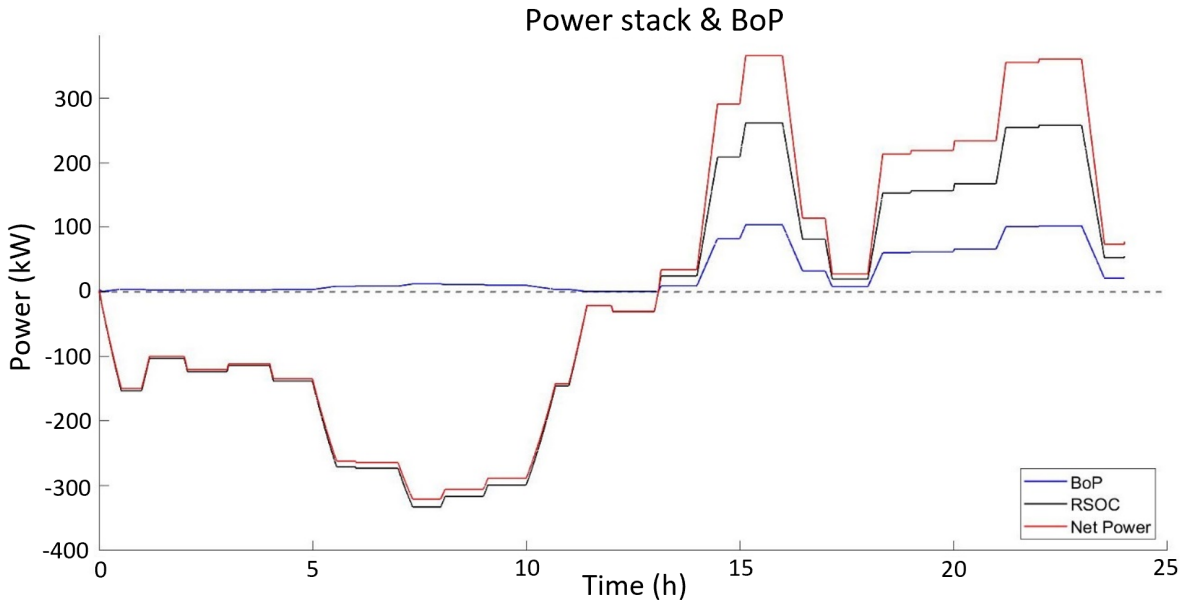

Figure 19: Balance-of-plant & air electric heater power consumption, June 30^{th}.

The performance of the systems for the different concepts for different thermal management strategies are presented in figure 20. The power input to the RSOC is substantially different for the three concepts. However, the largest differences are a result of the different control strategies to manage the temperature within the stack.

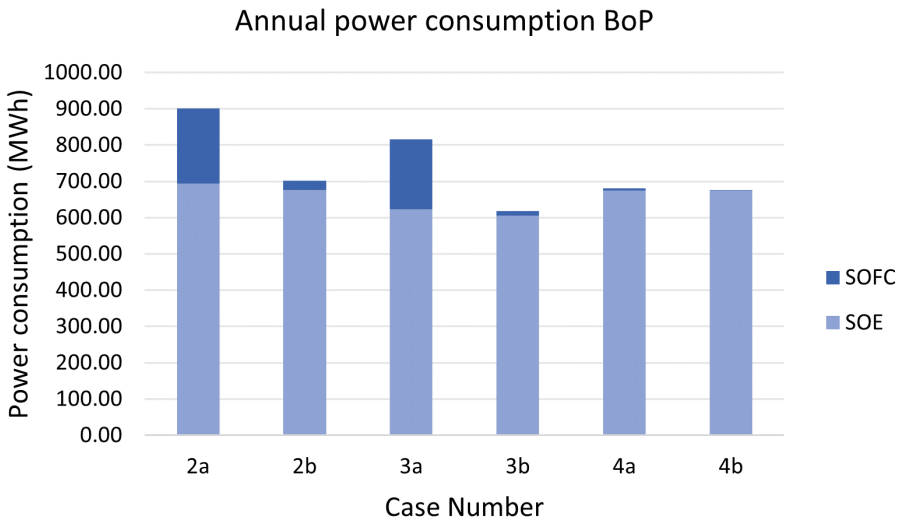

Figure 20: External power consumption of the BoP excluding the SOC, shown for SOFC and SOE.

5.2.2 Effects of varying rate of change of the current density

The response time of the BoP is determined by the limitations of the rate of change of the current density within the stack. Since all other components are assumed to have a faster response time or are modelled as zero-capacity models see section 4. The effect is the rate of change of the current is investigated with a sensitivity study the results are shown in figure 21. To determine the effect of the dynamic model concept 2 is used for the sensitivity study.

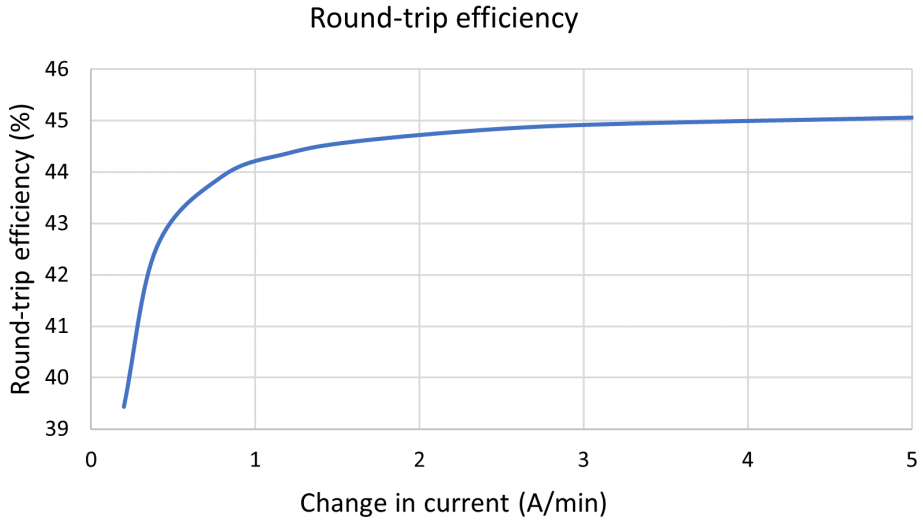

Figure 21: The effect of an increasing rate of change of the current density concept 2a.

Increasing the rate of change of the current density results in an increase of the round-trip efficiency. The delay in the response of the SOC results in electricity consumption while the grid requires electricity. As the change of the current results in a temporary mismatch between supply and demand compared to the grid and wind park, see figure 22. The increased efficiency is

a result of the faster response of the stack. This increases the amount of electricity produced at a time when the base load exceeds the produced electricity. Similarly, the amount of electricity consumed by electrolysis while the grid has a power deficit is reduced. Furthermore, the results do not include the additional power required for the deficit of actual power supplied and required from the grid.

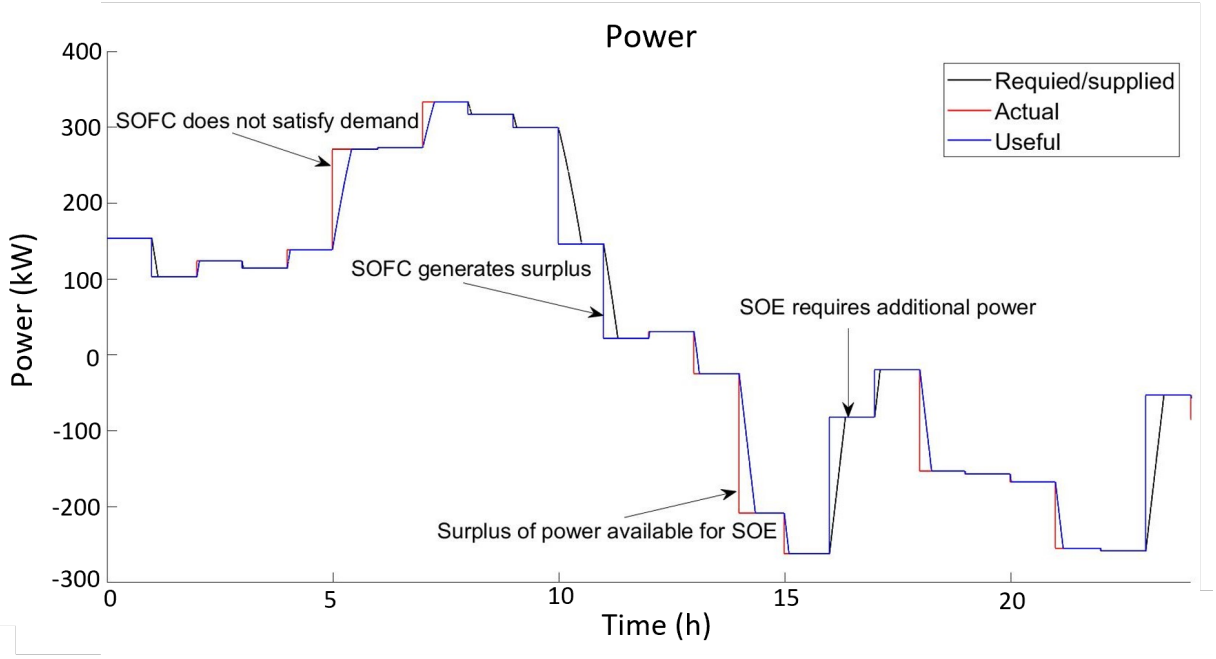

Figure 22: Required, actual and useful power.

5.3 Performance of concepts

In this section, concepts 2 to 4 are further investigated. This includes a breakdown of the electricity consumption. Furthermore, the effect of the size of the thermal energy storage on the performance of concepts 3 and 4 is investigated.

5.3.1 Heat recovery units (Concept 2

The electric boiler is the largest contributor to the power consumption of the BoP. Followed by the power consumed for the compression of hydrogen. The round-trip efficiency is determined by the temperature difference in the heat recovery units and the response time of the current. Based on a 25 °C difference over the stack and a rate of change of current rate of 5 A/min per 100x100mm. The round-trip efficiency of concept 2 is found to be 48.94%.

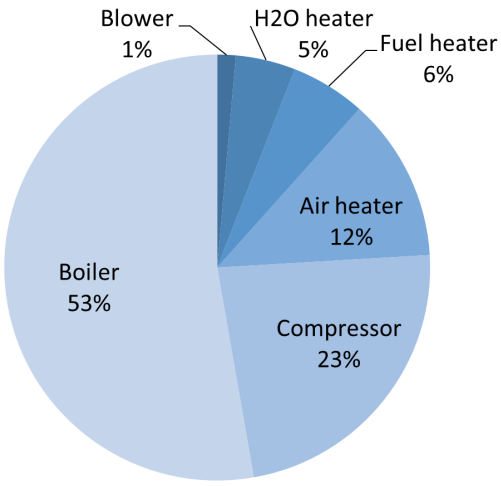

Figure 23: The power input to the BoP of concept 2 total input 702 MWh.

5.3.2 Heat pump and heat storage (concept 3)

This section shows the influence of TES integrated within the BoP in combination with a heat pump. The power consumption shown for systems with TES capacity up to 10 MWh of storage is presented in figure 25. The reduction of the power consumption of the BoP is during SOE mode. The breakdown of the power consumption is changed compared to concept 2. The power consumption of the boiler is lower compared to concept 2. However, the power consumption is increased by the heat pump. The overall BoP power consumption is reduced compared to concept 2, shown in 23 and 24. Due to the set boundary condition regarding the fuel composition and the set fuel utilization the SOC power requirement is reduced. The reduction compared to concept 2 utilization of non-utilized steam which heat of condensation is used as a heat source for the heat-pump. For SOFC mode sufficient heat is released due to condensation to function as a heat source of the heat-pump. Similarly, during electrolysis, the non-utilized steam could provide part of the heat required for evaporation even without heat storage. Figure 24 does not include thermal energy storage.

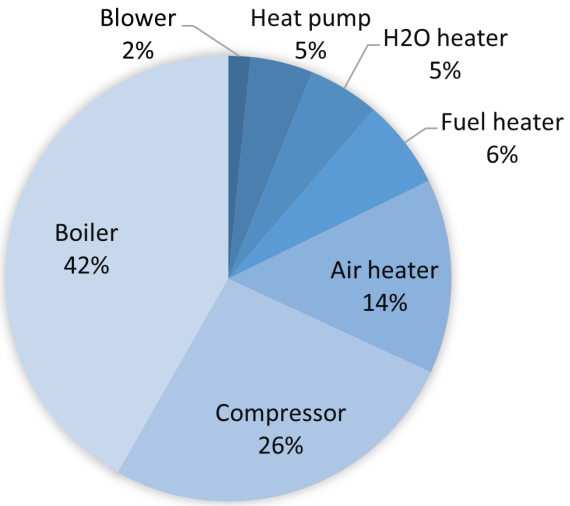

Figure 24: The power input to the BoP of concept 3 total input 618 MWh.

The effect of thermal energy storage on the performance of the SOE and SOFC is shown in figure 25. The effects of the size of the TES are affecting the required power consumption during SOEC mode. The size of TES does not affect the power consumption during SOFC mode due to the availability of heat during this time.

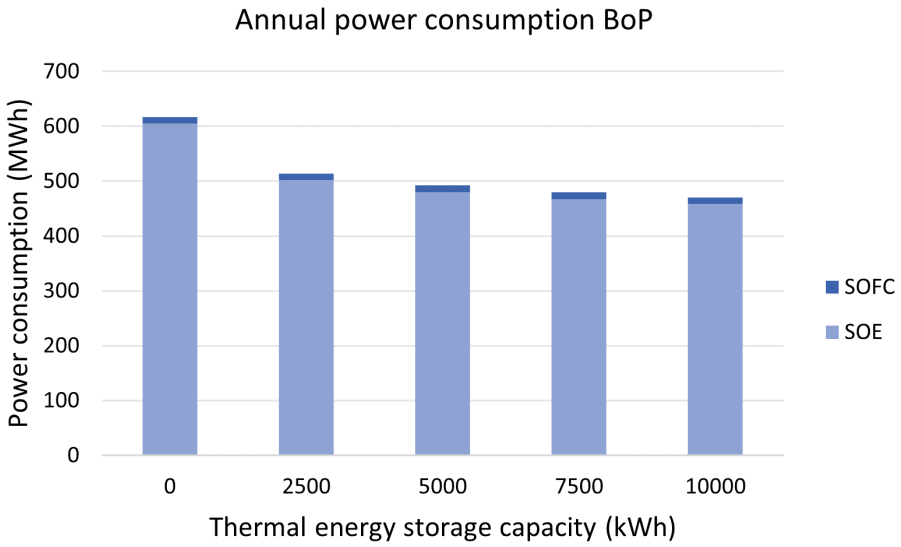

Figure 25: The effect of storage on the power consumption of BoP.

It is observed that the influence of increasing storage size diminishes for larger capacities of TES.

5.3.3 Integrated cooling and heat storage (concept 4)

Concept 4 uses two separate thermal energy storage tanks and integrated cooling. The first TES is a high-temperature storage used as a replacement for electric heaters. The second TES is a medium temperature storage between 100 - 700 °C to be used for the evaporation of water. Since both TES are charged by the SOFC the capacity of the storage affects the performance of

the other TES. This section describes the performance of multiple variations regarding storage. Firstly, the BoP without storage is expected to reduce the electricity consumption for evaporation during SOFC. Secondly, the variations in the capacity of the high and medium temperature TES respectively with the other set at zero. Thirdly, the combination of both storage shows the influence of one on the other.

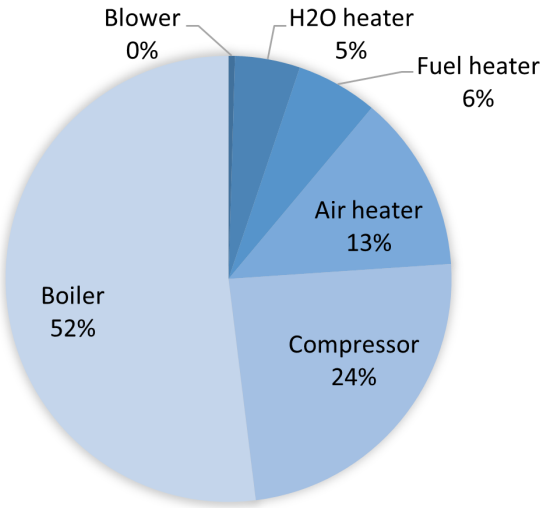

Figure 26: The power input to the BoP of concept 3 total input 675 MWh.

The high-temperature TES is charged prior to the medium-temperature TES. Therefore the size of the high-temperature TES affects the medium-temperature TES. The round-trip efficiency for variations in the size of the medium-temperature TES, with the high-temperature TES set at zero, is shown in figure 27.

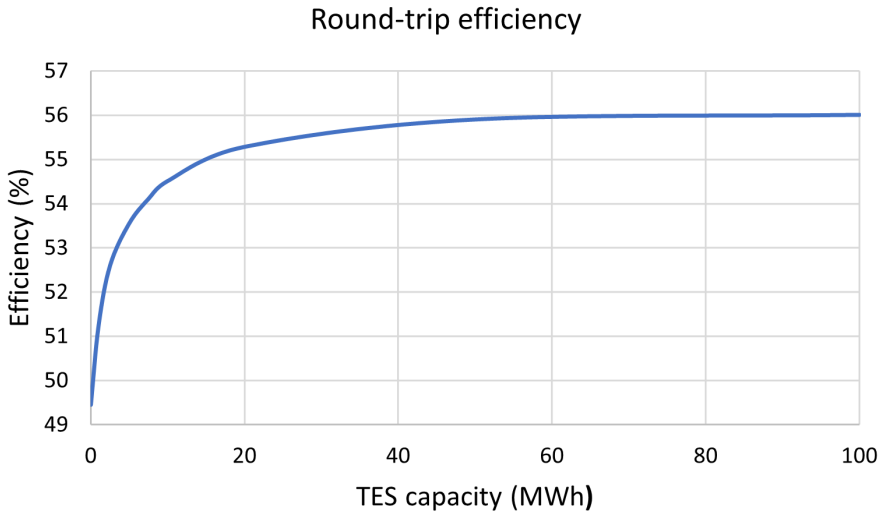

Figure 27: Round-trip efficiency related to medium temperature TES.

The effect of increasing TES of the high-temperature TES on the efficiency is shown in figure 28. The TES at medium temperature is set at zero.

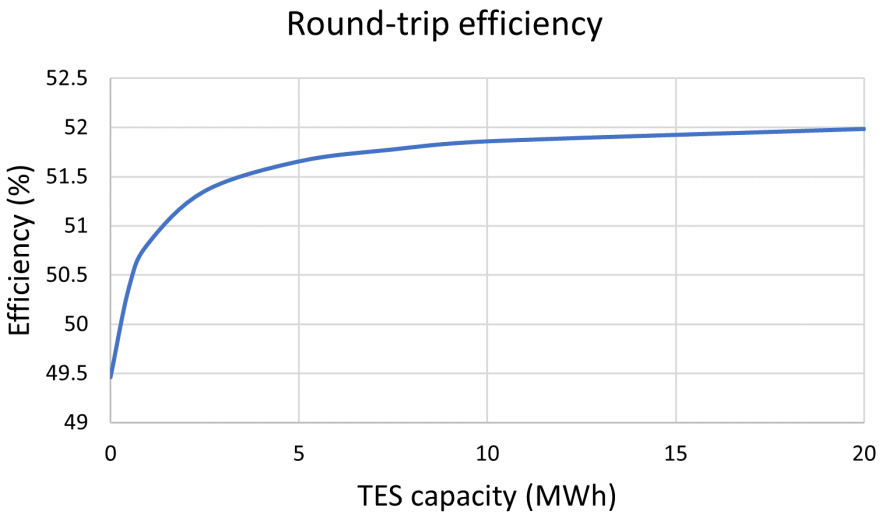

Figure 28: Round-trip efficiency related to the high-temperature TES.

Since both TES are charged by the RSOC during SOFC mode. The model is set so the high-temperature TES is charged prior to charging the medium-temperature TES. So the capacity of the high-temperature TES affects the input of the medium-temperature TES. The results for varying sizes of the medium-temperature TES for different high-temperature TES are shown in figure 29.

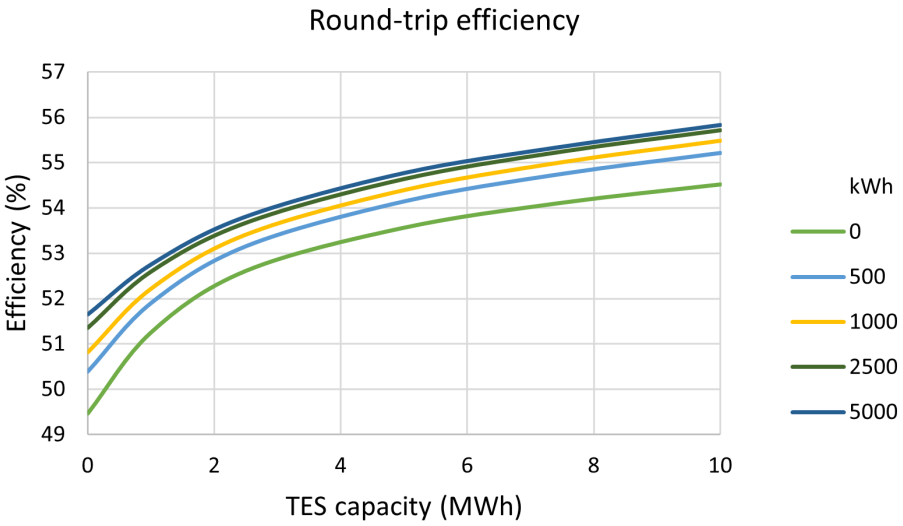

Figure 29: Round-trip efficiency for combined storage, for varying size of high-temperature over the size of low-temperature storage.

The effect of the capacity of the TES on the efficiency show a diminishing return for increasing the size of the TES. Furthermore, the effect of the capacity on the efficiency of the medium TES is larger compared to the high-temperature TES. This is caused by the differences in energy consumed for evaporation (medium-temperature TES) and superheating of the steam/hydrogen mixture (high-temperature TES). The larger capacity of the TES results in an increase of the efficiency. However, the larger size of the storage results in an increase in the cost. The costs

involved with the increased capacity are explained and evaluated in chapter 6.

5.4 Hydrogen production and consumption

The final component which is not included in the calculations of the BoP is the hydrogen storage. Since the auxiliary power for BoP components is assumed to be extracted from the grid. The hydrogen production and consumption are determined based on the power supply from the wind-park and base load. The summation of each transformation results in an annual level of hydrogen storage. The level of the storage of hydrogen is calculated as:

$$L_{H_2} = \sum_{n=1}^{n=t} R_{H_2}^n \tag{92}$$

Figure 30 shows the storage level over the year. The data obtained is used to determine the capacity of the storage. The level of hydrogen stored shows the seasonal behaviour of the generated power by wind energy to the base load of the grid.

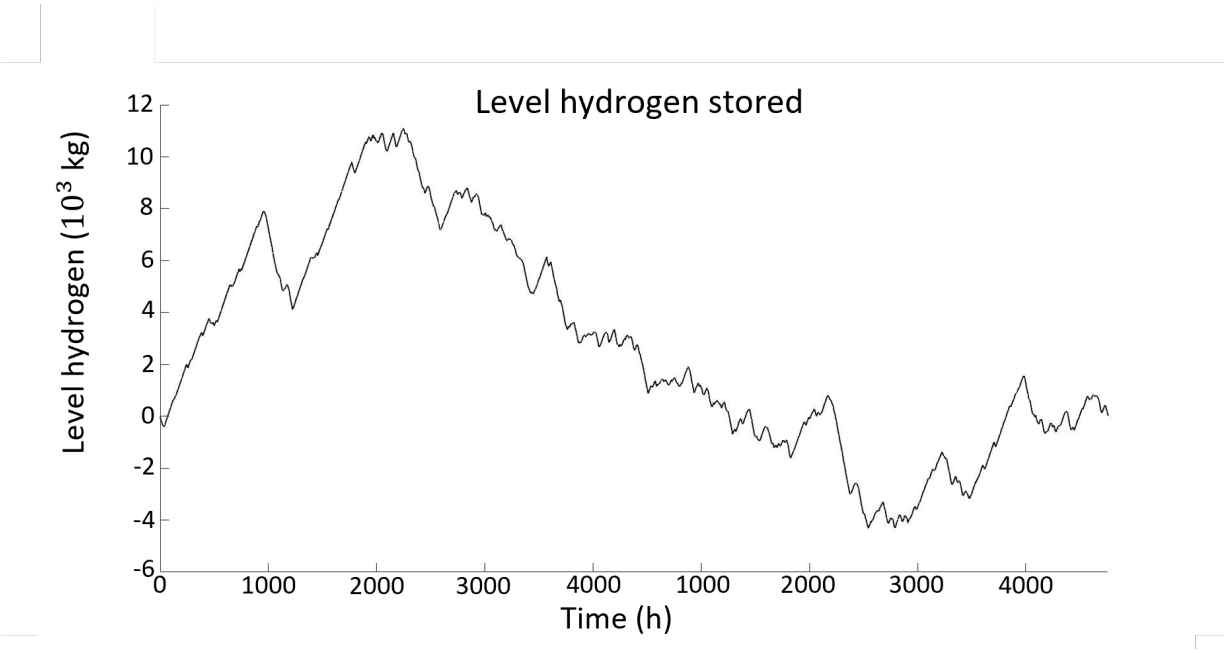

Figure 30: The level of H_2 required to be stored over a year.

The required capacity of the hydrogen storage is calculated at 15395 kg. The total amount of hydrogen produced is calculated at 50248 kg. The size of the storage is thus approximately 30% of the annual hydrogen production. The large required storage capacity is a significant component in the selection of the suitability of each concept. Two different solutions of hydrogen storage are used, compressed hydrogen and metal hydrides. The cost of metal hydrides as storage (concept 5) is substantially higher compared to concepts 2 till 4 and is therefore disregarded in the results, see section 6.2 for the techno-economic analysis regarding storage techniques.

6 Techno-economic analysis

An important aspect of the selection of the RSOC are the related costs. The goal of the chapter is to present the differences in the costs between the concepts. The techno-economic analysis is based on the required capacity.

6.1 Levelized cost

To be able to select the best economical suited option the method of levelized cost of energy is used (LCOE). The LCOE is equal to the life cycle cost if applied to the energy produced by the system during the analysed period [71].

$$LCOE = \frac{C_c}{E_l} \tag{93}$$

Where E is the electricity generation of the SOFC minus the power consumed during SOFC by the BoP ($E = P_{SOFC} - P_{BoP}$). C_c consists of the initial cost, operation and maintenance cost and cost of electricity during SOEC mode. The analysis period is set as one year. For the comparison the levelized cost is based on the annualized cost of the initial capital expenses, the cost of electricity and the operation and maintenance cost.

Table 6: Discount rate, O&M cost and electricity price

Discount rate	5%
O&M cost	2.5%
SOE electricity price ($/kWh)	0.05

6.2 Hydrogen storage

The cost of a storage vessel varies for different storage pressures. Whereas in general, the cost of hydrogen storage vessels increases with increasing pressure. For storage vessels intended for storage for mobility and transportation a low weight is desired. This weight reduction has consequences on the cost per kilogram of hydrogen stored, the lower weight results in higher initial cost [72]. It can be assumed that for the stationary situation, the weight of the storage vessel is not of importance.

In the concepts, shown in section 3, two alternatives are used for the storage of hydrogen. Concepts 1 to 4 use compressed hydrogen and concept 5 uses metal hydrides to store the hydrogen. Therefore a comparison is made between the two alternatives. The alternatives are compared based on the cost of storage. For the comparison, it is assumed that the exothermic reaction within the metal hydride, which occurs during electrolysis is included in the comparison. Furthermore, the cost related to the evaporation and compression is taken into account for storage by a pressure vessel. The two alternatives include the following components:

- Alternative 1: Compressor, pressure vessel and evaporator.
- Alternative 2: Metal hydride

Table 7: Initial cost of components

Component	Cost ($/kW)	Lifetime (years)	Source
Compressor	40035 $P^{0.6038}$	20	[73]
Evaporator	31 - 54	20	[74, 75]

Component	Cost ($/kg)	Lifetime (years)	Source
Storage vessel	83- 574	25	[72, 75]
Metal hydride	2000-3025, 14285	25	[76, 77]

It can be expected that the storage costs of alternative 1 will vary for different electricity prices. Similarly, the expected capital investment for alternative 1 is lower compared to alternative 2. However, alternative 2 is assumed to be able to operate without additional electricity supply for compression and evaporation. To determine the most economically viable storage solution the electricity price at which the cost are equal is determined.

Table 8: Annualized costs of components

Component	Cost ($/kW)	($)	($/year)	O&M ($)
Compressor	9 196	376 728	30 229	9413
Evaporator	31 (Low)	2709	217.38	68
Evaporator	54 (High)	4719	378.66	117

Component	Cost ($/kg)	($)	($/year)	O&M ($)
Storage vessel (low)	83	1 277 743	102 529	31 944
Storage vessel (high)	574	8 836 443	709 059	220 911
Metal hydride (low)	2000	30 789 000	2 470 589	799 725
Metal hydride (high)	3025	46 568 362	3 736 765	1 164 209

To evaluate the cost of the different methods the levelized cost of storage (LCOS) is compared. The LCOS is based on the initial purchasing price (CAPEX) and operation and maintenance cost (O&M). The initial cost and O&M are presented in table 8. The initial costs are calculated based on the size of the component and the cost per kW or kg found in the literature.

One of the methods used for the comparison of different alternatives is the annual worth or the capital return factor (CRF) [71].

$$CRF = \frac{i(1+i)^N}{(1+i)^N - 1} \tag{94}$$

The discount rate for both alternatives is set at 5%. The operational and maintenance costs are assumed to be 2.5 % of the initial investment.

The costs between the two storage solutions are compared to identify at which electricity price the cost of pressurized storage equals that of metal hydride. For this comparison, equal electricity prices for both operational modes are assumed. The comparison is made based on the Levelized cost of storage (LCOS) [71], which relates the cost to the amount of H_2 stored over a period of time.

$$LCOS = \frac{C_c}{\dot{M}} \tag{95}$$

Where C_c includes the initial investment, O&M cost and the cost of electricity (C_c) to power the steam generator and compressor.

$$C_c = CAPEX * CRF + O\&M + C_E \tag{96}$$

Where CAPEX is the capital expenditure, and CRF is the capital return factor. The comparison between the variations shows lower capital and O&M for the use of a compressor in combination with a pressure vessel. However, the cost of electricity consumed is higher compared the use of a metal hydride storage. It is found that the use of metal hydrides becomes economically feasible at a purchasing price of electricity of 4.31 $/kWh. It has to be noted that alternative 1 consumes most of the electricity during electrolysis (compressor & evaporator). As electrolysis takes place during a period with a surplus of power provided by the wind turbines relative to the demand of the grid. The cost of electricity provided by offshore wind energy parks is expected to be below 50 $/MWh or 0.05 $/kWh.

The cost of hydrogen storage by metal hydrides is therefore too expensive in comparison to the use of compressed hydrogen storage. The levelized cost of the lower and upper bound of compressed hydrogen is below the expected levelized cost of metal hydride storage. The effect of electricity consumed for compression and evaporation on the LCOS is limited. Metal hydride storage becomes the economically favourable solution at an electricity price of 4.31 $/kWh. However, the cost of electricity provided by offshore wind energy is expected to be substantially lower. Therefore concept 5 is expected to be not economically viable, due to the required size and corresponding cost of the metal hydride storage.

6.3 Balance-of-plant

This section focuses on the levelized cost of the three remaining concepts utilizing compressed hydrogen storage. Two of these concepts use thermal energy storage to optimize round-trip efficiency. However, similar to the use of metal hydride storage the size of the TES is significant compared to the power generated. Therefore, for concepts 3 & 4 the optimal size of the storage is determined based on the levelized cost of energy. These results are compared to a BoP without

energy storage. The concepts considered are:

- Concept 2: Heat recovery units
- Concept 3: Heat pump with TES
- Concept 4: TES with integrated cooling in RSOC

Table 9: Initial purchasing price and lifetime of components.

Component	Cost ($/kW)	Lifetime (years)	Source
RSOC	166-5387	5 -30	[78–80]
Condenser	19	20	[74]
Evaporator	31- 54	20	[74, 75]
Heat exchanger	40 - 46	20	[74, 81]
Pressure vessel	83	25	[72]

Component	Cost ($)	Lifetime (years)	Source
Blower	148	20	[74]
Heat pump	$\alpha_{\mathrm{k}}(CAP^{b_{\mathrm{k}}})CAP$	20	[82]
Electric heater	$\alpha_{\mathrm{k}}(CAP^{b_{\mathrm{k}}})$	20	[82]
Compressor	40035 $\mathrm{P}^{0.6038}$	20	[73]

The predicted cost of the RSOC varies greatly in the literature. However, it is assumed that the initial capital investment of a RSOC stack is 500 $/kW [78]. With an expected lifetime of approximately 10 years. To evaluate the cost of the BoP of the different concepts the levelized cost of electricity is used, see equation (93). The LCOE of the BoP includes all components, including the RSOC and the electricity consumed for the electrolysis process. The O& costs of the components are assumed to be constant over the lifetime. Similarly, the price of electricity is assumed to be constant over the lifetime of the BoP.

The additional costs for integrated cooling within the RSOC stack are not described in the literature. However, it will increase in complexity and costs [35]. Therefore the LCOE is calculated with the assumption that the costs of the RSOC stacks are equal. The use of thermal energy storage is excluded to determine the initial cost of the concepts. The levelized costs of electricity of the concepts are shown in table 10. The cost of concept 4 is found to be the lowest. This reduction in costs is a consequence of a different method of cooling the stack. This subsequently reduces the required size of the other components within the BoP. Most notably the size of the heat recovery units and blowers for the airflow.

Table 10: Levelized cost of energy without TES

Concept	LCOE ($/kWh)
2	0.1872
3	0.1833
4	0.1721

Since the costs of the RSOC are expected to increase for variation 3, due to the increased complexity of the stack. A sensitivity study was performed to investigate the maximum initial capital cost compared to concepts 2 and 3. The maximum cost of the RSOC with integrated cooling was found to be 700 and 750 $/kW for concepts 3 and 2 respectively, as shown in figure 32.

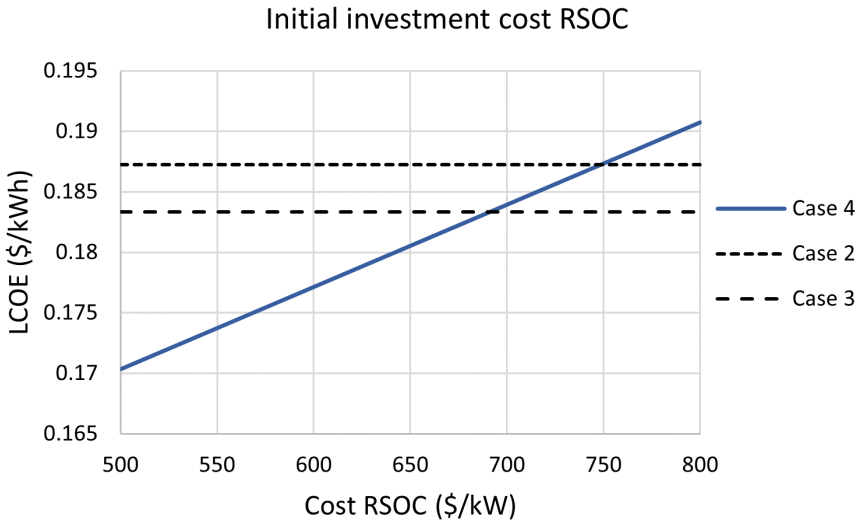

Figure 31: Effect of price per kW of the RSOC on the LCOE of concept 4. The price per kW of RSOC of concepts 2 & 3 is constant at 500 $/kW.

6.4 Thermal energy storage

The cost of TES could potentially reduce the cost of concepts 3 and 4. However, the reduction of the costs is limited and dependent on the cost of the TES. The energy storage could improve the efficiency with 4 to 5%.

For concept 3 sensible heat storage is used which is expected to be between 1 and 10 $/kWh. The found LCOE for different costs of storage and capacity of TES are shown in figure 32. The initial increase is due to the increased size of the heat pump. The size of components is determined at the maximum possible given the size of the heat storage.

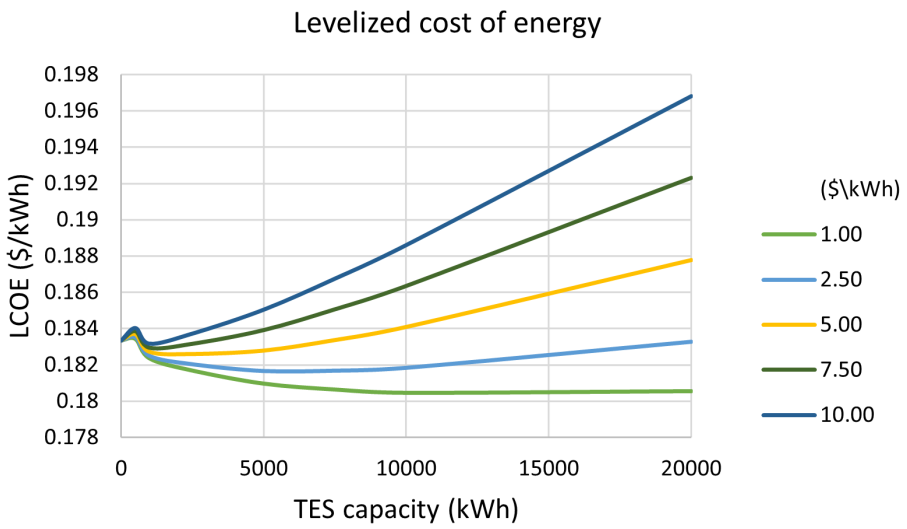

Figure 32: Effect of TES on LCOE of concept 3.

The energy storage for concept 4 is subdivided into two systems so that the storage can be set at different temperatures, see section 3.4. The costs of the TES are evaluated for both sections of the thermal energy storage. The cost of medium-temperature TES is expected to be equal to or lower compared to the high-temperature storage. The results for the heat storage connected to the evaporator are shown in figure 33.

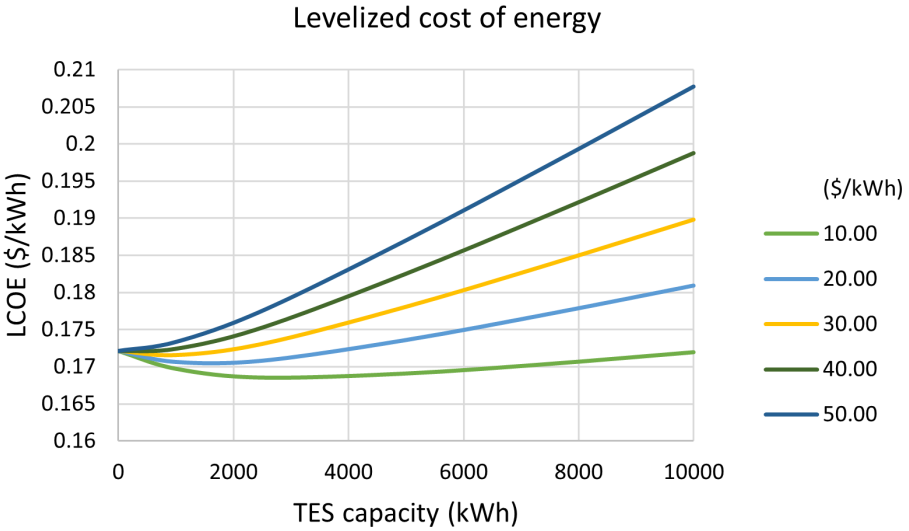

Figure 33: Effect of size and cost of medium-temperature TES for evaporation on the LCOE for concept 4.

The results for the heat storage connected to the fuel and air heaters are shown in figure 34.

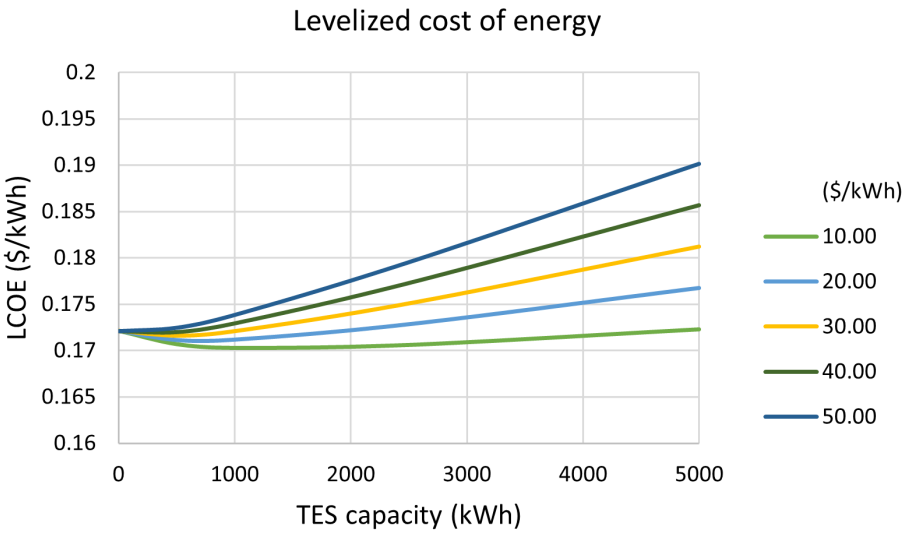

Figure 34: Effect of size and cost of high-temperature TES for air and fuel flow on the LCOE for concept 4.

7 Conclusion

The goal of this thesis was to find the optimal heat management of the balance-of-plant for a reversible solid oxide cell. This goal was subdivided into two objectives. The first objective is the development of a dynamic model of the balance-of-plant. The purpose of the model is to extract data regarding heat transfer and additional energy consumption. The second objective is to develop and analyze different concepts regarding the design of the balance-of-plant. The concepts are analyzed based on the round-trip efficiency of the BoP including the RSOC. In addition a techno-economic analysis was performed to obtain an indication of the economic feasibility.

7.1 Dynamic model

A dynamic model is developed with Matlab/Simulink. This dynamic model uses multiple sub-models for: the electrochemical cell, compressor, heat exchanger, evaporator and condenser. These are interconnected and dependent on each other. The developed model can perform time-dependent simulations and determine temperatures and transferred energy. The model is suitable to be incorporated into the electricity model. Since the model requires only a single input of the power imbalance between the supply and demand of the grid and wind park.

Parameters related to the response time of the stack and components of BoP were identified. A sensitivity analysis of the response time shows that the efficiency increase diminishes for the rate of change of 2 A/min and 5 A/min, per 10x10cm^2 cell. This is promising for the use of different heat management scenarios, including TES. Because the response of these different components is expected to be faster than the change of the current within the RSOC. Furthermore, the model can perform calculations regarding flow rates, temperature and energy transfer. The thermal management strategy of the air and cell temperature affects the round-trip efficiency. Because these affect the performance of the heat recovery units. The performance of the heat recovery units appears to have a major influence on the round-trip efficiency.

7.2 Concepts

Based on the dynamic model and steady-state calculations five different balance-of-plant concepts were compared. If the operating conditions of the RSOC are to be satisfied solely by electrical heaters the performance of the BoP is found to be low. During SOFC mode the required power input of the BoP exceeds the power output of the SOFC. With the use of heat recovery units and the management of exhaust gasses, the efficiency of the system could be increased. The efficiency increases to 45-50% due to the reuse of heat available in the exhaust streams of the RSOC. However, further improvements could be made to the BoP and stack. By implementing a heat pump for steam generation to utilize the heat of condensation during SOE and SOFC, the efficiency could be improved to 51%. The cooling with the airflow in the air channel requires large heat duties within the heat recovery units. It is found that with the use of an integrated

cooling system such as heat pipes, it is possible to remove the heat from the stack without increasing the airflow. This leads to a round-trip efficiency of 49% and smaller heat recovery units. The combination of TES and heat pipes results in the highest efficiency of 56%. Similarly, the use of metal hydrides results in relatively high round-trip efficiencies for the BoP.

From the economic analysis it is concluded that the use of metal hydrides is not a viable solution. Since the capacity of the metal hydrides is directly related to the hydrogen storage capacity. Literature shows that the costs of metal hydrides are significantly higher compared to pressurized hydrogen storage. It is therefore concluded that the use of metal hydride is not an economically viable solution for seasonal hydrogen storage.

The use of heat recovery is found to be of significance to operate efficiently and cost-effectively. However, the LCOE could be reduced further with the use of TES and integrated cooling. TES has however only a limited impact on the cost for each of the systems compared to a BoP only using heat recovery units. The use of TES reduces the overall electricity input and related costs. However, due to the increased initial cost of the TES, the price per kWh determines whether the improved performance of the BoP is economically feasible. The use of integrated cooling with heat pipes could reduce the cost of the BoP. However, the RSOC stack's initial costs are required to not substantially increase compared to an air-cooled RSOC stack. Based on the results of the techno-economical analysis, it can be concluded that integrated cooling has the potential to reduce the cost substantially. However, the sensitivity study shows that the cost of integrated cooling should not exceed 200 $/kW compared to the cost of RSOC without integrated cooling. The use of a heat-pump is economically possible if compared to a concept BoP using heat recovery units. However, the lower LCOE obtained due to the reduction of electricity consumed for evaporation is diminished by the higher initial cost related to the heat-pump compared to an electric boiler.

Multiple heat management scenarios were identified, developed and compared. It is concluded that the use of electrical heaters to achieve operational conditions is not a viable solution. The use of metal hydride is considered to be too expensive for seasonal storage. The optimal round-trip efficiency is achieved using integrated heat pipes and thermal heat storage. The costs are compared based on the levelized cost. It is found that the LCOE of the BoP heat recovery units, heat pump and heat pipes are too close. Due to the large uncertainty in the range of the initial purchasing price of various components.

8 Recommendations

This thesis contains an analysis of available information on thermal management in solid oxygen cells. This information has been integrated into a model that has been used to analyze various heat management concepts. This has increased the insight into how the heat management can be arranged as adequately as possible. This thesis does not answer all questions. In this chapter, recommendations are made to increase the knowledge of heat management.

8.1 Heat recovery units

The heat exchangers are modelled as zero-capacity models. However, the zero-capacity assumption is not a physical phenomenon. The heat exchangers are found to have a significant impact on the performance of the BoP. Therefore, the modelling of the heat exchangers should include the transient behaviour which includes the mass and specific heat.

8.2 Validation of the model

The dynamic model is based on information from the literature. However, the literature on the combination of multiple components within the RSOC balance-of-plant is limited. Furthermore, the models of the combinations and interaction with each other have not been validated for RSOC modelling. Therefore, it is recommended to experimentally determine the validation of the developed model.

8.3 Techno-economical analysis

The techno-economical analysis indicates the costs of the various heat management scenarios. It should be noted that several costs are not included like the piping between the components. Or components have a wide range in the analysis like the RSOC and TES. Furthermore, the differences in the levelized cost between the scenarios are found to be small. It is recommended to make a more thorough techno-economical analysis before opting for a specific method of the thermal management scenario.

8.4 Model RSOC

The electrochemical model is based on the ASR and current density. However, the model does not include the non-linear behaviour of the cell potential at higher current density. Furthermore, the model of the stack is modelled as a 0D model. This limits the ability to capture the variations within the stack. The variations may result in temperature variations within the stack, which could change the outlet temperature of the air. Therefore it is recommended to further investigate the effects of the model on the performance of the BoP.

References

[1] I. Garcia Torregrosa, "Modeling study of the heat management in solid oxide electrolyzer systems," 2019.

[2] S. Mekhilef, R. Saidur, and A. Safari, "Comparative study of different fuel cell technologies," *Renewable and Sustainable Energy Reviews*, vol. 16, no. 1, pp. 981–989, 2012.

[3] M. Ni, M. K. Leung, and D. Y. Leung, "Parametric study of solid oxide fuel cell performance," *Energy Conversion and Management*, vol. 48, no. 5, pp. 1525–1535, 2007. [Online]. Available: https://www.sciencedirect.com/science/article/pii/S0196890406003657

[4] A. Hauch, S. H. Jensen, S. Ramousse, and M. Mogensen, "Performance and durability of solid oxide electrolysis cells," *Journal of the Electrochemical Society*, vol. 153, no. 9, p. A1741, 2006.

[5] D. M. Bierschenk, J. R. Wilson, and S. A. Barnett, "High efficiency electrical energy storage using a methane–oxygen solid oxide cell," *Energy Environ. Sci.*, vol. 4, pp. 944–951, 2011. [Online]. Available: http://dx.doi.org/10.1039/C0EE00457J

[6] C. Song, "Fuel processing for low-temperature and high-temperature fuel cells: Challenges, and opportunities for sustainable development in the 21st century," *Catalysis today*, vol. 77, no. 1-2, pp. 17–49, 2002.

[7] P. Mottaghizadeh, S. Santhanam, M. P. Heddrich, K. A. Friedrich, and F. Rinaldi, "Process modeling of a reversible solid oxide cell (r-soc) energy storage system utilizing commercially available soc reactor," *Energy Conversion and Management*, vol. 142, pp. 477–493, 2017. [Online]. Available: https://www.sciencedirect.com/science/article/pii/S0196890417302121

[8] M. Singh, D. Zappa, and E. Comini, "Solid oxide fuel cell: Decade of progress, future perspectives and challenges," *International Journal of Hydrogen Energy*, vol. 46, no. 54, pp. 27 643–27 674, 2021.

[9] P. Kazempoor and R. Braun, "Model validation and performance analysis of regenerative solid oxide cells: Electrolytic operation," *International Journal of Hydrogen Energy*, vol. 39, no. 6, pp. 2669–2684, 2014. [Online]. Available: https://www.sciencedirect.com/science/article/pii/S036031991302908X

[10] P. Kazempoor, V. Dorer, and F. Ommi, "Modelling and performance evaluation of solid oxide fuel cell for building integrated co-and polygeneration," *Fuel Cells*, vol. 10, no. 6, pp. 1074–1094, 2010.

[11] P. Kazempoor and R. Braun, "Model validation and performance analysis of regenerative solid oxide cells for energy storage applications: Reversible operation," *international journal of hydrogen energy*, vol. 39, no. 11, pp. 5955–5971, 2014.

[12] X. Jin and X. Xue, "Mathematical modeling analysis of regenerative solid oxide fuel cells in switching mode conditions," *Journal of Power Sources*, vol. 195, no. 19, pp. 6652–6658, 2010. [Online]. Available: https://www.sciencedirect.com/science/article/pii/S0378775310006440

[13] K. Motylinski, J. Kupecki, B. Numan, Y. S. Hajimolana, and V. Venkataraman, "Dynamic modelling of reversible solid oxide cells for grid stabilization applications," *Energy Conversion and Management*, vol. 228, p. 113674, 2021. [Online]. Available: https://www.sciencedirect.com/science/article/pii/S0196890420312000

[14] V.-T. Giap, Y. D. Lee, Y. S. Kim, and K. Y. Ahn, "A novel electrical energy storage system based on a reversible solid oxide fuel cell coupled with metal hydrides and waste steam," *Applied Energy*, vol. 262, p. 114522, 2020.

[15] A. A. AlZahrani and I. Dincer, "Modeling and performance optimization of a solid oxide electrolysis system for hydrogen production," *Applied Energy*, vol. 225, pp. 471–485, 2018. [Online]. Available: https://www.sciencedirect.com/science/article/pii/S030626191830686X

[16] J. S. Herring, J. E. O'Brien, C. M. Stoots, G. Hawkes, J. J. Hartvigsen, and M. Shahnam, "Progress in high-temperature electrolysis for hydrogen production using planar sofc technology," *International Journal of Hydrogen Energy*, vol. 32, no. 4, pp. 440–450, 2007, path Forward to a Hydrogen Economy. [Online]. Available: https://www.sciencedirect.com/science/article/pii/S0360319906002709

[17] W. Becker, R. Braun, M. Penev, and M. Melaina, "Design and technoeconomic performance analysis of a 1mw solid oxide fuel cell polygeneration system for combined production of heat, hydrogen, and power," *Journal of Power Sources*, vol. 200, pp. 34–44, 2012. [Online]. Available: https://www.sciencedirect.com/science/article/pii/S0378775311020325

[18] W. A. N. W. Mohamed, S. F. A. Talib, I. A. Zakaria, A. M. I. Mamat, and W. R. W. Daud, "Effect of dynamic load on the temperature profiles and cooling response time of a proton exchange membrane fuel cell," *Journal of the Energy Institute*, vol. 91, no. 3, pp. 349–357, 2018.

[19] C. Mansilla, J. Sigurvinsson, A. Bontemps, A. Maréchal, and F. Werkoff, "Heat management for hydrogen production by high temperature steam electrolysis," *Energy*, vol. 32, no. 4, pp. 423–430, 2007, eCOS 05. 18th International Conference on Efficiency, Cost, Optimization, Simulation, and Environmental Impact of Energy Systems. [Online]. Available: https://www.sciencedirect.com/science/article/pii/S0360544206001964

[20] R. Peters, R. Deja, L. Blum, Q. Fang, D. Stolten *et al.*, "Influence of operating parameters on overall system efficiencies using solid oxide electrolysis technology," *International journal of hydrogen energy*, vol. 40, no. 22, pp. 7103–7113, 2015.

[21] S. Ali, K. Sørensen, and M. P. Nielsen, "Modeling a novel combined solid oxide electrolysis cell (soec) - biomass gasification renewable methanol production system," *Renewable Energy*, vol. 154, pp. 1025–1034, 2020. [Online]. Available: https://www.sciencedirect.com/science/article/pii/S0960148119319809

[22] M. Götz, J. Lefebvre, F. Mörs, A. McDaniel Koch, F. Graf, S. Bajohr, R. Reimert, and T. Kolb, "Renewable power-to-gas: A technological and economic review," *Renewable Energy*, vol. 85, pp. 1371–1390, 2016. [Online]. Available: https://www.sciencedirect.com/science/article/pii/S0960148115301610

[23] M. Z. Khan, M. T. Mehran, R.-H. Song, S.-B. Lee, and T.-H. Lim, "Effects of applied current density and thermal cycling on the degradation of a solid oxide fuel cell cathode," *international journal of hydrogen energy*, vol. 43, no. 27, pp. 12 346–12 357, 2018.

[24] W. Bujalski, C. M. Dikwal, and K. Kendall, "Cycling of three solid oxide fuel cell types," *Journal of Power Sources*, vol. 171, no. 1, pp. 96–100, 2007.

[25] H. Apfel, M. Rzepka, H. Tu, and U. Stimming, "Thermal start-up behaviour and thermal management of sofc's," *Journal of Power Sources*, vol. 154, no. 2, pp. 370–378, 2006.

[26] Y. Xie and X. Xue, "Transient modeling of anode-supported solid oxide fuel cells," *International Journal of Hydrogen Energy*, vol. 34, no. 16, pp. 6882–6891, 2009, 4th Dubrovnik Conference. [Online]. Available: https://www.sciencedirect.com/science/article/pii/S036031990900932X

[27] C.-Y. Wen, Y.-S. Lin, C.-H. Lu, and T.-W. Luo, "Thermal management of a proton exchange membrane fuel cell stack with pyrolytic graphite sheets and fans combined," *International Journal of Hydrogen Energy*, vol. 36, no. 10, pp. 6082–6089, 2011. [Online]. Available: https://www.sciencedirect.com/science/article/pii/S036031991100406X

[28] M. Ramezanizadeh, M. Alhuyi Nazari, M. Hossein Ahmadi, and L. Chen, "A review on the approaches applied for cooling fuel cells," *International Journal of Heat and Mass Transfer*, vol. 139, pp. 517–525, 2019. [Online]. Available: https://www.sciencedirect.com/science/article/pii/S0017931019310762

[29] G. Zhang and S. G. Kandlikar, "A critical review of cooling techniques in proton exchange membrane fuel cell stacks," *International Journal of Hydrogen Energy*, vol. 37, no. 3, pp. 2412–2429, 2012, 2010 AIChE Annual Meeting Topical Conference on Hydrogen Production and Storage Special Issue. [Online]. Available: https://www.sciencedirect.com/science/article/pii/S0360319911024980

[30] M. Zeng, J. Yuan, J. Zhang, B. Sundén, and Q. Wang, "Investigation of thermal radiation effects on solid oxide fuel cell performance by a comprehensive model," *Journal of Power Sources*, vol. 206, pp. 185–196, 2012. [Online]. Available: https://www.sciencedirect.com/science/article/pii/S0378775312002741

[31] M. Dillig and J. Karl, "Thermal management of high temperature solid oxide electrolyser cell/fuel cell systems," *Energy Procedia*, vol. 28, pp. 37–47, 2012.

[32] H. Zeng, Y. Wang, Y. Shi, N. Cai, and D. Yuan, "Highly thermal integrated heat pipe-solid oxide fuel cell," *Applied Energy*, vol. 216, pp. 613–619, 2018.

[33] M. Dillig, T. Meyer, and J. Karl, "Integration of planar heat pipes to solid oxide cell short stacks," *Fuel Cells*, vol. 15, no. 5, pp. 742–748, 2015.

[34] P. Marocco, D. Ferrero, A. Lanzini, and M. Santarelli, "Benefits from heat pipe integration in h2/h2o fed sofc systems," *Applied Energy*, vol. 241, pp. 472–482, 2019.

[35] M. Promsen, Y. Komatsu, A. Sciazko, S. Kaneko, and N. Shikazono, "Feasibility study on saturated water cooled solid oxide fuel cell stack," *Applied Energy*, vol. 279, p. 115803, 2020. [Online]. Available: https://www.sciencedirect.com/science/article/pii/S0306261920312848

[36] I. Sarbu and C. Sebarchievici, "A comprehensive review of thermal energy storage," *Sustainability*, vol. 10, no. 1, p. 191, 2018.

[37] A. V. Novo, J. R. Bayon, D. Castro-Fresno, and J. Rodriguez-Hernandez, "Review of seasonal heat storage in large basins: Water tanks and gravel–water pits," *Applied Energy*, vol. 87, no. 2, pp. 390–397, 2010.

[38] D. Enescu, G. Chicco, R. Porumb, and G. Seritan, "Thermal energy storage for grid applications: Current status and emerging trends," *Energies*, vol. 13, no. 2, p. 340, 2020.

[39] N. Brandon, J. Edge, M. Aunedi, P. Bruce, B. Chakrabarti, T. Esterle, J. Somerville, Y. Ding, C. Fu, P. Grant *et al.*, "Uk research needs in grid scale energy storage technologies," 2016.

[40] A. L. Nash, A. Badithela, and N. Jain, "Dynamic modeling of a sensible thermal energy storage tank with an immersed coil heat exchanger under three operation modes," *Applied energy*, vol. 195, pp. 877–889, 2017.

[41] N. Vitorino, J. C. Abrantes, and J. R. Frade, "Quality criteria for phase change materials selection," *Energy Conversion and Management*, vol. 124, pp. 598–606, 2016. [Online]. Available: https://www.sciencedirect.com/science/article/pii/S0196890416306410

[42] F. Schaube, A. Kohzer, J. Schütz, A. Wörner, and H. Müller-Steinhagen, "De-and rehydration of ca (oh) 2 in a reactor with direct heat transfer for thermo-chemical heat storage.

part a: Experimental results," *Chemical Engineering Research and Design*, vol. 91, no. 5, pp. 856–864, 2013.

[43] G. Alva, Y. Lin, and G. Fang, "An overview of thermal energy storage systems," *Energy*, vol. 144, pp. 341–378, 2018.

[44] M. Ghalambaz, S. Mehryan, A. Veismoradi, M. Mahdavi, I. Zahmatkesh, Z. Kazemi, O. Younis, M. Ghalambaz, and A. J. Chamkha, "Melting process of the nano-enhanced phase change material (nepcm) in an optimized design of shell and tube thermal energy storage (tes): Taguchi optimization approach," *Applied Thermal Engineering*, vol. 193, p. 116945, 2021. [Online]. Available: https://www.sciencedirect.com/science/article/pii/S1359431121003926

[45] A. Momma, K. Takano, Y. Tanaka, T. Kato, and A. Yamamoto, "Experimental investigation of the effect of operating pressure on the performance of sofc and soec," *ECS Transactions*, vol. 57, no. 1, p. 699, 2013.

[46] O. Posdziech, K. Schwarze, and J. Brabandt, "Efficient hydrogen production for industry and electricity storage via high-temperature electrolysis," *International Journal of Hydrogen Energy*, vol. 44, no. 35, pp. 19 089–19 101, 2019, a Special Issue with the Papers Selected from the 7th World Hydrogen Technologies Convention. [Online]. Available: https://www.sciencedirect.com/science/article/pii/S0360319918317737

[47] K. Sridhar and K. Bicha, "Comparative analysis of parallel and counter flow heat exchangers," *International Journal of Scientific Engineering and Technology Research*, vol. 6, no. 4, pp. 638–644, 2017.

[48] T.-M. Tveit, M. N. Johansson, and R. Zevenhoven, "Environmentally friendly steam generation using vhthps at a pharmaceutical research facility," in *Proceedings of the 13th IEA Heat Pump Conference, Jeju, Korea*, 2021, pp. 26–29.

[49] D. Wu, J. Jiang, B. Hu, and R. Wang, "Experimental investigation on the performance of a very high temperature heat pump with water refrigerant," *Energy*, vol. 190, p. 116427, 2020. [Online]. Available: https://www.sciencedirect.com/science/article/pii/S036054421932122X

[50] T.-M. Tveit, "Application of an industrial heat pump for steam generation using district heating as a heat source," in *12th IEA heat pump conference*, 2017.

[51] G. Masiwal, P. Kumar, and S. Chaudhary, "Performance analysis of surface condenser in 525mw thermal power plant," *International Journal of Engineering and Technology (IJET)*, vol. 9, no. 3, pp. 1931–1939, 2017.

[52] S. Hasnain, "Review on sustainable thermal energy storage technologies, part i: heat storage materials and techniques," *Energy conversion and management*, vol. 39, no. 11, pp. 1127–1138, 1998.

[53] F. Agyenim, P. Eames, and M. Smyth, "Heat transfer enhancement in medium temperature thermal energy storage system using a multitube heat transfer array," *Renewable energy*, vol. 35, no. 1, pp. 198–207, 2010.

[54] J. Wu, B. Tremeac, M.-F. Terrier, M. Charni, E. Gagnière, F. Couenne, B. Hamroun, and C. Jallut, "Experimental investigation of the dynamic behavior of a large-scale refrigeration – pcm energy storage system. validation of a complete model," *Energy*, vol. 116, pp. 32–42, 2016. [Online]. Available: https://www.sciencedirect.com/science/article/pii/S0360544216313688

[55] J. W. MacArthur, "Transient heat pump behaviour: a theoretical investigation," *International Journal of refrigeration*, vol. 7, no. 2, pp. 123–132, 1984.

[56] M. M. Kenisarin, "High-temperature phase change materials for thermal energy storage," *Renewable and sustainable energy reviews*, vol. 14, no. 3, pp. 955–970, 2010.

[57] P. Pardo, A. Deydier, Z. Anxionnaz-Minvielle, S. Rougé, M. Cabassud, and P. Cognet, "A review on high temperature thermochemical heat energy storage," *Renewable and Sustainable Energy Reviews*, vol. 32, pp. 591–610, 2014. [Online]. Available: https://www.sciencedirect.com/science/article/pii/S1364032113008289

[58] V. Yartys, M. Lototskyy, E. Akiba, R. Albert, V. Antonov, J. Ares, M. Baricco, N. Bourgeois, C. Buckley, J. Bellosta von Colbe, J.-C. Crivello, F. Cuevas, R. Denys, M. Dornheim, M. Felderhoff, D. Grant, B. Hauback, T. Humphries, I. Jacob, T. Jensen, P. de Jongh, J.-M. Joubert, M. Kuzovnikov, M. Latroche, M. Paskevicius, L. Pasquini, L. Popilevsky, V. Skripnyuk, E. Rabkin, M. Sofianos, A. Stuart, G. Walker, H. Wang, C. Webb, and M. Zhu, "Magnesium based materials for hydrogen based energy storage: Past, present and future," *International Journal of Hydrogen Energy*, vol. 44, no. 15, pp. 7809–7859, 2019, a special issue on hydrogen-based Energy storage. [Online]. Available: https://www.sciencedirect.com/science/article/pii/S0360319919300072

[59] B. Sakintuna, F. Lamari-Darkrim, and M. Hirscher, "Metal hydride materials for solid hydrogen storage: a review," *International journal of hydrogen energy*, vol. 32, no. 9, pp. 1121–1140, 2007.

[60] J. Larminie, A. Dicks, and M. S. McDonald, *Fuel cell systems explained*. J. Wiley Chichester, UK, 2003, vol. 2.

[61] J. Udagawa, P. Aguiar, and N. Brandon, "Hydrogen production through steam electrolysis: Model-based steady state performance of a cathode-supported intermediate temperature solid oxide electrolysis cell," *Journal of Power Sources*, vol. 166, no. 1, pp. 127–136, 2007.

[62] A. M. Murshed, B. Huang, and K. Nandakumar, "Control relevant modeling of planer solid oxide fuel cell system," *Journal of Power Sources*, vol. 163, no. 2, pp. 830–845, 2007.

[63] J. Kupecki, "Off-design analysis of a micro-chp unit with solid oxide fuel cells fed by dme," *International Journal of Hydrogen Energy*, vol. 40, no. 35, pp. 12 009–12 022, 2015.

[64] S. Jegadheeswaran and S. D. Pohekar, "Performance enhancement in latent heat thermal storage system: a review," *Renewable and Sustainable energy reviews*, vol. 13, no. 9, pp. 2225–2244, 2009.

[65] C. Schoeneberger, J. Zhang, C. McMillan, J. B. Dunn, and E. Masanet, "Electrification potential of u.s. industrial boilers and assessment of the ghg emissions impact," *Advances in Applied Energy*, vol. 5, p. 100089, 2022. [Online]. Available: https://www.sciencedirect.com/science/article/pii/S2666792422000075

[66] E. Rightor, A. Whitlock, and R. N. Elliott, "Beneficial electrification in industry," in *American Council for an Energy Efficient Economy*, 2020.

[67] Q. Cai, C. S. Adjiman, and N. P. Brandon, "Optimal control strategies for hydrogen production when coupling solid oxide electrolysers with intermittent renewable energies," *Journal of Power Sources*, vol. 268, pp. 212–224, 2014. [Online]. Available: https://www.sciencedirect.com/science/article/pii/S0378775314008817

[68] Y. Komatsu, K. Otsuka, A. Kurosaki, C. Kaseda, and S. Kimijima, "Development of an sofc dynamic simulation environment: Model extension for adopting heat loss analysis," in *2012 Proceedings of SICE Annual Conference (SICE)*, 2012, pp. 1081–1090.

[69] T. Gao, B. G. Sammakia, B. T. Murray, A. Ortega, and R. Schmidt, "Cross flow heat exchanger modeling of transient temperature input conditions," *IEEE Transactions on Components, Packaging and Manufacturing Technology*, vol. 4, no. 11, pp. 1796–1807, 2014.

[70] M. Sorrentino and C. Pianese, "Model-based development of low-level control strategies for transient operation of solid oxide fuel cell systems," *Journal of Power Sources*, vol. 196, no. 21, pp. 9036–9045, 2011, fuel Cells Science Technology 2010. [Online]. Available: https://www.sciencedirect.com/science/article/pii/S0378775311001017

[71] W. G. Sullivan, E. M. Wicks, and J. T. Luxhoj, *Engineering economy*. Prentice Hall Upper Saddle River, NJ, 2003, vol. 13.

[72] E. Rivard, M. Trudeau, and K. Zaghib, "Hydrogen storage for mobility: a review," *Materials*, vol. 12, no. 12, p. 1973, 2019.

[73] R. P. Micena, O. R. Llerena-Pizarro, T. M. de Souza, and J. L. Silveira, "Solar-powered hydrogen refueling stations: a techno-economic analysis," *International Journal of Hydrogen Energy*, vol. 45, no. 3, pp. 2308–2318, 2020.

[74] V.-T. GIAP, Y. D. LEE, Y. S. KIM, and K. Y. AHN, "Techno-economic analysis of reversible solid oxide fuel cell system couple with waste steam," *Transactions of the Korean hydrogen and new energy society*, vol. 30, no. 1, pp. 21–28, 2019.

[75] M. R. Akhtari, I. Shayegh, and N. Karimi, "Techno-economic assessment and optimization of a hybrid renewable earth-air heat exchanger coupled with electric boiler, hydrogen, wind and pv configurations," *Renewable Energy*, vol. 148, pp. 839–851, 2020.

[76] G. Amica, P. A. Larochette, and F. Gennari, "Light metal hydride-based hydrogen storage system: Economic assessment in argentina," *International Journal of Hydrogen Energy*, vol. 45, no. 38, pp. 18 789–18 801, 2020.

[77] K. Kumar, M. Alam, and V. Dutta, "Techno-economic analysis of metal hydride-based energy storage system in microgrid," *Energy Storage*, vol. 1, no. 3, p. e62, 2019.

[78] M. Wei, G. Levis, and A. Mayyas, "Reversible fuel cell cost analysis," *Lawrence Berkeley National Laboratory (LBNL), Berkeley, CA, USA. Available at: https://www. hydrogen. energy. gov/pdfs/review20/fc332_wei_2020_o. pdf*, 2020.

[79] R. Scataglini, M. Wei, A. Mayyas, S. H. Chan, T. Lipman, and M. Santarelli, "A direct manufacturing cost model for solid-oxide fuel cell stacks," *Fuel Cells*, vol. 17, no. 6, pp. 825–842, 2017.

[80] A. Chadly, E. Azar, M. Maalouf, and A. Mayyas, "Techno-economic analysis of energy storage systems using reversible fuel cells and rechargeable batteries in green buildings," *Energy*, vol. 247, p. 123466, 2022.

[81] M. S. Peters, K. D. Timmerhaus, R. E. West *et al.*, *Plant design and economics for chemical engineers*. McGraw-hill New York, 2003, vol. 4.

[82] M. H. Abokersh, M. Valles, K. Saikia, L. F. Cabeza, and D. Boer, "Techno-economic analysis of control strategies for heat pumps integrated into solar district heating systems," *Journal of Energy Storage*, vol. 42, p. 103011, 2021.

[83] L. Bi, S. Boulfrad, and E. Traversa, "Steam electrolysis by solid oxide electrolysis cells (soecs) with proton-conducting oxides," *Chemical Society Reviews*, vol. 43, no. 24, pp. 8255–8270, 2014.

[84] Y. Luo, Y. Shi, Y. Zheng, Z. Gang, and N. Cai, "Mutual information for evaluating renewable power penetration impacts in a distributed generation system," *Energy*, vol. 141, pp. 290–303, 2017. [Online]. Available: https://www.sciencedirect.com/science/article/pii/S0360544217315542

[85] M. Carmo, D. L. Fritz, J. Mergel, and D. Stolten, "A comprehensive review on pem water electrolysis," *International Journal of Hydrogen Energy*, vol. 38, no. 12, pp. 4901–4934, 2013. [Online]. Available: https://www.sciencedirect.com/science/article/pii/S0360319913002607

[86] M. Henke, J. Kallo, K. A. Friedrich, and W. G. Bessler, "Influence of pressurisation on sofc performance and durability: a theoretical study," *Fuel Cells*, vol. 11, no. 4, pp. 581–591, 2011.

[87] J. Mougin, S. Di Iorio, A. Chatroux, T. Donnier-Marechal, G. Palcoux, M. Petitjean, and G. Roux, "Development of a solid oxide electrolysis stack able to operate at high steam conversion rate and integration into a soe system," *ECS Transactions*, vol. 78, no. 1, p. 3065, 2017.

[88] S. D. Ebbesen and M. Mogensen, "Electrolysis of carbon dioxide in solid oxide electrolysis cells," *Journal of Power Sources*, vol. 193, no. 1, pp. 349–358, 2009.

[89] H. Yan, R. Wang, S. Du, B. Hu, and Z. Xu, "Analysis and perspective on heat pump for industrial steam generation," *Advanced Energy and Sustainability Research*, vol. 2, no. 5, p. 2000108, 2021.

A Solid oxide cell background information

To determine the heat and power consumption of the balance-of-plant the model of the solid oxide cell is developed. The reversible solid oxide cell is able to operate in two modes. These are electrolysis in which water and electricity are used to produce hydrogen. Secondly, the fuel cell in which hydrogen and oxygen react to form water generates power and heat. The operational temperature of both the fuel cell and electrolyser is between 700 and 750 °C. The reaction of hydrogen is dependent on multiple parameters, besides the physical parameters of the cell and stack. The three main influences regarding the performance of the SOC are the temperature, composition and pressure. Where increasing the pressure increases the potential electricity extracted from the hydrogen. However, for electrolysis, an increased pressure has the consequence of higher cell potential for an equal current density. Higher pressure increases the efficiency of fuel cells due to higher possible cell potentials. High temperatures reduce the cell potential which is advantageous for electrolysis. The increased temperature possible used SOC allows for the use of cheap nickel electrodes. Literature shows an increased cell potential for increasing H_2 fractions in the fuel channel within the stack [11].

Electrolysis is the operation in which H_2O and electricity are utilized to produce H_2. Due to the thermodynamics a substantial part of the required can be supplied as heat. Furthermore, the temperatures allow for water to be supplied as steam which reduces the required chemical potential substantially [83].

$$H_2O \rightarrow H_2 + \frac{1}{2}O_2 \tag{97}$$

The reaction for oxygen and water molecules. The process of the SOE and SOFC are shown in figure 35.

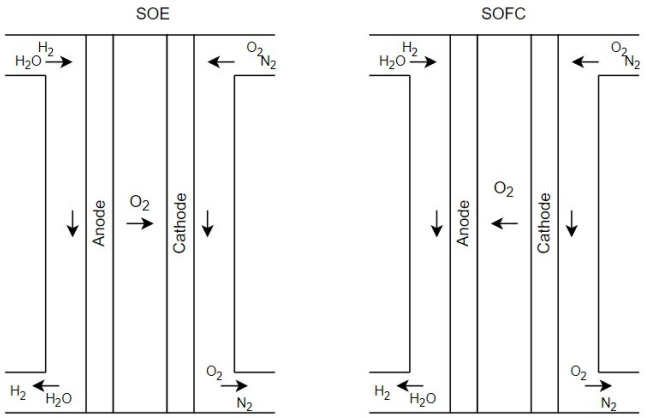

Figure 35: Schematic overview of Solid Oxide Electrolysis and the Solid Oxide Fuel Cell

A.1 Electrochemical reaction

This section describes the effects of different parameters on the open circuit voltage (OCV). The OCV is the difference in electrical potential between the anode and cathode without a current. To calculate the cell potential the standard cell potential could derived from the Gibbs free energy. Using the Gibbs free energy equation:

$$\Delta G = \Delta H - T\Delta S \tag{98}$$

A.1.1 Temperature

Both SOE and SOFC operate at high temperatures with temperatures of 600 to 1000 °C [3]. At these temperatures, the SOFC does not need a platinum catalyst [84], which consequently reduces the cost. Furthermore, the temperature affects the amount of energy which is required to be in the form of electricity. The additional energy could in this case be provided as heat. Which could potentially improve the performance of the RSOC if the heat is provided from a heat source within the stack or an external source. Due to the elevated temperatures, water could be provided in the form of steam which further reduces the power consumption during SOE. The effect of the temperature on the open circuit voltage is shown in figure 36, assuming other properties like composition and pressure are at the standard reference values.

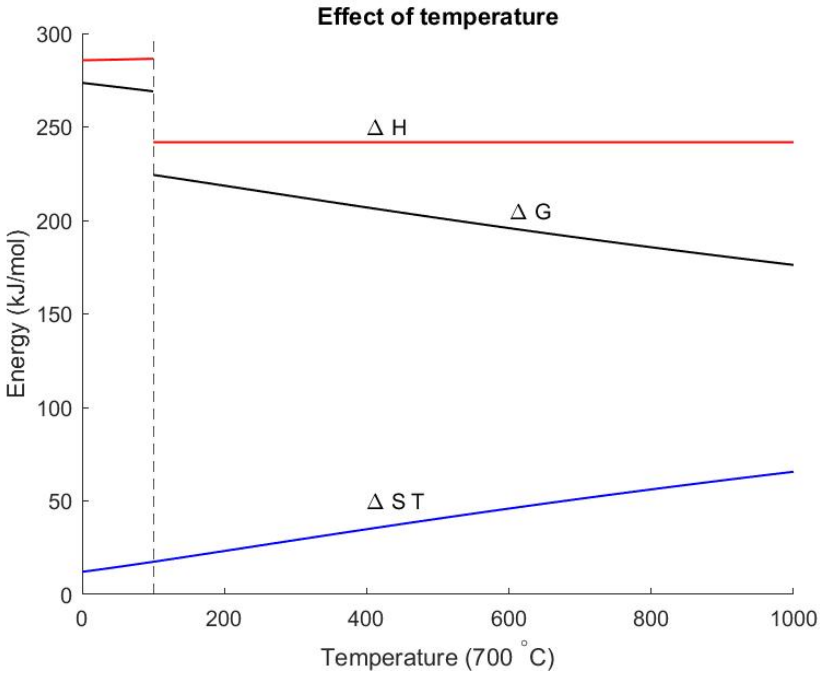

Figure 36: The effects of the temperature on the Gibbs free energy and thus the reversible energy

The resulting Gibbs free energy allows to calculate the maximum round-trip efficiency. Where it is assumed that the power input is at the thermoneutral voltage or the corresponding enthalpy

of formation ΔH. The effect of the temperature on the round trip efficiency is presented in figure 37. The round-trip efficiency decreases with increasing temperatures. The required energy is lower if H_2O is fed into the cell, $\Delta H_{gas} < \Delta H_{liquid}$, however the difference between ΔH_{gas} and ΔH_{liquid} equals the latent heat.

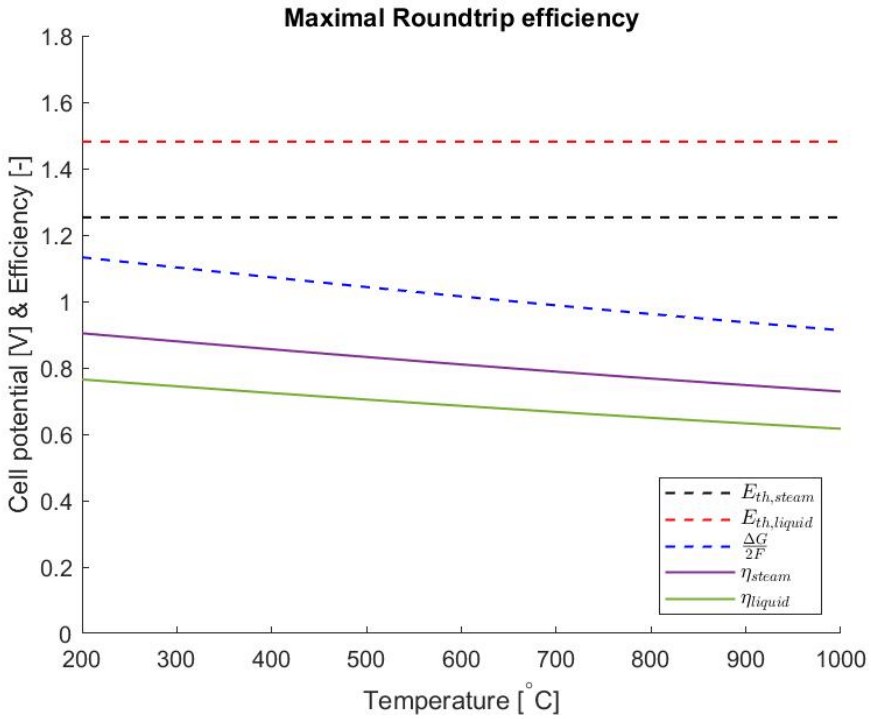

Figure 37: Maximum round trip efficiency related to temperature

A.1.2 Fuel composition

The open circuit voltage (OCV) for non-standard conditions is calculated with the Nernst Potential. The Nernst equation takes into account the non-standard conditions regarding pressure, temperature and composition of the electrochemical process.

$$E_{\text{Nernst}} = E_0 + \frac{RT}{2F} ln\left(\frac{x_{H_2}\sqrt{x_{O_2}}}{x_{H_2O}}\right) + \frac{RT}{2F} ln\left(\frac{P_A}{P_{amb}}\right) \tag{99}$$

Where the standard cell potential (E_0), ΔG follows from equation 98, F is Faraday's constant and R is the university gas constant. x is the molar fraction, P and T are the pressure (Pa) and temperature respectively (K).

$$E_0 = \frac{\Delta G}{2F} \tag{100}$$

The effect of the composition of the fuel on the OCV voltage is as follows, where the composition of hydrogen and water are related:

$$x_{H_2} = 1 - x_{H_2O} \tag{101}$$

Figure 38 shows the effect of the hydrogen content on the open circuit voltage of the cell.

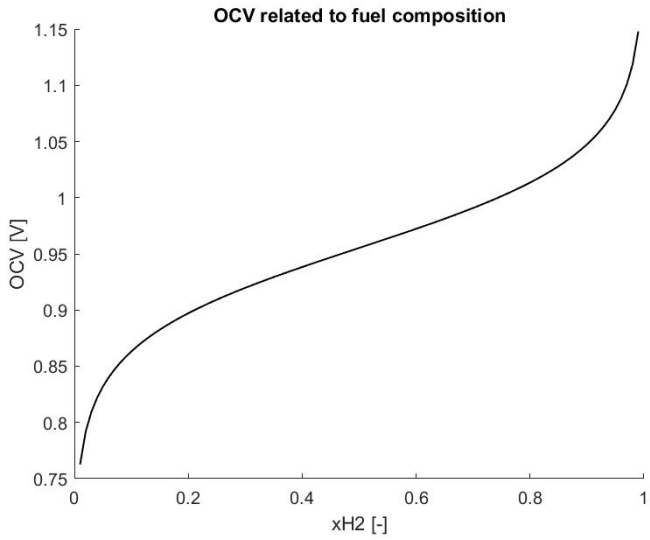

Figure 38: The open circuit voltage calculated at 700 ° at ambient pressure

The OCV increases for an increasing hydrogen fraction within the fuel. Therefore it is favorable to increase the hydrogen content in fuel cell mode and decrease the fraction of hydrogen during electrolysis.

A.2 Pressure effect

The pressurized operation of an electrolyzer has the advantage of delivering hydrogen at high pressure for the end user. Thus requiring less energy to compress and store the hydrogen. Another advantage is that it reduces the volume of the gaseous phase at the electrodes thus improving product gas removal which follows Fick's Law of diffusion [85]. Secondly, the efficiency of the fuel cell is improved if operated at higher pressures [11]. Since the increase of pressure positively affects the Nernst-potential and polarization curve for fuel cells [45]. Henke et al. state that increased pressure can reduce the concentration and activation overpotentials [86]. However, it states the increased pressure is a potential threat to the durability of the cell. Furthermore, the increased pressure requires the fuel and air to be pressurized. This requires additional energy consumption from the compression of air and fuel. Increased pressure can increase the cell efficiency with 5-7% points efficiency [46]. Mottaghizadeh investigated both the effects on cell efficiency as well as for the total BoP. They found a higher cell efficiency for higher pressure however the system efficiency is lower, this is attributed to the air compressor [7].

A.2.1 V-I curve

The V-I curve is the relation between the current density and the cell potential. This is related to the power density and thus the overall power. The V-I curve is dependent on multiple parameters, temperature, composition and pressure, as physical proprieties of the cell. For low current density as used in this model ($i \leq 1$ A/cm^2) the V-I curve can be assumed to be linear [87]. The approximation of the cell is the area-specific resistance (ASR) which can be experimentally determined, the ASR mainly varies for different compositions and temperatures [88].

B Concepts

This appendix includes the temperature and molar flow-rates corresponding to figures 2 to 6b.

B.1 Temperature & flow-rate of the concepts

Table 11: Temperature and molar-flow of concept 1 for SOEC and SOFC.

Stream	SOE	SOFC		SOE			SOFC	
	Temperature [° C]		$\dot{n}$	x_{H_2}	x_{H_2O}	$\dot{n}$	x_{H_2}	x_{H_2O}
1	20	20	0.1	1	0	0.95	1	0
2	100	100	0.1	1	0	0.95	1	0
3	20	20	0.9	0	1	0.050	0	1
4	20	20	0.9	0	1	0.050	0	1
5	100	100	0.9	0	1	0.050	0	1
6	100	100	0.9	0	1	0.050	0	1
7	100	100	1	0.1	0.9	1	0.95	0.05
8	700	700	1	0.1	0.9	1	0.95	0.05
9	700	750	1	0.82	0.18	1	0.19	0.81
10	100	100	0.82	1	0	0.19	1	0
11	25	25	0.82	1	0	0.19	1	0
12	192	192	0.82	1	0	0.19	1	0
13	25	25	0.82	1	0	0.19	1	0
14	20	20	11.01	-	-	39.85	-	-
15	20	20	11.01	-	-	39.85	-	-
16	700	700	11.01	-	-	39.85	-	-
17	700	700	11.01	-	-	39.85	-	-
18	100	100	0.18	0	1	0.81	0	1

Table 12: Temperature and molar-flow of concept 2 for SOEC and SOFC

Stream	SOE	SOFC		SOE			SOFC	
	Temperature [° C]		$\dot{n}$	x_{H_2}	x_{H_2O}	$\dot{n}$	x_{H_2}	x_{H_2O}
1	20	20	0	1	0	0.760	1	0
2	100	100	0	1	0	0.760	1	0
3	100	100	0.1	1	0	0.950	1	0
4	20	20	0.9	0	1	0.050	0	1
5	100	100	0.9	0	1	0.050	0	1
6	100	100	0.9	0	1	0.050	0	1
7	100	100	1	0.1	0.9	1	0.95	0.05
8	594	700	1	0.1	0.9	1	0.95	0.05
9	700	700	1	0.1	0.9	1	0.95	0.05
10	700	750	1	0.82	0.18	1	0.19	0.81
11	132	288	1	0.82	0.18	1	0.19	0.81
12	100	100	0.821	1	0	0.190	1	0
13	100	100	0.721	1	0	0	1	0
14	25	25	0.721	1	0	0	1	0
15	192	192	0.721	1	0	0	1	0
16	25	25	0.721	1	0	0	1	0
17	100	100	0.1	0	1	0.190	1	0
18	100	100	0.179	0	1	0.810	0	1
19	20	20	11.01	-	-	39.85	-	-
20	20	20	11.01	-	-	39.85	-	-
21	675	700	11.01	-	-	39.85	-	-
22	700	700	11.01	-	-	39.85	-	-
23	700	750	11.01	-	-	39.85	-	-
24	49	70	11.01	-	-	39.85	-	-

Table 13: Temperature and molar-flow of concept 3 for SOEC and SOFC

Stream	SOE	SOFC		SOE			SOFC	
	Temperature [° C]		$\dot{n}$	x_{H_2}	x_{H_2O}	$\dot{n}$	x_{H_2}	x_{H_2O}
1	20	20	0	1	0	0.760	1	0
2	100	100	0	1	0	0.760	1	0
3	100	100	0.1	1	0	0.950	1	0
4	20	20	0.9	0	1	0.050	0	1
5	100	100	0.9	0	1	0.050	0	1
6	100	100	0.9	0	1	0.050	0	1
7	100	100	1	0.1	0.9	1	0.95	0.05
8	594	700	1	0.1	0.9	1	0.95	0.05
9	700	700	1	0.1	0.9	1	0.95	0.05
10	700	750	1	0.82	0.18	1	0.19	0.81
11	132	288	1	0.82	0.18	1	0.19	0.81
12	100	100	0.821	1	0	0.190	1	0
13	100	100	0.721	1	0	0	1	0
14	25	25	0.721	1	0	0	1	0
15	192	192	0.721	1	0	0	1	0
16	25	25	0.721	1	0	0	1	0
17	100	100	0.1	0	1	0.190	1	0
18	100	100	0.179	0	1	0.810	0	1
19	20	20	11.01	-	-	39.85	-	-
20	20	20	11.01	-	-	39.85	-	-
21	675	700	11.01	-	-	39.85	-	-
22	700	700	11.01	-	-	39.85	-	-
23	700	750	11.01	-	-	39.85	-	-
24	49	70	11.01	-	-	39.85	-	-

Table 14: Temperature and molar-flow of concept 4 for SOEC and SOFC

Stream	SOE	SOFC		SOE			SOFC	
	Temperature [° C]		$\dot{n}$	x_{H_2}	x_{H_2O}	$\dot{n}$	x_{H_2}	x_{H_2O}
1	20	20	0	1	0	0.760	1	0
2	100	100	0	1	0	0.760	1	0
3	100	100	0.1	1	0	0.950	1	0
4	20	20	0.9	0	1	0.050	0	1
5	100	100	0.9	0	1	0.050	0	1
6	100	100	0.9	0	1	0.050	0	1
7	100	100	1	0.1	0.9	1	0.95	0.05
8	594	700	1	0.1	0.9	1	0.95	0.05
9	700	700	1	0.1	0.9	1	0.95	0.05
10	700	750	1	0.82	0.18	1	0.19	0.81
11	132	288	1	0.82	0.18	1	0.19	0.81
12	100	100	0.821	1	0	0.190	1	0
13	100	100	0.721	1	0	0	1	0
14	25	25	0.721	1	0	0	1	0
15	192	192	0.721	1	0	0	1	0
16	25	25	0.721	1	0	0	1	0
17	100	100	0.1	0	1	0.190	1	0
18	100	100	0.179	0	1	0.810	0	1
19	20	20	11.01	-	-	2.50	-	-
20	20	20	11.01	-	-	2.50	-	-
21	675	700	11.01	-	-	2.50	-	-
22	700	700	11.01	-	-	2.50	-	-
23	700	750	11.01	-	-	2.50	-	-
24	49	70	11.01	-	-	2.50	-	-

Table 15: Temperature and molar-flow of concept 5 for SOEC and SOFC

Stream	SOE	SOFC		SOE			SOFC	
	Temperature [° C]		$\dot{n}$	x_{H_2}	x_{H_2O}	$\dot{n}$	x_{H_2}	x_{H_2O}
1	20	20	11.01	-	-	2.50	-	-
2	20	20	11.01	-	-	2.50	-	-
3	675	700	11.01	-	-	2.50	-	-
4	700	700	11.01	-	-	2.50	-	-
5	700	750	11.01	-	-	2.50	-	-
6	45	370	11.01	-	-	2.50	-	-
7	100	100	0.10	1.00	0.00	0.19	1.00	0.00
8	287	287	0.10	1.00	0.00	0.19	1.00	0.00
9	100	287	0.72	1.00	0.00	0.76	1.00	0.00
10	100	100	0.18	0.00	1.00	0.81	0.00	1.00
11	20	100	0.72	0.00	1.00	0.76	0.00	1.00
12	20	100	0.90	0.00	1.00	0.05	0.00	1.00
13	287	287	0.90	0.00	1.00	0.05	0.00	1.00
14	287	287	1.00	0.10	0.90	1.00	0.95	0.05
15	610	700	1.00	0.10	0.90	1.00	0.95	0.05
16	675	700	1.00	0.10	0.90	1.00	0.95	0.05
17	700	750	1.00	0.82	0.18	1.00	0.19	0.81
18	312	392	1.00	0.82	0.18	1.00	0.19	0.81
19	100	287	0.82	1.00	0.00	0.81	0.00	1.00

B.2 Elaboration on the heat pump

The use of an electrically driven heat pump could increase the performance of the system. Very high-temperature heat pumps (VHTHP) release heat at temperatures above 100 °C and can operate with ambient temperature heat sources [48]. During both SOFC and SOE heat is removed within the condenser which could provide a high-temperature heat source. Heat pumps operate more efficiently when the temperate difference between evaporation and condensation is small. To determine the performance the coefficient of performance (COP) is used to investigate the performance of the heat pump. The COP is calculated by the heat output and the power input.

$$COP_{\text{heating}} = \frac{\dot{Q}_{\text{H}}}{\dot{Q}_{\text{H}} - \dot{Q}_{\text{C}}} \tag{102}$$

Where $\dot{Q}_{\text{H}}$ - $\dot{Q}_{\text{C}}$ is equal to the additional power input. The maximum theoretical performance of a heat pump is calculated by the Carnot Efficiency.

$$COP_{\text{heating}} = \frac{T_{\text{H}}}{T_{\text{H}} - T_{\text{C}}} \tag{103}$$

Literature indicates the performance achieved for steam-generating heat pumps. A COP of 6.1 has been achieved using water as a refrigerant with an evaporation temperature of 85 °C and condensation temperature of 117 °C [49]. Tveit et al. [50] present a series of heat pumps generating steam at 10 bar and a temperature of 184 °C with a source of 80-90 °C. Figure 39 shows that the temperature of the heat reservoir is an important factor for the performance of the heat pump. Where the temperature difference between the condensing flow of steam and the cooling fluid is desired to be small. The condensation is theoretically possible at a small temperature difference. The use of a logarithmic mean temperature difference (LMTD) of 9.5 °C is within the condenser of a power plant [51].

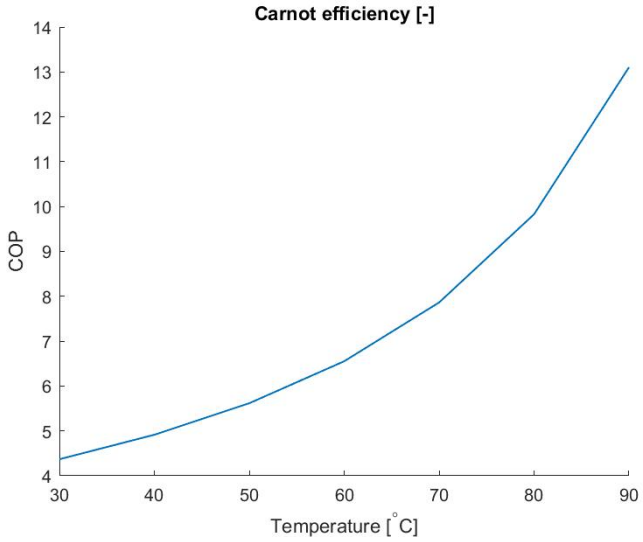

Figure 39: COP for varying temperatures of the lower reservoir (T_C), T_H = 120 °C

It is shown that an increase in the temperature of the lower reservoir increases the potential performance of the heat pump. However, the temperature of the lower reservoir is bound to at least two heat exchanges, $T_{con} > T_{cool} > T_{storage} > T_C$, where the storage might be used as the low-temperature reservoir. Equation 103 shows the COP is reduced by a larger temperature difference between the two reservoirs.

A second path for steam generation is reducing the pressure and subsequently reducing the boiling temperature of the water. This reduces the required temperature of the high-temperature reservoir of the heat pump. This increases the performance of the heat pump shown in equation 102. Yan et al. [89] propose a steam-generating heat pump which uses sub-atmospheric pressure to provide the latent heat for the transition from liquid to vapour. After which the vapour is pressurized by a compressor. This consequently reduces the absolute increase in performance of the steam generation process.

Both atmospheric and sub-atmospheric heat pumps might use a TES followed by a heat pump.

However, the response time of the heat pump increases as the heat is not directly available at the desired temperature for evaporation. A third option of steam generation is to change to order of the process of storage and the temperature elevation. The temperature is increased directly after condensation and stored at temperatures above the boiling temperature of the water vapour. The two orders of operation are:

- Condensation → TES → Heat pump → Evaporator (figure 40)
- Condensation → Heat pump → TES → Evaporator (figure 41)

The first possibility is that the heat of condensation is stored at a temperature below the temperature of the condenser. The stored heat is the reservoir of the heat pump from which the heat is extracted to increase the performance of the heat pump.

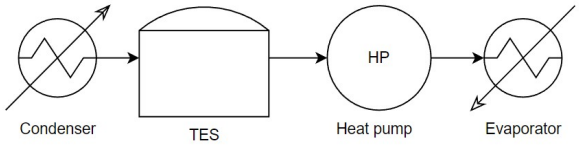

Figure 40: Path from condensation to evaporation, thermal energy storage followed by the heat pump

The second possibility to store heat is by increasing the temperature before storage of the thermal energy. This removes the response time of the heat pump if the heat is consumed by the evaporation.

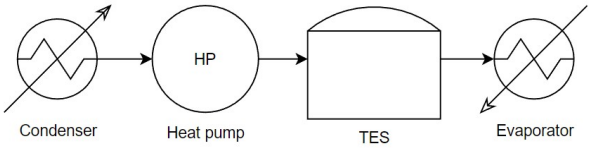

Figure 41: Path from condensation to evaporation, heat pump followed by thermal energy storage

Increasing the temperature before storage is not favourable due to higher losses during storage and the requirement of heat pump operations during SOFC. This increases the power requirement during a period when the demand from the grid requires additional electricity to be supplied. Water is selected as the favourable storage medium for this concept. Because of the relatively low temperatures required, low costs, fast response time and long-term storage possibilities.

C Additional equations for modelling

The additional equations related to various components of the modelling are presented in this appendix.

C.1 Calculation of the entropy

The entropy of the components at a reference temperature of 25 °C are given in table 16.

Table 16: Entropy of different components used within the model

	ΔS
H_2	131 J/molK
O_2	205 J/molK
$H_2O(l)$	69.9 J/molK
$H_2O(g)$	188.7 J/molK

The energy requirement and entropy difference of the reaction at the reference temperature at 25 °C are shown in table 17.

Table 17: Enthalpy and Entropy change in electrolysis operation

Phase	Enthalpy [kJ/mol]	Entropy [kJ/molK]
$H_2O(l) \rightarrow H_2 + \frac{1}{2}O_2$	-285.8	- 0.163
$H_2O(g) \rightarrow H_2 + \frac{1}{2}O_2$	-241.8	-0.045

The value C_p can be determined as a function of the temperature using:

$$C_p = A + Bt + Ct^2 + Dt^3 + \frac{E}{t^2} \tag{104}$$

In which $t = \frac{T}{1000}$ with T is the temperature in Kelvin.

Table 18: Parameters specific heat capacity

	H_2O (500-1700K)	O_2 (700-2000K)	H_2 (298-1000K)	N_2 (500-2000K)
A	30.092	30.032	33.066	19.506
B	6.833	8.773	-11.363	19.887
C	6793	-3.988	11.433	-8.599
D	-2534	0.788	-2.773	1.3698
E	0.082	-0.742	-0.159	0.528

C.2 Calculation compressor

Figure 42 shows the power consumption of the compressor for an increase from 1 to 350 bar with an inlet temperature of 25 °C.

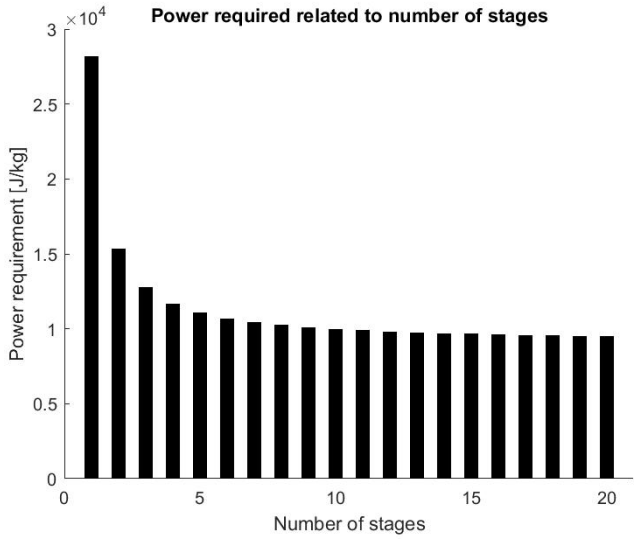

Figure 42: The energy required to increase the pressure from 1 to 350 bar is related to the number of stages in the compressor including inter-cooling

The reduction after five compressor stages is below 5% relative to a four-stage compressor. Therefore, a compressor with five stages is selected. The corresponding outlet temperature of the compressor is 192 °C as shown in figure 43 based.

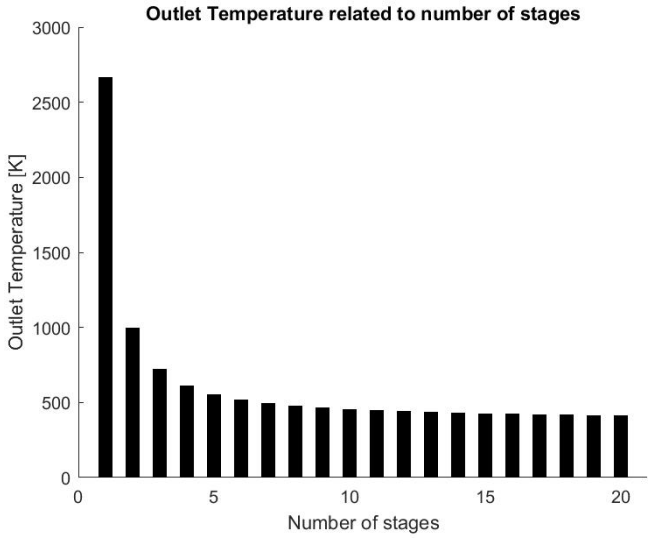

Figure 43: The outlet temperature of a compressor including the use of inter-cooling

The final power consumption for the compressor and blower are calculated with:

$$P = \frac{\rho Q W}{\eta_{\mathrm{m}} \eta_{\mathrm{t}} \eta_{\mathrm{mech}} \eta_{\mathrm{h}}} \tag{105}$$

Which include the efficiencies of the compressor. These include the mechanical efficiency (η_{mech}), motor efficiency (η_{m}), hydraulic efficiency (η_{h}), and transmission efficiency (η_{t}). The efficiencies used are presented in table 19.

Table 19: Efficiencies compressor

η_{pol}	0.85
η_{hyd}	0.95
η_{mech}	0.98
η_{t}	0.98
η_{m}	0.9

C.3 Algorithm heat storage

This section describes the algorithms used for the process of storing heat within the TES.

C.3.1 Concept 3: Heat storage

To model the storage levels of the heat storage the following algorithm is used. Firstly, the model is used to determine whether charging or discharging of the heat storage is required. The heat pump uses a fixed COP of 4, therefore three-quarters of the energy is supplied as heat from the heat storage or heat of condensation. The heat input of the heat pump is defined as:

$$Q_{\mathrm{req}} = Q_{\mathrm{SG}} - W \tag{106}$$

The required heat from the heat storage is calculated as the difference between the required heat input of the heat pump and the heat of condensation. In general, the heat of condensation is sufficiently large during SOFC therefore the heat storage is charged during SOFC. During SOE the heat required for evaporation exceeds the heat of condensation therefore heat is extracted from the heat storage.

$$Q = Q_{\mathrm{con}} - Q_{\mathrm{req}} \tag{107}$$

Where Q is the heat charging or discharging the heat storage. However, the capacity of the heat storage is limited. There are two boundary conditions set at the heat storage. No heat could be used if the storage is empty thus the heat storage cannot be below zero. Furthermore, the heat stored cannot exceed the maximum storage capacity of the storage.

$$x_{\mathrm{SOFC_{in}}} = \begin{cases} L_{\mathrm{min}} = 0 \\ L_{\mathrm{max}} = L_{\mathrm{max}} \end{cases}$$

Where L_{min} and L_{max} are the minimum and maximum state of charge. L is the new state of charge, L^{n-1} is the previous state of charge. The state of charge cannot be below the minimum.

$$Q_{\text{st}} = \begin{cases} -Q \;\; if \;\; L^{n-1} - Q > L_{\text{min}} \\ L^{n-1} - L_{\text{min}} \;\; if \;\; L^{n-1} + Q < L_{\text{min}} \end{cases} \tag{108}$$

Where if Qst cannot satisfy the required heat all heat is supplied by the electric boiler.

$$Q_{ext} = Q - Q_{st} \tag{109}$$

Similarly, the heat supplied to the heat storage should not exceed the maximum capacity of the storage.

$$Q_{\text{st}} = \begin{cases} L_{\text{max}} - L^{n-1} \;\; if \;\; L^{n-1} + Q > L_{\text{max}} \\ Q \;\; if \;\; L^{n-1} + Q < L_{\text{max}} \end{cases} \tag{110}$$

If the addition of heat results in a state of charge the storage is charged to the maximum. The excess heat is assumed to be waste released to the environment.

C.3.2 Concept 4: Heat storage

To model the storage levels of the heat storage the following algorithm is used. Firstly, the model is used to determine whether charging or discharging of the heat storage is required. The required heat from the heat storage is calculated as the difference between the required heat for heating and the heat generated by the SOFC. The RSOC only generated heat during SOFC mode. The model prioritizes the direct use of the heat for both heating the inlet flows and evaporation. The use of heat is used as follows for utilization and storage:

1. Pre-heating fuel and air flows
2. Heat for evaporation
3. Charging high-temperature TES
4. Charging medium-temperature TES

The direct use of heat for pre-heating of fuel and air flows is only used during the transition from SOE and SOFC and vice-versa. Heat generation and evaporation both take place during SOFC and therefore influence the amount of heat available for charging the TES.

$$Q = Q_{\text{SOFC}} - Q_{\text{req,A}} - Q_{\text{req,B}} \tag{111}$$

Where Q is the heat charging or discharging the heat storage. $Q_{req,A}$ is the heat required for pre-heating, $Q_{req,B}$ is the heat for evaporation and Q_{SOFC} is the available heat from the SOFC. It could be possible that the heat is only sufficient to supply heat for the pre-heating of fuel and

air.

$$Q_A = \begin{cases} 0 \ \ if \ \ Q_{\text{SOFC}} > Q_{\text{req,A}} \\ Q_{\text{req,A}} - Q_{\text{SOFC}} \ \ if \ \ Q_{\text{SOFC}} < Q_{\text{req,A}} \end{cases} \tag{112}$$

If $Q_{SOFC} < Q_{req,A}$ all heat for evaporation of water is supplied by electric boilers.

$$Q_{\text{B}} = \begin{cases} 0 \ \ if \ \ Q_{\text{SOFC}} - Q_{\text{req,A}} > Q_{\text{req,B}} \\ Q_{\text{SOFC}} - Q_{\text{req,B}} \ \ if \ \ 0 < Q_{\text{SOFC}} - Q_{\text{req,A}} < Q_{\text{req,B}} \end{cases} \tag{113}$$

Like the heat storage of concept 3, there are two boundary conditions set at the heat storage.

$$L_{\text{min}} = 0$$
$$L_{\text{max}} = L_{\text{max}}$$

Where L_{min} and L_{max} are the minimum and maximum state of charge. L is the new state of charge, L^{n-1} is the previous state of charge. The state of charge cannot be below the minimum.

$$Q_{\text{st,A}} = \begin{cases} Q_A \ \ if \ \ L^{n-1} + Q_{\text{AA}} > L_{\text{min}} \\ L^{n-1} - L_{\text{min}} \ \ if \ \ L^{n-1} + Q_{\text{A}} < L_{min} \end{cases} \tag{114}$$

Where if Q_{st} cannot satisfy the required heat all heat is supplied by the electric boiler.

$$Q_{\text{ext,A}} = Q_{\text{A}} - Q_{\text{st,A}} \tag{115}$$

Similarly, the heat supplied to the heat storage should not exceed the maximum capacity of the storage.

$$Q_{\text{st,A}} = \begin{cases} L_{\text{max}} - L^{n-1} \ \ if \ \ L^{n-1} + Q > L_{\text{max}} \\ Q \ \ if \ \ L^{n-1} + Q < L_{\text{max}} \end{cases} \tag{116}$$

If the addition of heat results in a state of charge the storage is charged to the maximum. The excess heat is assumed to be used for charging the medium-temperature storage.

$$Q_{\text{av,B}} = Q - Q_{\text{st,A}} \tag{117}$$

Where $Q_{av,B}$ is the heat available to be used for charging the medium-temperature storage. Similar to the high temperature storage the level of the medium temperature storage.

$$L_{\text{min}} = 0$$
$$L_{\text{max}} = L_{\text{max}}$$

$$Q_{\text{st,B}} = \begin{cases} Q_{\text{B}} \ \ if \ \ L^{n-1} + Q_{\text{B}} > L_{\text{min}} \\ L^{n-1} - L_{\text{min}} \ \ if \ \ L^{n-1} + Q_{\text{B}} < L_{\text{min}} \end{cases} \tag{118}$$

Where if Q_{st} cannot satisfy the required heat all heat is supplied by the electric boiler.

$$Q_{\text{ext,B}} = Q_{\text{B}} - Q_{\text{st,B}} \tag{119}$$

Similarly, the heat supplied to the heat storage should not exceed the maximum capacity of the storage.

$$Q_{\text{st,B}} = \begin{cases} L_{\max} - L^{n-1} \;\; if \;\; L^{n-1} + Q_{\text{av,B}} > L_{\max} \\ Q_{\text{av,B}} \;\; if \;\; L^{n-1} + Q_{\text{av,B}} < L_{\max} \end{cases} \tag{120}$$

D Steady-state Results

The efficiency is thus defined as: Figures 44 to 46 show the power input from external sources during SOE and SOFC. The reduction in power consumption is caused by lower flow rates in both the fuel and air sides of the BoP. The lower flow rates are a result of a change in the efficiency of the electrochemical process. The higher efficiency of the SOC results in less hydrogen and steam being produced and thus improves the relative performance of the BoP. For concepts 2 to 4 the power input required during SOFC is caused by the blower and evaporation. The increase in required power for concept 5 is a result of the increasing efficiency of the SOFC. The generated heat as shown in equation 47 is lower than the required heat, see equation 7. For low current densities and high cell potential equation 6 is not satisfied. To release hydrogen from the metal hydride storage additional energy is required.

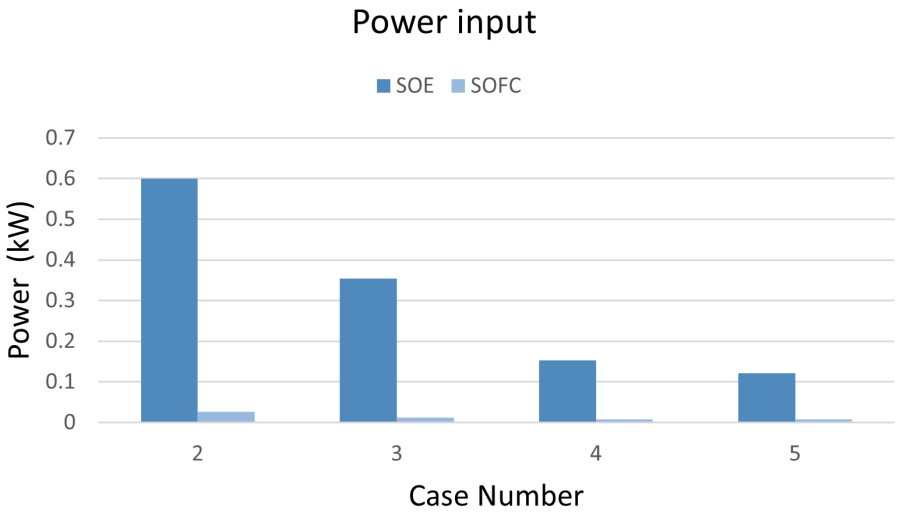

Figure 44: Power consumption for a current density of 1 A/cm^2

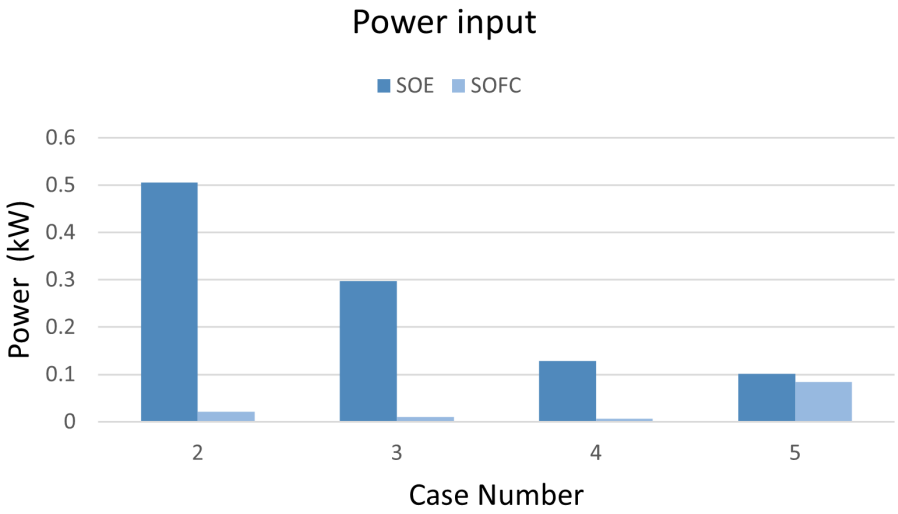

Figure 45: Power consumption for a current density of 0.5 A/cm^2

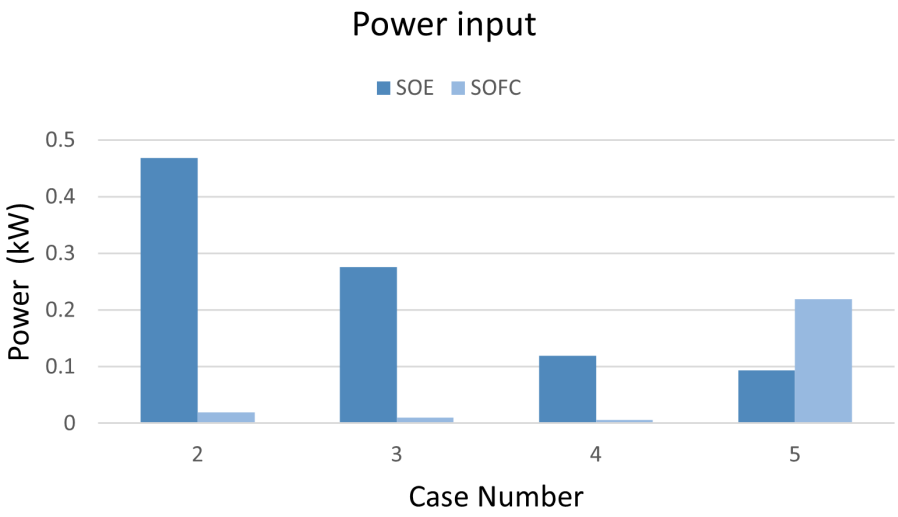

Figure 46: Power consumption for a current density of 0.25 A/cm^2

E Performance of varying variables

E.1 Pinch point of the Heat exchangers

Figure 18 shows the energy consumption of the BoP for a temperature difference within the heat recovery units of 25 °C. However, the first method of reducing the parasitic power consumption by the electric heaters is by reducing the required temperature difference within the heat recovery units. The effects of different temperature differences within the stack are presented in tables 20 and 21. The heating of air requires substantially more electricity for larger temperature differences within the heat recovery units. These results are representative of the heat recovery units required for concepts 2 & 3.

Table 20: The size and energy transfer by heat recovery and electric heaters respectively used for pre-heating the airflow for concepts 2 & 3

Temperature Difference (°C)	Energy Transfer (kWh)	Maximum Power (kW)	Electricty Consumption (kWh)	Maximum Power (kW)
0	16247183.34	3785.40	0	0
10	16172749.82	3785.37	74433.53	56.1
25	15971426.36	3785.13	275756.99	144.74
50	15472826.31	3704.64	774357.04	291.79

Table 21: The size and energy transfer by heat recovery and electric heaters respectively used for super-heating the H_2 and H_2O for concepts 2 & 3

Temperature Difference (°C)	Energy Transfer (kWh)	Maximum Power (kW)	Electricity Consumption (kWh)	Maximum Power (kW)
0	341285.91	104.24	32748.32	8.13
10	338290.66	104.25	35744.66	8.85
25	333098.82	104.24	40935.07	9.92
50	321796.09	104.24	52237.42	11.70

The results show increasing demand for electrical heaters for increasing temperature differences in heat recovery. For fuel, a second aspect is of importance, which is the changing composition of the fuel. The high-temperature stream entering the heat recovery during SOE contains less heat than is required to heat the inlet stream. This results in additional heat being supplied by electrical heaters even when a zero temperature difference is allowed.

Table 22: The size and energy transfer by heat recovery and electric heaters respectively used for pre-heating the airflow for concept 4

Temperature Difference (°C)	Energy Transfer (kWh)	Maximum Power (kW)	Electricty Consumption (kWh)	Maximum Power (kW)
0	2693912.04	550.53	0.00	0.00
10	2659280.99	541.92	34632.82	8.61
25	2607412.67	529.03	86501.07	21.49
50	2505314.79	507.63	188598.96	42.89

Table 23: The size and energy transfer by heat recovery and electric heaters respectively used for super-heating the H_2 and H_2O for concept 4

Temperature Difference (°C)	Energy Transfer (kWh)	Maximum Power (kW)	Electricity Consumption (kWh)	Maximum Power (kW)
0	341285.91	104.24	32748.32	8.13
10	338290.66	104.25	35744.66	8.85
25	333098.82	104.24	40935.07	9.92
50	321796.09	104.24	52237.42	11.70

E.2 Efficiency of different thermal management scenarios

Table 24: Energy consumption System

Concept Number	Energy Input SOE (kWh)	Energy Input SOFC (kWh)	Energy Output SOFC (kWh)	Efficiency (-)
Concept 2a	2395675.16	207638.41	1176922.72	45.21
Concept 2b	2378557.22	26291.26	1176922.72	48.94
Concept 3a	2325317.26	193711.87	1176922.72	46.72
Concept 3b	2308199.31	12365.88	1176922.72	50.72
Concept 4a	2376636.81	7668.33	1176922.72	49.36
Concept 4b	2377438.48	1264.87	1176922.72	49.48

Since the required power supplied and consumed by the grid and wind-park varies over the year an investigation of the annual performance is executed. The annual output of the stack is determined as P = 1.18 GWh. The efficiency of the system is determined by the net power output, P_{net} = P - P_{SOFC} and the power input during SOE (P_{SOE}). This method of determining efficiency gives a better representation of the performance. The method presented in equation 121 is the round-trip efficiency of the entire system.

$$\eta = \frac{P - P_{\text{SOFC}}}{P_{\text{SOE}}} \tag{121}$$

F List of variables

Latin symbols

A	area	cm^2
ΔE	energy released	J
F	Faraday's constant	C/mol
ΔG	molar gibbs free energy	J/mol
h	molar enthalpy	J/mol
ΔH	molar enthalpy of formation	J/mol
i	current density	A/cm^2
I	current	A
ΔS	molar entropy	J/(mol K)
C	specific heat capacity	J/(kg K)
C_E	cost of electricity input	$
C_c	all cost involved for the generation of electricity	$
c_p	molar heat capacity	J/(mol K)
E_0	open circuit voltage under standard conditions	V
E_{cell}	cell potential	V
n	number of moles	mol
E_{Nernst}	open circuit voltage under non-standard conditions	V
E_l	Power generated	kW
$\dot{n}$	molar flux	mol/s
M	mass	kg
N	time periods	years
p	pressure	Pa
P	power	W
Q	heat transfer	J
$\dot{Q}$	heat flux	W
r	specific resistance	Ω/cm^2
R_{H_2}	hydrogen consumption rate	mol/s
R_{H_2O}	water consumption rate	mol/s
R_{O_2}	oxygen consumption rate	mol/s
R	universal gas constant	J/(K /mol)
t	time	s
T	temperature	K
U_f	utilization factor	-
U_{th}	thermoneutral voltage	V
V	voltage	V
x	molar fraction	

Greek symbols

η_{act}	activation losses	V
η_{conc}	concentration losses	V
η_{ohm}	ohmic losses	V
η	efficiency	-
ρ	density	kg/m^3

G Abbreviation list

ASR	area specific resistance
BoP	balance of plant
CAPEX	capital expenditure
CRF	capital return factor
HEX	heat exchanger
HHV	higher heating value
int	interconnect
LCOE	levelized cost of electricity
LCOS	levelized cost of storage
LHV	lower heating value
OCV	Open circuit voltage
O&M	operation and management cost
PEN	positive-electrolyte-negative
PH	pre-heating
RSOC	reversible solid oxide cell
SG	steam generation
SOC	solid oxide cell
SOE	solid oxide electrolyser
SOFC	solid oxide fuel cell
TES	thermal energy storage